

Abundances and distribution of chalcogen volatile elements in chondritic meteorites and their components

Inaugural-Dissertation

zur

Erlangung des Doktorgrades

der Mathematisch-Naturwissenschaftlichen Fakultät

der Universität zu Köln

vorgelegt von

Claudia Funk

aus Hagenow

Köln, 2015

Berichtersteller:
(Gutachter)

Prof. Dr. Carsten Münker

PD Dr. Dominik Hezel

Tag der mündlichen Prüfung:

8. Mai 2015

„0 ist Nichts & Alles ist 1“

Thomas. R. Pennington

CONTENTS

Abstract	1
Kurzzusammenfassung	3
1. Introduction	
1.1. The origin of the elements	7
1.2. Solar system abundance of the elements	9
1.3. CI chondrites	10
1.4. Cosmochemical classification of the elements	12
1.5. Primary element fractionation	15
1.6. Chondritic components	19
1.7. Primary classification of chondrites	22
1.8. Secondary and tertiary classification parameters	24
2. Quantification of novel calibration and reference materials for LA-ICP-MS analysis	
2.1. INTRODUCTION	28
2.2. SAMPLE AND CALIBRATION MATERIALS	29
2.3. EXPERIMENTAL – QUANTIFICATION OF CANS AND COBO	30
2.3.1. Solution nebulization SF-ICP-MS and ICP-OES	30
2.3.2. Isotope dilution ICP-MS analysis of S, Se and Te	37
2.3.3. Additional analysis by Q-ICP-MS, EMS, INAA, XRF, and Karl Fischer titration	39
2.4. RESULTS AND DISCUSSION	40
2.4.1. Composition of CANS	40
2.4.2. Composition of COBO	45

3. Quantification of trace elements in chondritic components using

femtosecond LA-ICP-MS

3.1. INTRODUCTION	51
3.2. EXPERIMENTAL	53
3.2.1. Femtosecond LA-ICP-MS	53
3.2.2. Data treatment and ablation yield correction	54
3.3. RESULTS AND DISCUSSION	57
3.3.1. Homogeneity of CANS, COBO, and NIST SRM 612	57
3.3.2. Comparison of ablation yields for NIST SRM 612, CANS and COBO.....	59
3.3.3. Evaluation by 100% sum standardization with external CANS-NIST calibration using COBO as a test sample.....	63
3.4. CONCLUSION	64

4. Sulfur, selenium, and tellurium abundances and distributions in chondrites

And their components

4.1. INTRODUCTION	67
4.2. ANALYTICAL METHODS	69
4.2.1. Isotope dilution ICP-MS analysis of S, Se and Te	69
4.2.2. Femtosecond laser ablation ICP-MS analysis	72
4.3. RESULTS.....	73
4.3.1. Reproducibility and accuracy	73
4.3.2. Sulfur, selenium and tellurium concentrations in bulk chondrites	81
4.3.3. Abundances and distribution of S, Se and Te in chondritic components	86
4.4. DISCUSSION	96
4.4.1. Primary (pre-accretionary) depletion during chondrule formation.....	96
4.4.2. Decoupling of Te during chondrule formation	99
4.4.3. Secondary depletion - Redistribution of Te on the parent body	100
4.4.4. Aqueous alteration	101
4.4.5. Sample heterogeneity.....	102
4.4.6. Comparison of chondritic ratios with the Earth.....	102
4.6 CONCLUSION	103

5. References	105
6. Danksagung	125
7. Erklärung	127
8. Lebenslauf	128

Abstract

The Sun comprises approximately 99.8 % of the matter of the solar system. Thus, the chemical composition of the Sun is considered representative for the composition of the solar system in cosmochemistry. Based on spectroscopic studies of the solar photosphere and chemical investigations on meteorites, the composition of the solar system is now relatively well known. There is one group of meteorites – the CI chondrites – that are of special interest as their composition is nearly indistinguishable from the composition of the solar photosphere for non-atmophile elements. Thus, the composition of CI chondrites is broadly used for reference purposes in cosmochemistry. Compared to CI chondrites all other inner solar system materials are depleted in volatile elements. The reasons for this pervasive primary depletion of volatile elements are still under debate.

Chondritic meteorites contain the most pristine solar system materials available for scientific investigations. They consist of different components such as chondrules (small melt droplets), refractory inclusions (e.g. Ca, Al-rich inclusions), metals, and sulfides embedded in fine-grained matrix material. Some of these components are thought to have formed under different spatio-temporal conditions (e.g. Chondrules and CAIs) before they assembled to form the chondrite parent bodies. After accretion, processes such as thermal metamorphism, aqueous alteration, and shock metamorphism during collisions may have further changed the chemical composition of chondritic material. Investigations on chondrites that largely escaped such secondary processes yield information about the pre-accretionary processes that were involved in the primary depletion of volatile elements in the early solar system. To better understand these processes the focus of this work was on the development and utilization of novel analytical methods to study the elemental abundances in chondritic components and in bulk chondrites. A special focus was on the chalcogen and moderately volatile elements sulfur, selenium and tellurium.

The first chapter of this dissertation contains a general introduction to the topic. **Chapter 2** comprises the analytical protocols of all methods that were applied within this thesis. These methods were utilized for the quantification of major-, minor-, and trace elements in two novel reference materials developed for laser ablation inductively coupled plasma mass spectrometry

(LA-ICP-MS) during this PhD. This chapter includes the reference concentrations determined for the reference materials and the data assessment. For the determination of major-, minor-, and trace element concentrations by sector field ICP-MS in “synthetic” and natural chondritic reference materials matrix-matched calibration solutions were developed and prepared. An isotope dilution ICP-MS method for the highly precise and accurate determination of Se and Te concentrations was refined and adjusted to chondrites, while a second isotope dilution ICP-MS method to determine S concentrations in bulk chondrites was set up completely new. Both methods are now routinely implemented and allow the determination of accurate and precise S, Se and Te concentrations from the same sample aliquot.

Chapter 3 comprises the analytical approach to determine the abundances and distributions of elements in chondritic components using femtosecond LA-ICP-MS. The focus was on the elaborative quantification of elements in chemically and physically heterogeneous and thus challenging chondritic matter. Because common procedures to correct for different ablation yields between sample and external calibration material failed, an alternative strategy was applied. However, this strategy in which the ablation yield is corrected by the total material requires a suitable external calibration material for major and minor element calibration in chondrites. According to this, matrix-matched calibration and reference materials (based on synthetic and natural nano-particles) were designed, prepared, quantified (Chapter 2) and applied (Chapter 4) during this PhD project. This chapter thus contains the application and applicability of the novel reference materials as well as the analytical setup and the strategy for data evaluation.

In **Chapter 4** highly precise and accurate isotope dilution ICP-MS concentration data for S, Se, and Te in 54 chondrites of different classes and groups of carbonaceous, ordinary, enstatite, and Rumuruti chondrites are presented. Furthermore, this chapter presents the first data obtained from the newly developed femtosecond LA-ICP-MS method described in Chapter 3. In-situ laser ablation ICP-MS data yield information about the distribution and the relative abundances of S, Se and Te in sulfides and metals in different chondritic components such as chondrules, matrix, and refractory inclusions. Initial results indicate that S, Se, and Te depletion and in particular the decoupling of Te from Se in ordinary chondrites might be related to chondrule formation. It is demonstrated that bulk analyses are instructively complemented by the in-situ LA-ICP-MS analysis.

Kurzzusammenfassung

Da die Sonne mit ~99.8 % den Hauptteil der Materie unseres gesamten Sonnensystems umfasst wird die chemische Zusammensetzung der Sonne in der Kosmochemie mit der chemische Zusammensetzung unseres Sonnensystems gleichgesetzt. Mit Hilfe spektroskopischer Untersuchungen der Photosphäre der Sonne und chemischer Untersuchungen an Meteoriten sind die Häufigkeiten der meisten Elemente des Sonnensystems mittlerweile relativ gut bekannt. CI Chondriten kommt dabei eine besondere Rolle zu, da die relative Häufigkeit für fast alle non-volatilen Elemente in CI Chondriten nahezu identisch ist mit denen der solaren Photosphäre. Aufgrund dessen wird die chemische Zusammensetzung dieser Meteorite in der Kosmochemie als Referenz benutzt. Im Vergleich zu CI Chondriten sind alle anderen Materialien des inneren Sonnensystems an kosmochemisch flüchtigen Elementen wie K, Zn oder S verarmt. Die Prozesse die zur primären Verarmung flüchtiger Elemente geführt haben sind noch nicht endgültig geklärt. CI und andere chondritische Meteorite sind das ursprünglichste Material des inneren Sonnensystems, welches für Laboruntersuchungen zur Verfügung steht. Sie bestehen aus unterschiedlichen Komponenten wie Chondren (kleine Schmelzkügelchen), und refraktären Einschlüssen (z. B. Ca, Al-reiche Einschlüsse), Metallen und Sulfiden, eingebettet in feinkörnigem Matrixmaterial. Einige dieser Komponenten sind zeitlich und/-oder räumlich unabhängig voneinander entstanden (z. B. Chondren und CAIs) bevor sie sich gemeinsam zu Mutterkörpern zusammengefügt haben. Nach der Akkretion können weitere Prozesse wie thermische Metamorphose und wässrige Alteration auf dem Mutterkörper oder auch Schockmetamorphose aufgrund von Kollisionen die chemische Zusammensetzung verändert haben. Betrachtet man jedoch die Chondrite und deren Komponenten die durch solche sekundären Prozesse weitgehend verschont geblieben sind, erhält man Informationen über die prä-akkretionären Prozesse die an der Verarmung flüchtiger Elemente im frühen inneren Sonnensystem beteiligt waren. Um diese Prozesse besser zu verstehen wurden in dieser Arbeit gezielt neue analytische Methoden zur Untersuchung der Elementhäufigkeiten in chondritischen Komponenten und in gesamtchondritischem Material entwickelt und angewendet. Ein besonderer Focus lag dabei auf den chalcogenen, moderat flüchtigen Elementen Schwefel, Selen und Tellur.

Nach der Einleitung in **Kapitel 1**, werden in **Kapitel 2** der vorliegenden Arbeit die Protokolle für alle analytischen Methoden die im Rahmen dieser Arbeit verwendet, und in diesem Kapitel in Verbindung mit der Quantifizierung von Haupt-, Neben-, und Spurenelementen zweier neu entwickelter Referenzmaterialien für die Laserablations ICP-MS (induktiv gekoppelte Plasma Massenspektrometrie) angewendet wurden. Somit enthält dieses Kapitel auch die für diese Referenzmaterialien ermittelten Referenzwerte und deren Bewertung. Für die Bestimmung der Haupt-, Neben-, und Spurenelemente mittels Sektorfeld-ICP-MS in „synthetischen“ und natürlichen chondritischen Referenzmaterialien wurden matrixangepasste Kalibrierlösungen entwickelt und hergestellt. Die Isotopenverdünnungs-ICP-MS Methoden für die präzise und akkurate Bestimmung der Gesamtkonzentration an Schwefel, Selen und Tellur in Chondriten wurden für Se und Te verfeinert und an chondritisches Material angepasst und für S neu aufgesetzt. Beide Messverfahren wurden als Routinemethoden etabliert.

In **Kapitel 3** wird die Herangehensweise zur Bestimmung der Konzentration und Verteilung von Elementen in chondritischen Komponenten per Femtosekunden-, Laserablations-ICP-Massenspektrometrie (LA-ICP-MS) dargelegt. Da die komplexe chemische und physikalische Beschaffenheit von chondritischem Material gewöhnliche Verfahren zur Korrektur unterschiedlicher Ablationsraten zwischen externem Kalibrierungsmaterial und Probe schwer möglich macht, wurde ein alternatives Korrekturverfahren angewendet bei dem die vorherige Bestimmung der Konzentration für ein internes Standardelement durch externe Verfahren (z. B. Elektronenstrahlmikrosonde) nicht erforderlich ist. Der Korrekturfaktor für die unterschiedlichen Ablationsraten wird hier über die Summe der Haupt- und Nebenelemente berechnet, welche hierfür per Laserablations ICP-MS mitgemessen werden. Zur externen Kalibrierung der Haupt- und Nebenelemente wurde eine matrixangepasste Pulverpresstablette aus Nanopartikeln hergestellt, welche diese Elemente etwa in CI-chondritischer Häufigkeit enthält. Eine weitere Presstablette wurde für die Qualitätskontrolle aus dem CM2 Chondriten Cold Bokkeveld hergestellt und auf die Anwendbarkeit als externes Kalibrierungsmaterial getestet. Die Anwendung und Anwendbarkeit der beiden neuen Referenzmaterialien, sowie der analytische Aufbau und die Auswertungsstrategie der Laserdaten sind in diesem Teil der Arbeit abgefasst.

In **Kapitel 4** werden die Ergebnisse von hochpräzisen S, Se, und Te Konzentrationsdaten für 54 Gesamtchondrite unterschiedlicher Klassen und Gruppen kohligler, gewöhnlicher, Enstatit-, und Rumurutichondrite aus Isotopenverdünnungs ICP-MS Messungen präsentiert. Des Weiteren

werden hier die ersten Ergebnisse, die mit der in Kapitel 3 beschriebenen Laserablations-ICP-MS Methode gewonnen wurden vorgestellt. Die in-situ Laserablations ICP-MS Analysen geben Aufschluss über die Verteilung, die Konzentrationen und die relativen Häufigkeiten von S, Se und Te in Sulfiden und Metallen, welche Bestandteil der unterschiedlichen chondritischen Komponenten wie Chondren, Matrix, und refraktäre Einschlüsse sind. Erste Ergebnisse verweisen darauf dass die Verarmung der moderat flüchtigen Elemente S, Se und Te und insbesondere die Entkopplung von Te in gewöhnlichen Chondriten, im Zuge der Chondrenentstehung stattgefunden haben kann. Es wird gezeigt dass die in-situ Analysen an chondritischen Komponenten Informationen hervorbringen die gesamtchondritische Konzentrationsmessungen ergänzen.

Chapter 1

INTRODUCTION

1.1 The origin of the elements

The first elements of the Universe (H ~75%, He ~25%, and traces of Li, Be, and B) formed during the “primordial nucleosynthesis” which occurred in the first minutes subsequent to the „Big Bang“, a massive explosion thought to have formed our universe 13.5 billion years ago. Elements heavier than hydrogen were primarily produced by stellar nucleosynthesis processes (*e.g.* Hoyle 1946, 1954; Merrill 1952). With onward cooling and expansion of the universe, the first galaxies including the Milky Way formed within a billion years after the Big Bang by gravitational attraction due to small density variations. Simultaneously, the first stars were formed from a gas of extremely low metallicity, composed almost entirely of H and He. It is assumed that some of these first generation stars (population III stars) must have been extremely massive with >100 solar masses (M_{\odot}) and formed isolated contemporary to galaxies (*e.g.* Bromm et al. 1999, 2004; Nakamura & Umemura 2001; Abel et al. 2000, 2002). Due to their extreme mass such stars rapidly exhausted their fuel (within a few million years) and would have exploded in extremely energetic supernovae in which they released most of their mass in the form of heavy elements, the metals. Although low-mass and intermediate-mass stars are far more abundant than high mass stars ($>10 M_{\odot}$), the high mass stars have been the primary contributors of heavy elements to the intergalactic and interstellar medium for a long time as their lifetimes are far shorter (a few million years) when compared to the lifetimes of low-mass and intermediate-mass stars, whose lifetimes tend towards billions of years (*e.g.* McSween & Huss 2010).

Different stages of stars lifetimes cause different processes whereby the extent and the rate of these processes strongly depend on the mass of the star. Hydrogen burning is the initial and longest fusion process in the lifetime of every star. During this stage H is converted into He, in the core of the star until H is exhausted and gravitational collapse occurs due to decreasing radiation pressure. However, the dominating and increasing gravitational compression is

accompanied by an increase in core temperatures which can reach those necessary for further nuclear fusion reactions such as helium burning, and in the more massive stars carbon burning, neon burning, oxygen burning, and silicon burning, each of which require higher temperatures for ignition and generate new and more heavy elements up to iron and nickel which have the highest binding energy per nucleon.

The synthesis of elements heavier than iron and nickel requires energy input and are produced by different neutron capture processes (Burbidge et al. 1957; Seeger et al. 1965). Burbidge et al. (1957) provided the first description of neutron capture processes in stars to generate heavier elements than iron. The general process is driven by the capture of a neutron by a nucleus, increasing the atomic mass by one unit. The resulting nucleus may become a stable isotope of the original element. If it is unstable the atom undergoes β -decay during which a neutron emits an electron, converting to a proton and becoming an isotope of a heavier element. Depending on the velocity of capture compared to the velocity of decay this process can be subdivided into the slow s-process and the rapid r-process. The s-process occurs during alternate hydrogen-shell and helium-shell burning at low neutron density in the AGB stage of low- and intermediate mass stars where neutron capture is slow when compared to the rate of β -decay. The r-process occurs during supernovae in which heavy seed nuclei are in the presence of neutron flux with extremely high densities. Under these conditions many neutrons can be captured, particularly by unstable nuclei prior to radioactive decay which yielding the potential to generate the heaviest elements up to Uranium. Another process that is able to generate different nuclides or isotopes is irradiation of matter by high-energy particles (*e.g.* protons and α -particles), in cosmic rays which can originate in the Sun and cause spallation reactions in which a nucleus is split into two or more smaller nuclides. By this, neutrons can be released and captured by other nuclides.

The quantity and composition of the gas in the interstellar medium of a galaxy is generally affected by infalling metal-poor gas, the removal of gas due to star formation and the returning gas enriched in heavy elements from dying stars. Stellar nucleosynthesis changed the initial composition of the gaseous and dusty interstellar medium extensively by enrichment of heavy elements so that the elemental and isotopic composition of next generation stars became increasingly complex (*e.g.* Ostriker & Gnedin 1996; Bromm et al. 2004; Yoshida et al. 2004).

1.2 Solar system abundance of the elements

Because the Sun contains ~99.8 % of the total mass of the solar system the composition of the Sun can be considered as equivalent to the composition of the solar system. The formation of the solar system occurred ~4.57 billion years ago from the gravitational collapse of a part of a molecular cloud, a dense region of the interstellar medium. The elemental abundance of our solar system is primarily inherited from its parent molecular cloud, a mixture of gas and dust composed of elements which originated from nucleosynthesis during the Big Bang, from several generations of massive and intermediate-mass stars that had contributed their material to the interstellar medium by supernovae and novae explosions until the Sun was formed. Knowing the composition of the material from which the solar system was formed helps to understand the evolution of the solar system as well as the chemical and physical processes that produced the different elemental and isotopic compositions of solar system materials. The solar system elemental abundances were mainly determined by spectroscopy of the stellar photosphere and chemical analyses of chondritic meteorites (especially CI chondrites). Indirect information about solar system abundances comes from investigations of comets, interplanetary dust particles, the nearby interstellar medium, hot B stars, and planetary nebulae (*e.g.* Lodders et al. 2009). Recent compilations for solar system elemental abundances are mainly based on spectroscopic data from the solar photosphere, chemical analyses of CI chondrites (mainly Orgueil) and indirect methods or theoretical considerations to estimate the abundances of elements which cannot be directly measured (*e.g.* He, Ne, Ar, Kr, Xe). The first comprehensive table of solar system elemental abundances based on compilation of chemical data from terrestrial rocks, meteorites, and individual phases of meteorites was published by Victor Moritz Goldschmidt in 1937. This table also included abundance data of highly volatile elements like C, O, and N, from spectroscopic measurements of the solar photosphere provided by H. N. Russell (1929). Together, these data covered most of the major features of the solar system abundances such as the dominance of H and He, the decrease of element abundance with increasing atomic number, the abundance peak at ^{56}Fe and the low abundance of Li, Be, and B. Additionally, they confirmed the higher abundance of elements with even atomic numbers when compared to elements with odd atomic numbers as discovered by Giuseppe Oddo (1914) and William D. Harkins (1917). The basis of modern tables on elemental abundances of the solar system was given by Suess & Urey in 1956.

Their table was based on meteorite data, spectroscopic solar abundances, and theoretical arguments based on a better understanding of nucleosynthesis and nuclear physics. Subsequent element and isotope abundance tables as given by *e.g.* Anders & Grevesse 1989; Palme & Beer 1993; Grevesse & Sauval 1998; Palme & Jones 2003; Lodders 2003; Lodders et al. 2009; Palme et al. 2014 are permanent updates and refinements of solar and solar system elemental abundances.

1.3 CI chondrites

Carbonaceous chondrites of the Ivuna-type, the CI chondrites represent the most primitive material available for laboratory investigations. Comparisons of the element abundances of CI chondrites and the solar photosphere showed that a large number of elements are present in the same relative abundance in both, the photosphere and in CI chondrites (Figure 1.1). Exceptions are highly volatile elements like H, He, O, C, N, and the noble gases which are depleted in CI chondrites relative to the solar photosphere, whereas Li is depleted in the photosphere due to nuclear burning in the Sun. Even if the elemental abundances of CI chondrites are the most unfractionated relative to the Sun their textures and mineralogy are rather complex. CI chondrites have a brecciated structure, consisting of millimeter to submillimeter sized clasts of different composition, which in turn consist almost entirely of extremely fine-grained hydrous silicates and magnetite. Chondrules and CAIs are absent and high-temperature phases like olivine and pyroxene are extremely rare (Hyman & Rowe 1983; Dodd 1981; Lodders & Fegley 2011). Furthermore, they are traversed by fractures filled with calcium and magnesium sulfates, as well as carbonates, demonstrating that these meteorites are extensively affected by aqueous alteration on the parent body (Morlok et al. 2006). Currently there are only five known CI chondrites: Orgueil, Ivuna, Alais, Tonk, and Revelstoke. Because Orgueil is the most massive of the five CI chondrite falls, most abundance data comes from this chondrite. Uncertainties in abundance data can be huge and reflect problems with the sample size, the mobility of some elements as reflected in the chemical heterogeneity within Orgueil, and sample preparation (*e.g.* Morlok et al. 2006; Lodders et al. 2009; Palme et al. 2014). As demonstrated by Barrat et al. (2012) Orgueil is chemically homogeneous on the one-gram scale, with the exception of water-soluble elements

which are somewhat more variable based on redistribution by fluids on the parent body. On the micrometer scale heterogeneities are much more pronounced (*e.g.* Morlok et al. 2006).

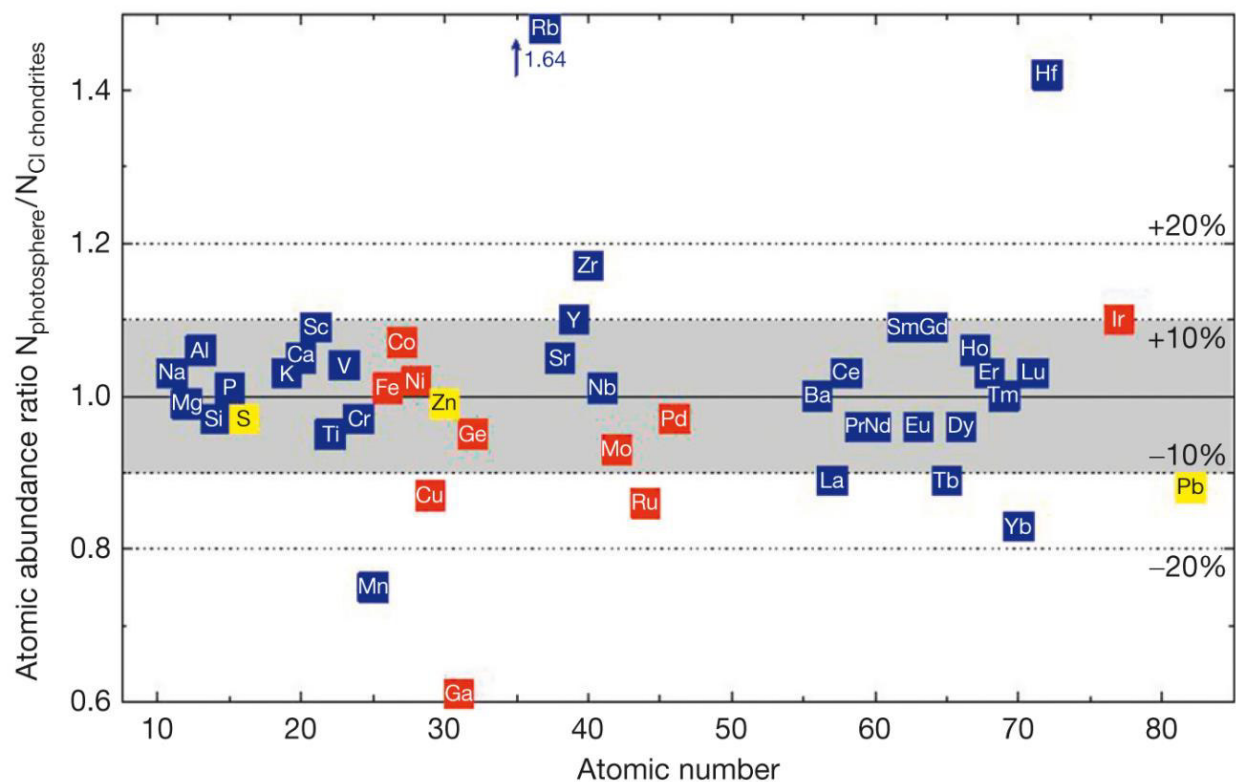


Figure 1.1 Comparison of photospheric and CI chondritic abundances (Palme et al. 2014). CI chondritic and photospheric abundances agree for 36 elements within $\pm 10\%$. Lithophile elements are blue, siderophiles red, and chalcophile elements yellow.

1.4 Cosmochemical classification of the elements

Almost all inner solar system materials experienced some thermal processing during the evolution of the solar system. Chondrules for example formed during high-temperature events in which precursors were molten, elements evaporated, and partly recondensed. For some other solar system materials like Ca, Al-rich inclusions (*e.g.* Scott & Krot 2001; Kurat et al., 2002; Lin et al., 2003), amoeboid olivine aggregates (*e.g.* Krot et al. 2004; Weisberg et al. 2005), metal grains in CB and CH chondrites (*e.g.* Meibom et al. 2001; Petaev et al. 2001, 2003; Campbell et al. 2001), PGE nuggets, relict hibonite and fassaite in CAIs (*e.g.* El Goresy et al. 1979, 1984; Lin & Kimura 2000), relict olivine in chondrules and matrix (*e.g.* Pack et al. 2004, 2005), it is assumed that they directly condensed from a gaseous phase. Furthermore, bulk chondrites display a smooth fractionation pattern which reflects element abundances in bulk chondrites being strongly controlled by the volatility of these elements. According to these observations, (re)condensation and evaporation played an important role and affected most inner solar system materials during solar system evolution. The cosmochemical classification of elements is therefore mainly based on the volatility of the elements. A good measure for volatility is the temperature at which an element condenses from the gas phase into solids, the condensation temperature (T_c). Since most elements condense over a certain temperature range it is also convenient to use the temperature at which 50% of an element condensed into a solid phase, the 50% condensation temperature (50% T_c). Both, T_c and 50% T_c are defined to study the transition of phases from a gas of solar composition to solid phases and vice versa and are fundamental to study fractionation processes.

Calculations of condensation temperatures are based on thermodynamic data and started in the 1950s with relatively simple calculations to model the condensation behavior of elements in different astrophysical settings. Today these calculations are much more complex, considering total ambient pressures, the starting composition of the gas and the changes in gas composition with ongoing condensation of phases and therefore removal of elements, as well as the diverse components that can potentially form from these elements. Important studies include Larimer 1967, Grossman 1972, Grossman & Larimer 1974, Boynton 1975, Wai & Wasson 1977, Fegley & Palme 1985, Kornacki & Fegley 1986, Ebel & Grossman 2000, and Lodders 2003. From these calculations the condensation sequence (Figure 1.2) of minerals evolved which is widely used to

describe the formation of minerals and components in the early solar system and provide an important and useful framework for the interpretation of the compositions of chondritic components like CAIs, chondrules and matrix, metals and sulfides, bulk meteorites and planets.

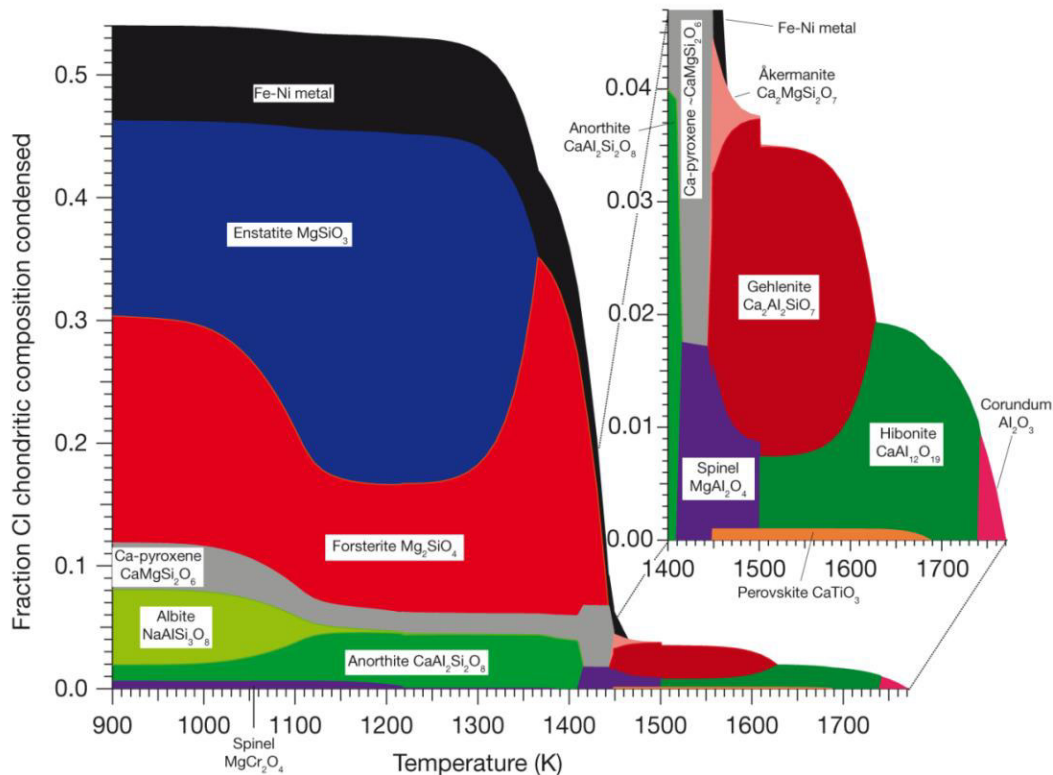


Figure 1.2 Condensation of major phases from a gas of solar composition at a total pressure of 10^{-3} atm (Davis & Richter 2003).

The 50% condensation temperatures form the basis of the cosmochemical classification in which the elements are subdivided into: (1) *Refractory elements* which condense at high temperatures between 1850 - 1355 K and would form the first condensates from a cooling gas of solar composition; (2) the *major components* which include the three most abundant elements heavier than oxygen: Si, Mg and Fe. They condense within a temperature range of 1355-1250 K as magnesium silicates and metallic iron, the most abundant phases in meteorites. (3) The *moderately volatile elements* that condense between 1250 and 252 K, and (4) the *highly volatile elements* with 50% $T_c < 252$ K.

Analog to the geochemical classification developed by Victor M. Goldschmidt (1937) in which the elements are grouped according to their preferred host phases, elements are subdivided into (1) *lithophile* (rock-loving) elements which tend to form silicates and oxides, (2) *siderophile* (iron-loving) elements which react with iron and are incorporated into metal alloys, (3) *chalcophile* (sulfur-loving) elements which prefer to coalesce with sulfur to form sulfides, and (4) *atmosphile* elements which tend to reside as gaseous species in the atmosphere (Table 1.1). Some elements tend to have more than one affinity, such as being both siderophile and chalcophile. Furthermore, the chemical affinity can be different under different p/T-conditions and oxygen fugacities and/or depend on the availability of host phases into which the elements (especially trace elements) can condense in solid-solution.

Table 1.1 Cosmochemical classification of the elements

Elements	Lithophile (silicates & oxides)	Siderophile & Chalcophile (metals & sulfides)
Refractory 1850 - 1355 K	Zr, Hf, Sc, Y, Gd, Tb, Dy, Ho, Er, Tm, Lu, Th, Al, U, Nd, Sm, Ti, Pr, La, Ta, Nb, Ca, Yb, Ce, Sr, Ba, Be, V, Eu	Re, Os, W, Ir, Mo, Ru, Pt, Rh
Main component 1355 - 1250 K	Mg, Si, Cr	Ni, Co, Fe, Pd
Moderately volatile 1250 - 252 K		
Above T _c of sulfur	Mn, Li, K, P, Na, Cl, B, Rb, Cs, F, Zn, Sn	P, As, Au, Cu, Ag, Sb, Ga, Ge, Bi, Pb, Te, Se, S
Below T _c of sulfur	Br, I, Tl	Cd, In, Tl, Hg
Highly volatile < 252 K	O, N, Xe, Kr, Ar, C, Ne	

1.5 Primary element fractionation

The formation of the solar system and the accompanied formation and evolution of inner solar system materials like chondritic components, planetesimals, and the planets involved various stages of thermal processing at which volatile elements were fractionated from the solar system elemental abundance. The fractionation patterns especially in carbonaceous chondrites are generally a smooth function of the half-mass condensation temperature ($50\%T_c$) and must have been originated in the very early stages of solar system evolution prior to the accretion of parent bodies. Furthermore, chondritic components like chondrules, matrix, refractory inclusions, and presolar grains, which experienced very different degrees of thermal processing were physically mixed and in some cases likely sorted by size and/or density in turbulent nebular environments (e.g. Huss et al. 2005). After accretion parent body processes like thermal metamorphism and aqueous alteration may have led to further fractionation or redistribution of elements in chondritic meteorites.

Evaporation and condensation – Primary depletion of volatile elements

Except for the highly volatile elements H, C, N, O, and the noble gases CI chondrites match the bulk elemental composition of the solar photosphere (e.g. Anders & Grevesse 1989; Lodders 2003; Lodders et al. 2009). Compared to CI chondrites all other inner solar system materials are depleted in volatile elements. The cause for this pervasive loss of volatile elements was extensively studied but is still under discussion. As demonstrated in Fig. 1.3 the extent of volatile element depletion differs from group to group, but share the common characteristic of being a function of the volatility of the elements independent of their geochemical character. Based on this, most of the proposed models are based on condensation and/or evaporation.

Anders (1964) and Larimer and Anders (1967) proposed that fractionation of volatile elements occurred by evaporation during chondrule formation and that the depletion of bulk chondrites reflect a mixture of volatile depleted chondrules and volatile enriched CI-like matrix. This model was questioned because simple mixing of two independent components would not create the smooth fractionation patterns as observed in bulk chondrites (Wasson & Chou (1974); Wai & Wasson 1977) and missing mass-dependent fractionations of stable isotopes do not

support evaporative processes (*e.g.* Humayun et al. 1995; Alexander et al. 2000). However, considering that: (1) volatile depleted chondrules and volatile enriched matrix are genetically related and formed in the same environment (Wood 1963, 1985; Klerner 2001; Bland et al. 2005; Hezel & Palme 2008, 2010; Ebel et al. 2009; Palme et al. 2015; Hezel & Palme 2008, 2010), (2) that these environments were most likely dust enriched and dense which would largely prevent mass-dependent isotope fractionation because isotopic re-equilibration between chondrule melts and the surrounding gas is possible (*e.g.* Alexander 2004; Alexander et al. 2008), and (3) that chondrules are not as volatile depleted as initially predicted, acting like open systems and allow re-introduction of volatile elements into chondrules during cooling (Matsunami et al. 1993; Scott 1994; Sears & Lipschutz 1994; Alexander & Grossman 2005; Grossman et al. 2007; Hezel et al. 2014), implies that evaporative processes related to chondrule formation could be responsible for volatile loss and the smooth fractionation pattern observed for bulk chondrites.

Wasson & Chou (1974) and Wai & Wasson (1977) explained these patterns by equilibrium condensation of elements from an initially hot gas of solar composition with continuous loss of nebular gas. This was based on the suggestion of Cameron (1962, 1963) and Cameron & Pine (1973) that the gravitational potential energy during the collapse of the solar system produced temperatures high enough to vaporize the inner solar nebula completely. Further support was given by the model of Cassen (1996, 2001) in which a high mass accretion rate ($>10^{-7} M_{\odot} \text{ yr}^{-1}$) is assumed so that evaporation occurred out to 3 AU and in which chondrites achieve their volatility related fractionation pattern in their final formation location. Partial condensation is supported by the CAI mineralogy which confirms the predicted condensation sequence of minerals but has problems explaining the presence of presolar materials (Huss et al., 2003; Huss, 2004) and isotopic differences in Ti, Cr, and Mo (Niemeyer & Lugmair, 1984; Niederer et al., 1985; Lugmair & Shukolyukov, 1998; Dauphas et al., 2002; Yin et al., 2002) which would have been destroyed in an initially hot solar nebula. Huss et al. (2003) and Huss (2004) demonstrated that there is a correlation between chondrite group specific assemblages of presolar grains with characteristic thermal and chemical resistance and the abundances of volatile elements. They pointed out that this implies a common and in some groups repeated thermal processing that removed volatile elements and the most fragile presolar components simultaneously from molecular cloud material (the precursor material for all solar system materials) and suggested partial evaporation prior to chondrule formation. Spectroscopic studies of the absorption lines of

the gas phase of the interstellar medium (ISM) show an increasing abundance of volatile elements with decreasing condensation temperature, while refractory elements are complementary depleted. Based on this observation, Yin (2005) proposed a model in which the depletion pattern observed in chondrites were inherited from the interstellar medium. In this model Yin suggests that refractory elements are enriched in dusty cores while the volatiles (except H and He) are enclosed in icy mantels around the dusty cores during the cold and dense molecular cloud stage. Adiabatic compression during the collapse stage of the parent molecular cloud or passages of shock waves in the early solar nebula stage could have then evaporated these icy mantels, putting the volatiles back into the gas phase. Yin suggests that the different chondrites formed at locations of the nebula where the ambient temperatures were slightly different, so that the most depleted chondrites formed at the highest temperatures.

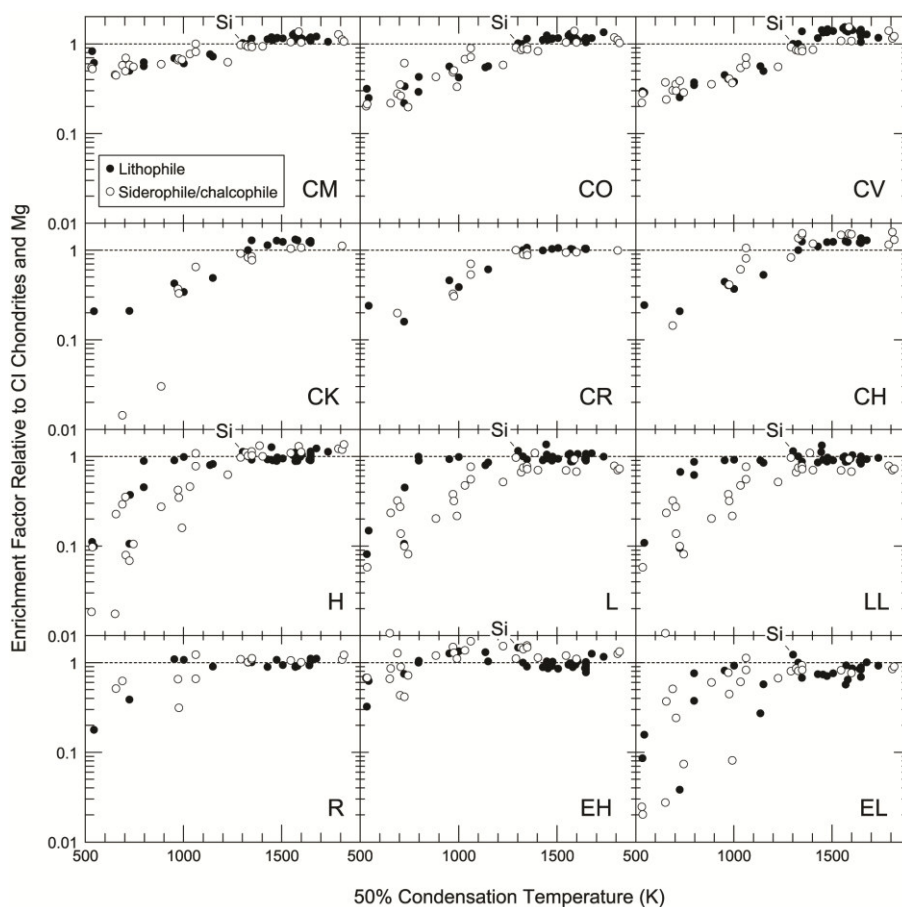


Figure 1.3 Mg and CI-normalized element abundances for elements with different geochemical affinity (lithophile, chalcophile, siderophile) plotted vs. 50% condensation temperatures. Element abundances in different chondrites decrease with increasing volatility of the elements, independent of the geochemical character. (Figure from Davis, A. M., 2006)

Physical fractionation

From smooth depletion patterns in bulk chondrites it is evident that volatility controlled fractionations due to thermal processing occurred. However, chondrites are a mixture of different components with very different compositions. Chondrules and CAIs for example are mostly depleted in moderately volatile elements while the fine-grained matrix is typically volatile rich. However, bulk compositions and element ratios of chondrites other than CI, also reflect mixing of different components with different elemental compositions (Figures 1.3 and 1.4). As an example, elements with 50% T_c at about 1400 K are enriched over CI ($\sim 1.25 \times \text{CI}$) in CM chondrites, reflecting the presence of chondrules and CAIs which are absent in CI chondrites. Furthermore, the presence of refractory inclusions (CAIs and AOAs) results in further enrichment in refractory lithophile and siderophile elements in chondrites relative to CI which implies that variable amounts of a refractory component was incorporated. The plateau formed by highly volatile elements with 50% T_c between 800 – 400 K in Figure 1.4 reflects the fine-grained matrix that obviously retained volatiles to a certain level ($\sim 0.7 \times \text{CI}$) in CM chondrites. This demonstrates that physical mixing of compositionally distinct components affect the bulk chemistry of different chondrites to various degrees. As shown in Figure 1.3, these effects are also present in other chondrites.

Another example for fractionation by physical processes is the metal-silicate fractionation visible on the micro scale in many chondrules, where immiscible metal melts separated from silicate melt in the form of droplets which could have been partly expelled physically from the chondrule's interior (e.g. Zanda et al. 2000; Bland et al. 2005). In ordinary chondrites the abundance of siderophile elements increases from LL to L to H, which is consistent with the metal abundance in these chondrites, which increase in the same order. It is assumed that sorting by mass or aerodynamic size sorting in the nebula (e.g. Kuebler et al. 1999) might have incorporated variable fractions of metal which resulted in the variations in concentrations of Fe and other siderophile elements in chondrites (e.g. Lodders et al. 2009). As mentioned by Lodders et al. (2009), the incorporation of various amounts of early-formed forsterite can produce the variations in Mg/Si, while variable incorporation of early condensed refractory phases (e.g. CAIs) is most likely responsible for variations in e.g. Al/Si and Ca/Si in chondrites different than CI.

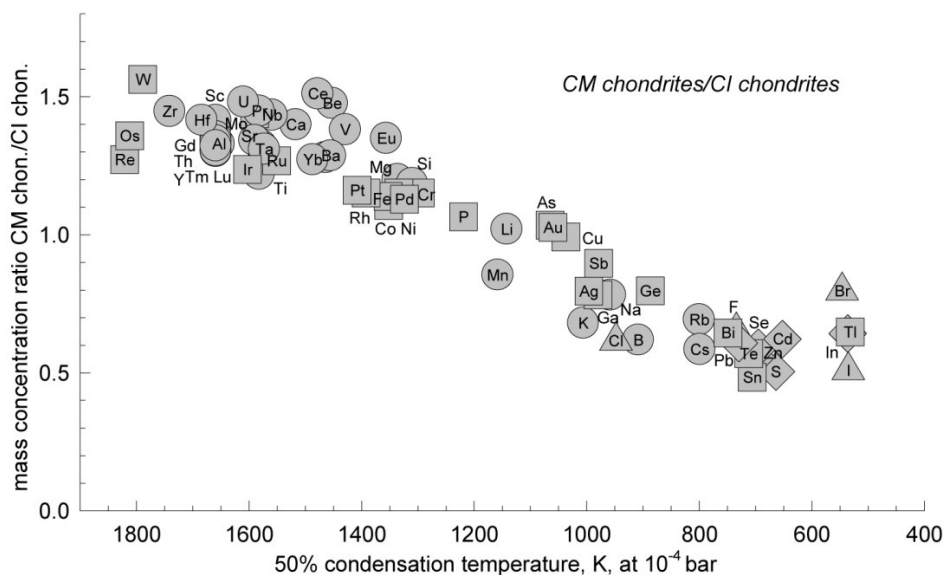


Figure 1.4 Element abundances of CM chondrites normalized to CI. Elements are plotted in order of increasing volatility from left to right. The geochemical character of the elements is indicated by different symbols: square = siderophile; circle = lithophile; diamond = chalcophile; triangle = halogen. (Diagram from Lodders et al. 2009)

1.6 Chondritic components

Chondrites consist of mixtures of sub-millimeter- to centimeter-sized components such as refractory inclusions, chondrules, metals and sulfides, silicates, oxides, and fine-grained matrix. Some of these components are thought to have formed independently under different conditions, most of them at different times, and possibly in different environments of the protoplanetary disk. In the following chapter major components as chondrules, matrix, and refractory inclusions are defined and briefly described.

Refractory inclusions

Refractory inclusions can be subdivided into Ca, Al-rich inclusions (CAI) and amoeboid olivine aggregates (AOA). They occur predominantly in carbonaceous and Rumuruti chondrites but also in ordinary and enstatite chondrites. CAIs are the oldest known materials formed in our solar system (*e.g.* Amelin et al. 2002, 2010; Connelly et al. 2011) and formed during the most

energetic phase of protosolar disk evolution (*e.g.* Ireland & Fegley 2000; Wood 2000, Ebel & Grossman 2000). They contain high concentrations of refractory elements like Ca, Al, and Ti in phases such as corundum, hibonite, grossite, perovskite, spinel, melilite, fassaite, rhoenite, and precious metals (*e.g.* Bischoff 1989; Scott 2007). Some fine-grained CAIs are thought to be direct condensates from a cooling gas of solar composition because of their irregular shapes, fluffy textures, and a mineralogy that is consistent with the condensation sequence (*e.g.* Simon et al. 2002; Lodders et al. 2009). However, the preservation of large isotopic anomalies (*e.g.* ^{48}Ca and ^{50}Ti), their lack of ^{26}Al , and the presence of mass-fractionation effects implies that other CAIs might be evaporative residues (Scott & Krot 2014).

Amoeboid olivine aggregates are irregularly shaped μm - to cm -sized fine-grained objects found within all carbonaceous chondrites except CI. They are mainly composed of olivine and minor Fe, Ni- metal, spinel, anorthite, and Al, Ti-pyroxene (Komatsu et al. 2001). In the least altered chondrites, AOAs are porous and their mineralogy matches that expected for high-temperature condensates (*e.g.* forsteritic olivine). In metamorphosed chondrites the olivine in AOAs is more Fe-rich, whereas the fayalite concentration correlates with the degree of metamorphism (Chizmadia et al. 2002). Some AOAs display recrystallized textures indicating high-temperature annealing with minor melting. About 10% contain low-Ca pyroxene replacing forsterite at grain boundaries in the outer edges of AOAs or rimming the AOA (Krot et al. 2004). It is assumed that amoeboid olivine aggregates formed in a similar environment as CAIs (Itoh et al. 2002) and represent the least refractory endmember of refractory inclusions (Brearley & Jones 1998).

Chondrules

Chondrules are μm - to mm -sized rounded droplets with magmatic textures and belong to the major components in chondritic meteorites. They formed within the first few million years after CAI formation in the solar system within minutes to hours from the melting of precursor materials in dust enriched environments (*e.g.* Kita & Ushikubo 2012). The processes that produced the heat (up to 2000 K) is still unknown but a wide range of possible mechanisms like (1) condensation of melts or melts and crystals from a hot solar gas (Ebel & Grossmann 2000; Krot et al. 2001), (2) formation close to the Sun with transport by proto-solar jets to the outer

regions of the protoplanetary disc (Shu et al. 1996, 2001), (3) collision of (partially) molten planetesimals (Zook 1981; Asphaug et al. (2011); Sanders and Scott 2012), (4) local heating by shock waves due to gravitational instabilities in the nebula (Desch et al. 2005; Connolly & Love 1998), and (5) heating by electromagnetic processes (Ciesla 2005) have been proposed. According to their FeO content chondrules are often divided into Type I and Type II chondrules. Type I chondrules are characterized by Mg-rich olivine and pyroxene, varying low-Ni metal contents, and Si, Al-rich mesostasis which can also contain some alkalis. Different, Type II chondrules have Fe-rich silicates, low metal contents, and higher contents of volatile elements (*e.g.* Huss et al. 2005).

Matrix

Matrix is generally defined as the optically dark, fine-grained material interstitial to chondrules, CAIs, metals, and sulfides (Scott et al. 1988). Characteristic for matrix is the small grain size (<5 μm) of its constituents which are a complex mixture of silicates (mostly olivine and pyroxene), oxides, sulfides, Fe, Ni-metal, and in Type 2 and 1 chondrites phyllosilicates, and carbonates (Weisberg et al. 2006). It is thought that matrix constituents are a mixture of presolar materials and nebular condensates, mixed with fine chondrule fragments (Scott & Krot 2014). Relative to other chondritic components, matrix is rich in volatile elements but is depleted relative to CI (*e.g.* Bland et al. 2005). The modal abundance of matrix varies from group to group with CI chondrites (>99 vol. %) consisting almost entirely of fine-grained hydrated matrix down to less than 1 vol. % in CB chondrites. The origin of matrix is still uncertain but there is growing evidence that matrix is closely related to chondrules and that both, matrix and chondrules were formed or at least processed by the same processes (*e.g.* Bland et al. 2005; Hezel & Palme 2008, 2010; Ebel et al. 2009; Palme et al. 2014).

Metal and Sulfide

Metals can be subdivided into refractory alloys and metallic iron (Fe, Ni-alloys). Refractory alloys consist of transition metals like W, Re, Os, Ir, Mo, Pt, Rh, and Ru and are predicted to condense prior to iron metal at temperatures >1600 K from a gas of solar composition (*e.g.*

Lodders 2003; Scott & Krot 2014). They occur in the form of small nuggets in refractory inclusions (*e.g.* Palme & Wlotzka 1976).

Primitive Fe, Ni-alloys have compositions that are consistent with condensation about 1400 K (Lodders 2003). However, such primitive Fe, Ni-metals are scarce since most of the metals have been modified by subsequent heating events including in many cases repeated sulfurization and desulfurization cycles, and oxidation of the metal (Scott & Krot 2014). The main metal phases in chondrites are kamacite and taenite which are mostly associated with troilite and in some cases with magnetite. They occur in the form of spherules or blebs within chondrules and as isolated irregularly shaped grains of different sizes outside chondrules or at the surface of chondrules, within fine-grained silicate rims on chondrules, or in the form of tiny grains within fine-grained matrix (Brearley & Jones 1998). Bevan & Axon (1980) and Nagahara (1982) described large rounded to subrounded clusters of metal and sulfide grains which are often referred to as “metallic chondrules” in ordinary chondrites. Finally, metals and troilite form porous or “sponge-like” continuous rims around chondrules and chondrule fragments (*e.g.* Bevan and Axon 1980; El Goresy et al. 1981). It is assumed that some of the metal outside chondrules may have formed originally within chondrules and was expelled during chondrule formation (*e.g.* Zanda et al. 2000; Huss et al. 2005).

1.7 Primary classification of chondrites

The classification of chondrites is largely based on primary parameters like petrological characteristics including texture, mineralogy, mineral compositions, whole-rock chemical compositions, and O-isotopic compositions. The currently used classification scheme divides meteorites into chondrites, primitive achondrites, and achondrites. Chondrites are defined as meteorites derived from asteroids that did not experience planetary differentiation, whereas the achondrites are igneous rock (melts, partial melts, melt residues) or breccias of igneous rock fragments from differentiated bodies. Achondrites have achondritic textures (igneous or recrystallized) but retain a primitive chemical affinity to their chondritic precursors (*e.g.* Weisberg et al. 2006). Primitive achondrites take an intermediate position between chondrites and achondrites showing characteristics of both. Figure 1.5 shows the systematics of chondrite

classification according to Weisberg et al. (2006), including the major meteorite divisions (classes, clans, and groups) and relationships between chondrite groups. Because this study focuses on chondritic meteorites, the following descriptions are restricted to the chondrites.

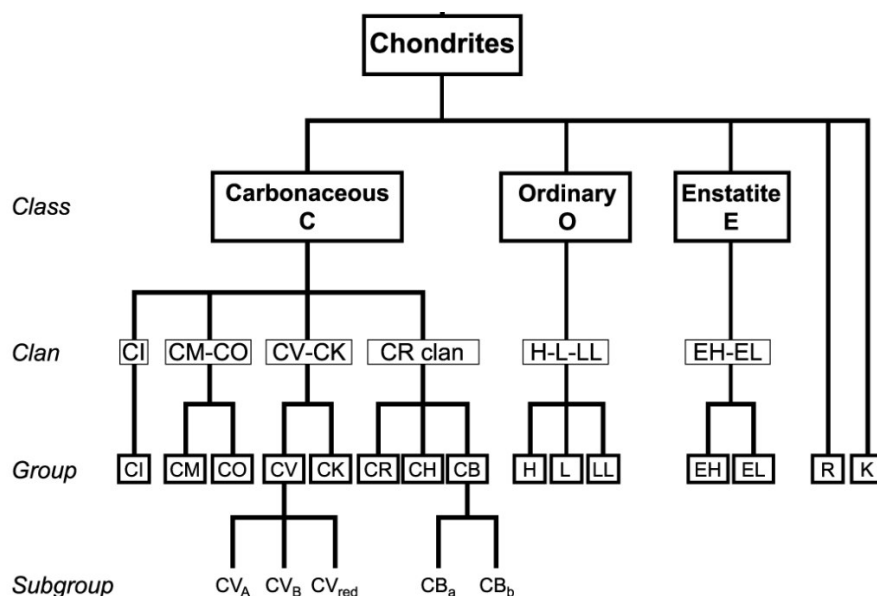


Figure 1.5 Systematics of chondrite classification (modified from Weisberg et al. 2006)

Chondrites are divided into the carbonaceous (C), ordinary (O), and enstatite (E) classes and into the Rumuruti (R) group and Kakangari grouplet. Each of the classes contains two or more groups sharing primary whole-rock, chemical, and O-isotopic properties. The class of carbonaceous chondrites can subdivide into four clans (CI, CM-CO, CV-CK, CR). Chondrites within a clan have chemical, mineralogical, and isotopic similarities suggesting a petrogenetic relationship, but have petrologic and/or bulk chemical characteristics excluding a group relationship. The groups of the O and E chondrite classes overlap in O-isotopic compositions and petrologic characteristics indicating a close relationship at the clan-level, therefore the O and E chondrite classes consist in each case only of one clan.

The term group is commonly interpreted to indicate that the meteorites originate from the same parent body. A group comprises a minimum of five unpaired chondrites with closely similar petrologic, whole-rock chemical and O-isotopic characteristics. For the case in which

there are less than five members, the term grouplet has been applied. Systematic petrologic differences in some chondrite groups led to the division into subgroups. Chemically and mineralogically unique chondrites are designated as ungrouped.

1.8 Secondary and tertiary classification parameters

Secondary processes like thermal metamorphism, aqueous alteration, and shock metamorphism have affected most chondritic meteorites to some extent, whereby the primary characteristics of the chondrites have been modified to various degrees. The following chapter briefly describes the classification schemes that have been evolved to identify the grade of modification by secondary and tertiary processes on the parent bodies and on Earth.

Petrologic types

The petrologic type defines the degree of aqueous alteration and thermal metamorphism affecting chondritic matter on the parent body. A classification scheme to identify these processes was developed from Van Schmus & Wood (1967) (see also Table 1.2). The assignment of petrologic types is based on petrologic observations, mineral compositions, and thermoluminescent properties of the meteorite. In the current usage of this scheme type 3.0 represent the most pristine materials. Types 3.1 to 6 indicate increasing degree of petrologic equilibration and recrystallization (increasing thermal metamorphism). In the so called “onion-shell model” it is assumed that asteroids were heated internally by the decay of the short-lived nuclide ^{26}Al , leading to a layered structure of the asteroid with decreasing thermal metamorphosis from the center (petrologic type 6) to the surface (petrologic type 3) (*e.g.* McSween et al. 2002). In contrast, the petrologic types 2 to 1 represent increasing degrees of aqueous alteration at low temperatures (<150°C) at which different anhydrous phases convert into secondary minerals like layered silicates and carbonates, sulfates and magnetite which precipitate into pore spaces and fractures. Sears et al. (1980) extended the Van Schmus & Wood classification by an additional division of the petrologic type 3 into the subtypes 3.0 – 3.9. Type 3.0 designates meteorites that

have experienced very little metamorphism whereas type 3.9 designates those that have nearly reached the degree of chemical equilibrium associated with type 4.

Table 1.2 Criteria for petrologic types (After Van Schmus & Wood (1967) with modifications from Sears & Dodd (1988))

Criterion	Petrologic type					
	1	2	3	4	5	6
Homogeneity of olivine and low-Ca pyroxene compositions		>5% mean deviations		<5%	Homogeneous	
Structural state of low-Ca pyroxene		Predominantly monoclinic		>20% monoclinic	<20% monoclinic	Orthorhombic
Feldspar		Minor primary grains only		Secondary, <2 μm grains	Secondary, 2–50 μm grains	Secondary, >50 μm grains
Chondrule glass		Altered, mostly absent ^a	Clear, isotropic, variable abundance		Devitrified, absent	
Maximum Ni in metal		<20 wt%; taenite minor or absent	>20 wt% kamacite and taenite in exsolution relationship			
Mean Ni in sulfides		>0.5 wt%	<0.5 wt%	<0.5 wt%	<0.5 wt%	<0.5 wt%
Matrix	All fine-grained, opaque	Mostly fine, opaque	Clastic, minor opaque	Transparent, recrystallized coarsening from 4 to 6		
Chondrule–matrix integration	No chondrules	Chondrules very sharply defined		Chondrules well defined	Chondrules readily delineated	Chondrules poorly defined
Carbon (wt%)	3–5	0.8–2.6	<1.5	<1.5	<1.5	<1.5
Water (wt%)	18–22	2–16	0.3–3			

^aChondrule glass is rare in CM2 chondrites, but preserved in many CR2 chondrites.

Shock stage classification

The degree of shock metamorphism due to impacts is discernable in various mineralogical and textural characteristics (see Table 1.3) Six different shock stages (1 to 6) have been defined by Stöffler et al. (1991) for ordinary chondrites. This classification is based on the shock effects observable by optical microscopy in olivine and plagioclase. Rubin et al. (1997) extended the shock classification scheme to orthopyroxene because of the lack of olivine in enstatite chondrites using the same shock stages (1 to 6). The same scheme can also be applied to carbonaceous chondrites. General information about shock effects for the classification is outlined in Table 1.3.

Table 1.3 Criteria for shock stage classification (After Stöffler et al. 1991 & Rubin et al. 1997)

Shock stage	Description	Effects resulting from equilibration peak shock pressure			Shock pressure [Gpa]*
		OLIVINE	PLAGIOCLASE	ORTHOPIROXENE	
S1	unshocked	sharp optical extinction, irregular fractures			< 4 - 5
S2	very weakly shocked	undulatory extinction, irregular fractures	undulatory extinction, irregular fractures	undulatory extinction, irregular fractures, some planar fractures	5 - 10
S3	weakly shocked	planar fractures, undulatory extinction, irregular fractures	undulatory extinction	clinoenstatite lamellae on (100), undulatory extinction, planar fractures, irregular fractures	15 - 20
S4	moderately shocked	weak mosaicism, planar fractures	undulatory extinction, partially isotropic, planar deformation features	weak mosaicism, twinning on (100), planar fractures	30 - 35
S5	strongly shocked	strong mosaicism, planar fractures, planar deformation features	maskelynite	strong mosaicism, planar fractures	45 - 55
S6	very strongly shocked	solid state recrystallization and steining, ringwoodite, melting	shock melted (normal glass)	majorite, melting	75 - 90
	shock melted	whole rock melting (impact melt rock and melt breccias)			> 90

*Shock pressure for ordinary chondrites only.

Degree of terrestrial weathering

An additional classification parameter is used to describe the degree of terrestrial weathering, experienced by a meteorite. There are two classification schemes which are currently used. One scheme describes the weathering degrees for hand specimens of Antarctic meteorites with: A = minor rustiness; B = moderate rustiness; C = severe rustiness; and E = evaporative minerals visible to the naked eye. Wlotzka (1993) evolved a weathering scale based on observations in the

optical incident light microscopy on polished sections, with progressive alteration stages: W0 = no visible oxidation of metal or sulfide, some limonite staining; W1 = minor oxide rims around metal and troilite, minor oxide veins; W2 = moderate oxidation of about 20-60% of metal; W3 = heavy oxidation of metal and troilite. 60-95% being replaced; W4 = complete oxidation of metal and troilite, but no oxidation of silicates; W5 = beginning alteration of mafic silicates, mainly along cracks; W6 = massive replacement of silicates by clay minerals and oxides.

Chapter 2

Quantification of novel calibration and reference materials for LA-ICP-MS analysis

2.1 INTRODUCTION

Chondritic meteorites (chondrites) provide the most primitive solar system materials that are readily available for scientific investigation in the laboratory. They are variable mixtures of up to \leq mm sized silicate dominated components such as chondrules and refractory inclusions, fine-grained matrix, with more or less abundant metal and sulfide.

Microanalysis using laser ablation - inductively coupled plasma - mass spectrometry (LA-ICP-MS) provides a quantitative technique, able to resolve the spatial distribution of elemental abundances at the tenth of μm scale and sub-ppm level (*e.g.* Gao et al. 2002, Jochum et al. 2007, Liu et al. 2008). This spatial resolution and abundance level allows addressing fundamental questions in cosmochemistry aiming at the environmental conditions and processes relevant for the early evolution of the inner solar system. For example (i) the chemical affinity of trace elements (*cf.* Goldschmidt 1937) in different chondrite classes and groups can be evaluated, (ii) the distribution and host components of parent and daughter elements used for chronology can be inferred (Humayun et al. 2007, Krot et al. 2009), and (iii) the fate of volatile elements can be studied (Bland et al. 2005, Grossman et al. 2007).

The accuracy of LA-ICP-MS data depends heavily on the external calibration material that should ideally be of similar chemical composition and physical properties as the samples under investigation (*e.g.* Guillong et al. 2005; Kroslakova & Günther 2007, Koch & Günther 2011). Thus, the most suitable calibration material should be similar to bulk chondrite material. To this end, two very fine-grained powders suitable for the preparation of binder free pressed powder tablets have been prepared. First, a custom-tailored chondrite analog nanoparticle standard (CANS) was prepared for external major, minor and Se and Te calibration in chondrites. A second powder tablet has been prepared from the CM2 chondrite Cold Bokkeveld (COBO),

mainly used as a test sample for quality control. The element and water contents of the new calibration materials have been determined by means of solution nebulization sector-field and quadrupole ICP-MS, ICP-optical emission spectrometry (ICP-OES), electron microprobe, X-ray fluorescence (XRF) instrumental neutron activation analysis (INAA) and Karl Fischer titration. In addition, S, Se and Te abundances were determined by isotope-dilution single or multiple collector-ICP-MS. Quantification procedures and reference compositions of the two powder calibration and reference materials are presented in this section, while the applicability and homogeneity of powder pellets prepared from the new calibration materials will be assessed in Chapter 3 of this thesis.

2.2 SAMPLE AND CALIBRATION MATERIALS

The accurate spatial matching of internal standard values from an external method (e.g. electron microprobe) with laser spots is generally not feasible for heterogeneous chondritic materials. In particular electron microprobe analysis only captures the sample surface, while laser ablation liberates particles from depths of several tens of micrometres.

As an alternative to internal standardisation to a single element, standardisation to the sum of all major element components can be applied (Hoffmann et al. 1997; Leach and Hieftje 2000; Halicz and Günther 2004; Liu et al. 2008). This requires that all major element abundances are precisely and accurately determined in the sample and in the standard. Therefore the external calibration material needs to contain all major elements at suitable concentrations, ideally in chondritic abundances. Compared to CI chondrites, NIST SRM 610 and 611 glasses are 100, 200 and 400 times lower in S, Mg and Fe and are therefore poorly suited for 100% sum standardisation. This difference is even more extreme for the more depleted NIST glasses. Likewise, USGS and MPI-DING glasses differ from chondrite compositions in particular in their low sulfur abundance (Jochum et al., 2000; Jochum et al., 2005; Jochum et al. 2006).

Nanoparticle based calibration materials produced by flame spray synthesis (Athanasios et al. 2010) can be custom-tailored (Tabersky et al. 2014) to obtain matrix-matched compositions and allow for enhanced 100% sum standardisation. The relative abundances of non-atmophile

elements in CI chondrites match those of the solar photosphere. Therefore CI chondrites are representative for the relative solar system abundances of non-atmophile elements (e.g. Lodders 2003; Palme and Jones 2003; Lodders et al. 2009; Palme et al. 2014) and their composition provides the most commonly used reference for normalization. For this reason, the most useful composition for a custom-tailored chondrite calibration material is that of CI chondrites. To evaluate the suitability of such a custom tailored calibration material, a nanoparticle powder of chondritic composition (CANS) was obtained from Nano SRM Ltd in Staefa/Switzerland. CANS comes as a brownish powder with particle sizes expected to be in the range of 20 to 50 nm (Athanassiou et al. 2010), that comprises all major and minor elements except K and V, and the trace elements Se and Te in the form of oxides (Na_2O , MgO , Al_2O_3 , SiO_2 , P_2O_5 , CaO , TiO_2 , Cr_2O_3 , MnO_2 , Fe_2O_3 , SO_3 , CoO , NiO , CuO , ZnO , TeO_2 and SeO_2) in approximately CI chondritic abundances, except for S, some of which was lost in the production process. For laser ablation analysis, the nanoparticles were compacted without the use of binders into tablets of 7 mm diameter and ~2 mm thickness using a mechanical press.

In addition to CANS, a very fine grained powder was prepared from the CM2 chondrite Cold Bokkeveld by wet-milling (Garbe-Schönberg & Müller 2014). According to Garbe-Schönberg & Müller (2014), the typical grain size is expected to be somewhat larger than 1 μm . The Cold Bokkeveld (COBO) chondrite powder was also compacted into a tablet and used for quality control purposes.

2.3 EXPERIMENTAL - QUANTIFICATION OF CANS AND COBO

2.3.1 Solution nebulization SF-ICP-MS and ICP-OES

The elemental compositions of CANS and COBO powder were determined using a ThermoScientific ElementXR™ sector-field ICP-MS at the University of Bonn/Germany, equipped with an Elemental Scientific SC-2 DX autosampler, a microconcentric PFA nebulizer with about 140 $\mu\text{l min}^{-1}$ uptake rate, a Scott type PFA spray chamber and a sapphire injector. Table 2.1 lists details of the instrumental settings, performance and acquisition parameters.

CANS was also analysed at the University of Cologne/Germany using a AMETEC Spectro Arcos ICP-OES equipped with an Elemental Scientific SC4-DX autosampler, a standard glass spray chamber and a cross-flow nebulizer with a pumped flow rate of about 1 mL min^{-1} . In order to obtain reliable calibrations and equivalent matrix effects for samples and standards, two different sets of calibration solutions with major element compositions and acid molarities closely matched to the CANS and COBO measurement solutions were prepared. The later quantification of COBO included two further digestions of the CANS powder in order to cross check the results. Quantification was based on mass fractions using a micro balance for the dilution of samples, the addition of internal standards and the preparation of calibration solutions. Results are given in Tables 2.2 and 2.3.

Quantification of CANS (SF-ICP-MS session #1)

With the exception of K and V, all major and minor elements and Se and Te were analysed. Six aliquots of about 25 mg CANS powder were weighted into 7 ml PFA beakers. To half of the samples and one blank, 0.714 ml 14 M HNO_3 and 0.205 ml 24 M HF were added, beakers were capped and placed onto a hotplate for 48 h at 120°C . In an attempt to quantify Si, these solutions were not dried down to prevent the loss of SiF_4 . After digestion, 2.5 g of an internal standard solution containing about $2 \mu\text{g/g}$ Be, $1 \mu\text{g/g}$ Sc and V, and $0.2 \mu\text{g/g}$ Y in 0.28 M HNO_3 , additional HNO_3 , ultrapure water (18.2Ω) and HF for Si bearing solutions were added to obtain a final weight of $\sim 50 \text{ g}$ (i.e. 2000-fold sample dilution). The internal standard solution was added by a pipette, but precisely weighted for later offline correction of intensities for slightly inaccurate internal standard additions. Three other aliquots of CANS and one blank were digested using 2.5 ml 14 M HNO_3 and 0.5 ml 24 M HF. Capped beakers were placed onto a hotplate at 150°C for 48 h. Subsequently, samples were dried down at low temperature (70°C) to avoid the loss of volatile Se species. Samples were then dissolved in 2 ml 6 M HCl, capped and placed onto a hotplate for another 24 h at 120°C and again evaporated at 70°C . Dry samples were then redissolved in 0.95 ml 14 M HNO_3 and 2.5 g of the internal standard solution were added as described above and the sample weight was adjusted to $\sim 50 \text{ g}$. The 2000-fold dilutions were analysed by ICP-OES and quantified as detailed below for the SF-ICP-MS procedure. For SF-ICP-MS analysis, the samples were again diluted 5-fold with 0.28 M HNO_3 (10,000-fold sample

dilution in 0.28M HNO₃ (+ trace HF (0.0112 M) for Si bearing samples). Three point calibration was applied with calibration solutions prepared from highly pure single element solutions (Alfa Aesar, Merck) in such a way that the composition of CANS (as determined during an earlier SF-ICP-MS measurement) is closely matched by one calibration solution while the other two calibration solutions contain the same elemental mix at 20 % higher and lower concentration. Thus, the calibration solutions (with and without Si and HF) were prepared to match the matrix of the two sets of digestions. Calibration solutions were mixed and diluted right before analysis from a multi-element solution in 0.28 M HNO₃ that contains Fe, Mg, Ni, Ca, Al, Mn, Se, Te, Na Co, Cu and Cr, a solution containing P and S in H₂O and two single element solutions of Si and Ti in 0.28 M HNO₃ – 0.112 M HF, the internal standard solution and the acids required to match the final acid concentration. In the course of the analysis, the three calibration solutions were analysed right before and right after the analysis of the three CANS aliquots and the concentrations were calculated based on both calibration sets. This “double calibration“ was carried out twice with Si bearing samples and calibration solutions and twice with Si-free solutions. Thus, for most elements the abundance was calculated 24 times. The Si and Se data are based on results from the HF bearing sample set only. While this is obvious for Si, the HF free calibration resulted in less reproducible and higher values for Se for unknown reasons. Due to a mistake in the production of the multi-element calibration solutions, the Zn data is based on a one point calibrations ran with the HF free analysis only. The mean values and standard deviations reported in Table 2.2 are based on the 24 (or 12 for Si, Zn and Se) values determined (i.e. 12 or 6 analysis with “double calibration”).

To correct for the instrumental background, a 0.28 M HNO₃ (\pm trace HF) solution blended with the internal standard elements was measured prior to every calibration and sample solution. Before the background measurement, the sample introduction system was first rinsed for 2 minutes with 0.56 M HNO₃ followed by a 4 minute rinse with the background solution. After determination of the instrumental background, the sample or calibration solutions were taken up for 1.2 minutes and the measurement started. The background values were always subtracted. The background contributed less than 1% for all element signals in sample and calibration solutions, except for S, Na and Te (2 – 5 %), and 45 to 57 % for ⁷⁷Se (probably mainly due to ³⁶Ar⁴⁰ArH⁺). Signal intensities for every measured element were always far above the quantification limit, as calculated based on the average signal intensities of the background

measurements plus six times the standard deviation. While Y served as the internal standard for the low resolution measurements of Se and Te, Sc was used for elements measured in medium resolution mode. If V rather than Sc were used for internal normalization, results were by 0 to 0.8% lower.

Quantification of COBO and additional analysis of CANS (SF-ICP-MS session #2a and b)

After the quantification of major elements in CANS, Garbe-Schönberg & Müller (2014) demonstrated that nanoparticulate powder tablets can be prepared from natural samples. This opened up the possibility to prepare a powder tablet from a chondrite sample for the purpose of quality control and as an alternative laser ablation calibration material. To obtain data for comparison, a procedure for major and trace element analysis of chondrites by SF-ICP-MS was developed that is detailed in the following. About 50 mg of fine-grained Cold Bokkeveld (COBO) CM2 chondrite powder and 25 mg CANS powder were weighted into 7 ml PFA beakers in duplicate. In order to oxidize organic compounds 1 ml concentrated HNO₃ was added to the samples and blanks that were then dried down to incipient dryness at 70°C, followed by the addition of two ml of 14 M HNO₃ and 24 M HF each. To one aliquot of COBO and CANS and to one blank, one ml of ~10 M HClO₄ was added. Capped beakers were placed onto a hotplate for 48 h at 150°C. The HClO₄ free samples were dried down at 70°C, refluxed in 2 ml 6 M HCl at 120°C for 24 h and again dried down at 70°C. For samples containing HClO₄, open beakers were placed onto a hotplate at 120°C for 12 h prior to final evaporation at 180°C. Subsequently, samples were taken up in 0.5 ml (CANS) and 1 ml (COBO) 14 M HNO₃ and refluxed for another 4 h at 120°C. About 0.5 g (COBO) and 0.25 g (CANS) of internal standard solution containing about 60 µg/g Sc and Y and 6 µg/g Ho were added by a pipette. The same internal standard solution was proportionally added to blanks, calibration and background solutions and always precisely weighted for later offline correction of intensities for slightly variable internal standard additions. COBO naturally contains the internal standard elements Sc, Y and Ho. The contribution from these elements in COBO to the total signal of the internal standard elements, as estimated based on typical CM2 chondrite abundances (Lodders & Fegley, 1998), amounts to no more than 0.7% for Sc, < 0.2% for Y and < 0.1% for Ho which is considered to be insignificant for the current purpose. Sample solutions were then diluted with 0.012 M HF to a final solution

weight of 50 g (COBO) and 25 g (CANS) to obtain a 2000-fold dilution which was used for some major and all trace element analyses (Table 2.1). Additional major and minor element analyses including Na, Mg, and Fe were carried out on 20,000-fold dilutions in the same acid mix. Four point calibration was applied, whereby a new set of calibration solutions (independent from the calibration in session #1) that cover the compositions of CI and CM chondrites were prepared from highly pure single element solutions (Alfa Aesar, Merck, NIST). To this end, the calibration solutions were freshly prepared at the day of the analysis in 0.28 M HNO₃ - 0.012 M HF, from six cosmochemically meaningful multi-element solutions with roughly CI chondritic relative abundances: the ultra-refractory elements Al, Ca, Ti, Zr, Nb, Mo, Hf, Ta and W, the refractory trace elements Be, V, Sr, Ba, REE (except Sc, Y and Ho), Th and U, the highly siderophile elements Ru, Rh, Pd, Re, Ir, Pt, the main compound elements Mg, P, Cr, Fe, Co and Ni, the alkali/volatile elements Li, Na, K, Mn, Cu, As, Rb, Cs and the more or less chalcophile volatile elements S, Zn, In, Cd, Te, Tl, Bi and Pb. Furthermore, some elements that are notoriously unstable in solution (Ge, Ga, Sn, Ag and Sb) were added to the calibration solutions from single element solutions at the day of measurement right before the final dilution. Apart from Be, all the above elements were analysed. However results obtained from ⁷Li, ⁷⁰Ge (in high resolution), ¹⁰¹Ru, ¹²¹Sb, ¹³³Cs, ²⁰⁵Tl, ²⁰⁹Bi were irreproducible or completely off the expected values and are therefore discarded. To recognize detrimental effects of isobaric interferences, two isotopes were monitored for many elements. Isotopes that have been used for data evaluation are given in Table 2.1, but results from the alternative isotopes ²⁵Mg, ³⁴S, ^{42,44}Ca, ⁴⁹Ti, ⁵³Cr, ⁶²Ni, ⁶⁵Cu, ⁶⁸Zn, ⁷¹Ga, ⁸⁸Sr, ⁹⁰Zr, ¹¹⁹Sn, ¹³⁵Ba, ¹⁴³Nd, ¹⁵³Eu, ¹⁸⁷Re, ¹⁹¹Ir were consistent within a few %. However, inconsistent results were obtained from ¹⁰⁷Ag and ¹²⁸Te.

No data was rejected for CANS. However, results for S, K, Ti and Fe obtained for the COBO sample treated with HClO₄ during the major element session #2a were 10 to 50% lower than that obtained from the digestion without HClO₄. Furthermore, Al in the COBO sample without HClO₄ was by a factor of 4 lower than for COBO with HClO₄ in session #2a and in all analysis during the trace element session #2b. This data was rejected. For ¹²⁵Te, the data obtained for COBO with the use of HClO₄ was by a factor of 2.5 higher. The higher value was rejected as it is in gross disagreement with the isotope dilution measurement.

During both measurements sessions (#2a and b; Table 2.1), six sample solution analysis (two aliquots as digested with and without HClO_4 of COBO, CANS and one more chondrite sample that is not of interest here) were bracketed by the calibration solutions and the sample solution analysis repeated three times. Abundances were calculated based on the prior and succeeding calibration sets. Thus, for most elements in each sample solution the abundances were calculated six times from three actual sample measurements and more often for elements that were included in measurement sessions #2a and b or analysed at different mass resolutions. To correct for the instrumental background, a 0.28 M HNO_3 – 0.012 M HF background solution blended with the internal standard was measured prior to every calibration and sample solution. Before the background measurement, the sample introduction system was rinsed for 2 minutes with 0.56 M HNO_3 followed by the background solution for another 4 minutes. After determination of the instrumental background, the sample or calibration solutions were taken up for one minute and the measurement started. The background values were always subtracted. For the elements and isotopes reported, the background contribution to the sample or calibration solutions was: Less than 1 % during major element session #2a, except up to 2% for P and 5 to 7% for Na, S and K. During the trace element session #2b, background contributions were typically much less than 3%, but 5 to 6% for Sr, Zr, Tb and Er, 8 to 9% for Pd and Sn, 14% for Hf and 20 to 30% for Rb, Ag, W and Th. The largest background contribution was commonly observed in the most diluted calibration solution. For the few trace elements above detection limit reported in the Table 2.2 caption for CANS, background signals contributed the most to Mo and Gd with 6 and 9%, respectively.

Blank contributions were negligible for major elements. Trace element blanks in COBO contributed usually much less than 3 %, but 4 to 7% for As, Rb, Sr, Zr, Mo, Pd and U, 11% for Hf and Re, 17, 22, 24 and 28% for Th, Ag, Sn and W, respectively. However, the reproducibility of blank contributions is difficult to assess at this stage and comparison with literature data shows that apart from Ag, Sn and W most the above elements tend to fall below literature values. Therefore, blank subtraction was only carried out for the four elements where blanks were largest: Th, Ag, Sn and W.

Table 2.1 Solution nebulization SF-ICP-MS (ElementXR): parameter for CANS and COBO analysis**Instrument settings and performance**

RF power	1200 W
Cool gas	16 L min ⁻¹
Auxillary gas	0.8 to 0.85 L min ⁻¹
Sample gas	1.2 L min ⁻¹
BaO/Ba	3.5 to 4.0 %
Ba ⁺⁺ /Ba	0.12 to 0.2 %
sensitivity	~1 * 10 ⁶ cps for ¹³⁸ Ba per ng/g Ba
Resolution	Low (LR~400), medium (MR~4700), high (HR~10000)
Scanning mode	Triple
E-scan range	30%
Samples per peak	LR = 100, MR = 20 (CANS-1) or 40, HR = 25
Sample time [ms]	LR = 1 – 5, MR = 1 – 5, HR = 2 - 20
Mass window [%]	LR = 10, MR = 80 – 120, HR = 120 -125
Search window [%]	LR = 10, MR = 80, HR = 80
Integration window [%]	LR = 10, MR = 40, HR = 40 - 60

#1 CANS: data acquisition major and minor elements 1:10,000 dilution, 0.28M HNO₃ (- 0.0112 M HF if Si)**LR:** background: 15 scans; samples and standards: 45 scans; each scan 50 ms on peak / scan⁷⁷Se, ⁸⁹Y, ¹²⁵Te**MR:** background: 15 scans; samples and standards: 90 scans; each scan 16 - 40 ms on peak / scan²³Na, ²⁶Mg, ²⁷Al, ³⁰Si, ³¹P, ³²S, ⁴³Ca, ⁴⁵Sc, ⁴⁷Ti, ⁵²Cr, ⁵⁵Mn, ⁵⁷Fe, ⁵⁹Co, ⁶⁰Ni, ⁶³Cu, ⁶⁶Zn**#2a COBO; CANS: data acquisition major and minor elements 1:20,000 dilution, 0.28M HNO₃ - 0.012 M HF****MR:** background: 10 scans; samples and standards: 30 scans; each scan 16 to 40 ms on peak / scan²³Na, ²⁶Mg, ³¹P, ³²S, ⁴³Ca, ⁴⁵Sc, ⁴⁷Ti, ⁵¹V, ⁵²Cr, ⁵⁵Mn, ⁵⁷Fe, ⁵⁹Co, ⁶⁰Ni, ⁶³Cu, ⁶⁶Zn**HR:** background: 10 scans; samples and standards: 30 scans; each scan 200 ms on peak³⁹K, ⁴⁵Sc**#2b COBO; CANS: data acquisition minor and trace elements 1:2,000 dilution, 0.28M HNO₃ - 0.012 M HF****LR:** background: 20 scans; samples and standards: 60 scans; each scan 20 ms on peak (Sc to Mo: 10 ms)⁸⁵Rb, ⁸⁶Sr, ⁸⁹Y, ⁹¹Zr, ⁹³Nb, ⁹⁵Mo, ¹⁰¹Ru, ¹⁰³Rh, ¹⁰⁸Pd^{\$}, ¹⁰⁹Ag, ¹¹¹Cd, ¹¹⁵In^{\$}, ¹¹⁸Sn, ¹²⁵Te * ¹³⁷Ba,
¹³⁹La, ¹⁴⁰Ce, ¹⁴¹Pr, ¹⁴⁶Nd, ¹⁴⁷Sm, ¹⁵¹Eu, ¹⁵⁷Gd, ¹⁵⁹Tb, ¹⁶³Dy, ¹⁶⁵Ho, ¹⁶⁶Er, ¹⁶⁹Tm, ¹⁷²Yb, ¹⁷⁵Lu, ¹⁷⁸Hf
¹⁸²W, ¹⁸⁵Re, ¹⁹³Ir, ¹⁹⁵Pt, ²⁰⁵Tl, ²⁰⁸Pb, ²³²Th, ²³⁸U**MR:** background: 20 scans; samples and standards: 60 scans; each scan 40 ms on peak (16 ms for S)²⁷Al, ³¹P, ³²S, ⁴³Ca, ⁴⁵Sc, ⁴⁷Ti, ⁵¹V, ⁵²Cr, ⁵⁵Mn * ⁵⁹Co, ⁶⁰Ni, ⁶³Cu, ⁶⁶Zn, ⁸⁹Y**HR:** background: 20 scans; samples and standards: 60 scans; each scan 20 ms on peak³⁹K, ⁴⁵Sc * ⁷¹Ga, ⁷⁵As, ⁸⁹Y

Given are only the isotopes used for data evaluation; those used as internal standards are underlined

The star (*) separates where different internal normalisation was applied to lower or heavier mass regions

^{\$}corrected for isobaric interferences from ¹⁰⁸Cd and ¹¹⁵Sn (max. <7%)

2.3.2 Isotope dilution ICP-MS analysis of S, Se and Te

Sulfur, Se and Te abundances in CANS and COBO were also determined by isotope dilution multi-collector (Se, Te, e.g. König et al. 2012; Wang & Becker 2014a) or single-collector sector field (S, e.g. Makishima & Nakamura 2001; Wang & Becker 2014a) ICP-MS. Three isotope tracer solutions (spikes) were prepared, containing $1195 \pm 26 \mu\text{g/g}$ S, $420.1 \pm 2.7 \text{ ng/g}$ Se and $56.97 \pm 0.83 \text{ ng/g}$ Te, enriched in ^{34}S , ^{77}Se and ^{125}Te to 99.9, 96.4 and 95.5%. The ^{34}S spike solution was prepared as described in Wang & Becker (2014a). Each tracer solution was repeatedly calibrated against two commercial Merck and Alfa Aesar calibration solutions. The isotope tracer solutions were added to 19 to 26 mg of CANS and to 50 mg Cold Bokkeveld powders. CANS was digested four times for the analysis of Se and Te and later four times for S isotope dilution analysis, as this method was set up later. For COBO, two digestions were made for Se and Te and six for S. For all Se and Te analysis, sample-spike mixtures were first oxidized in 7 ml PFA beakers with 1 ml 14 M HNO_3 and 0.1 ml H_2O_2 and then dried down. This and all subsequent drying steps were carried out at low temperature of 65°C to avoid possible loss of volatile Se species. The oxidation step was omitted for one out of four CANS samples and five out of six COBO samples because some S could be lost as H_2S or SO_2 (Okai et al. 2001; Ackermann et al. 2012; Wang & Becker, 2014a). However, results with and without the preoxidation step were not significantly different. Two ml each, 14 M HNO_3 and 24 M HF were then added for sample digestion and capped beakers were placed on a hot plate at 120°C for 48 h. For comparison, two out of six COBO samples were digested with Savillex beakers placed into Parr bombs at 150°C for 48 h. Again, results did not differ outside the stated uncertainty.

Sulfur isotope ratio measurements were carried out in medium resolution mode without further purification using an ElementXR SF-ICP-MS, a Scott type PFA spray chamber, a microconcentric PFA nebulizer, and counting mode. An aliquot containing ca. $15 \mu\text{g}$ of S was taken, dried down, redissolved in 3 ml of 0.14 M HNO_3 and then diluted to S contents of about $1 \mu\text{g/g}$ in 0.14 M HNO_3 for analysis. Sensitivity was $\sim 2 \times 10^6$ cps for ^{32}S . Mass, search and integration windows are set to 80, 80 and 40%. Data acquisition consists of 25 runs, 25 passes each, with 12, 60 and 24 ms on ^{32}S , ^{33}S and ^{34}S peaks. After rinsing for 2 minutes, the background that typically corresponds to 1 % of the sample intensities, is determined, the sample solution taken up and the measurement started. The background was always subtracted.

The remaining bulk of the sample solution is then dried down, taken up in 2 ml 6 M HCl and refluxed for 24 h at 80°C to ensure complete conversion of Se(VI) and Te(VI) to the 4+ oxidation state (e.g. Marin et al. 2001). This solution is dried down again, taken up in 6 ml 6 M HCl and refluxed for another 24 h at 80°C. After cooling, the sample was diluted with ultrapure water (18.2 M Ω) to achieve 36 ml of 1 M HCl sample solution. Thiol cotton fibre (TCF) was employed for the separation of Se and Te from sample matrices. Preparation of TCF followed the protocols of Yu et al. (2002); Rouxel et al. (2002); Elwaer and Hintelmann (2008); König et al. (2012) and Mitchell et al. (2012). For this purpose, a mixture of 20 ml thioglycolic acid (96-99%), 14 ml acetic anhydride (99.9%), 6.4 ml glacial acetic acid, 0.064 ml sulphuric acid (97.5%) and 2.5 ml 18.2 Ω water is added to 6 g medical grade hydrophilic cotton in a brown wide mouth borosilicate glass bottle. The capped bottle is then placed into a water bath at 40 \pm 2°C for 5 days with the mixture slued gently twice a day. The treated cotton was then air dried for two days. While Se(IV) and Te(IV) have a strong affinity for the thiol cotton fibers (Yu et al. 2002), all major elements pass through the columns. Following the protocol of Rouxel et al. (2002), diluted sample solutions were loaded onto 5 ml polypropylene columns. The columns were filled with 140 mg of TCF, previously washed with 3 ml H₂O and conditioned with 2 ml of 6 M HCl and 2 ml of 1 M HCl. Both Se and Te are finally eluted together by destruction of the functional groups of the TCF. For destruction the TCF was transferred to 10 ml test tubes and mixed with 0.5 ml 7 M HNO₃. Test tubes were capped and left at room temperature for 20 minutes. Afterwards, the test tubes were put into a boiling water bath for another 20 minutes, and subsequently diluted with 4.6 ml ultrapure water. Samples were centrifuged and filtered through a 0.45- μ m filter with a syringe to remove the cotton fibers from the sample solution. For Se and Te analyses the solution was split and mixed with 0.25 ml 10 M HCl to ensure that both, Se and Te are in the reduced 4+ state.

For Se and Te isotope ratio analysis a Thermo Finnigan Neptune MC-ICP-MS equipped with an ESI SC-2 autosampler and a home-made hydride generator (cf. Wombacher et al. 2009; König et al. 2012) was utilized. Hydride-liquid separation was achieved within a borosilicate glass spray chamber consisting of a cyclonic and Scott type chamber arranged in tandem. Using the built-in peristaltic pump, about 0.7 ml/min of the sample solution (in 0.56 M HNO₃) and the reducing agent (freshly prepared 0.13 M NaBH₄ - 0.05 M NaOH) are fed via capillary tubes through the drain into the cyclonic chamber where both solutions mix at the spray chamber wall. The volatile

Se and Te hydrides are carried to the plasma by an Ar gas flow of about 1.1 ml/min provided by a concentric nebulizer with a sealed sample inlet. Using a set of two Y connectors, the waste solution is removed by a second peristaltic pump through the same drain port that is used to introduce the sample solution and reductant. Hydride generation provides an extra separation from remaining matrix elements and, taking the higher uptake rate into account, a 10 – 15 times higher ion yield. The higher sensitivity is probably mainly due to the far more efficient delivery of Se and Te to the plasma. A one ppb solution yields about 20 mV for ^{82}Se and 400 mV for ^{128}Te using $10^{11} \Omega$ resistors. The cup configuration includes ^{76}Se , ^{77}Se , ^{78}Se and ^{82}Se and ^{124}Te , ^{125}Te , ^{126}Te , ^{128}Te and ^{130}Te . Each analysis comprises 20 cycles with an integration time of 4.2 s. Because Se and especially Te can be rather sticky, rinsing with 0.56 M HNO_3 sometimes took up to 20 minutes. The background was then determined right prior to every standard and sample analysis. Measured background intensities are subtracted offline from the signal intensities recorded, subtracting both, residual Se and Te signals and contributions from gas blanks, e.g. $^{40}\text{Ar}^{36}\text{ArH}$ on ^{77}Se , ^{82}Kr on ^{82}Se and ^{126}Xe on ^{126}Te . Instrumental mass bias was monitored externally by repeated analysis of standard solutions and corrected using the natural $^{77}\text{Se}/^{82}\text{Se}$ of 0.87447 and $^{125}\text{Te}/^{126}\text{Te}$ of 0.376688 (Berglund & Wieser, 2011).

The external reproducibility is evaluated from two relative standard deviations with n = number of measurements and d = number of digestions. For sulfur, $\pm 2.3\%$ for CANS ($n=14$; $d=4$), $\pm 2.7\%$ for COBO ($n=18$; $d=6$) was obtained. Repeated analysis for two more chondrite samples yielded $\pm 1.5\%$ ($n=11$; $d=4$) for Murchison, another CM2 chondrite and $\pm 4.0\%$ ($n=20$; $d=8$) for a slightly weathered piece of the Allende CV3 chondrite. For Se, the external reproducibility was $\pm 0.63\%$ for CANS ($n=4$; $d=4$), $\pm 1.5\%$ for Murchison ($n=5$; $d=5$), $\pm 2.9\%$ for the weathered Allende sample ($n=16$; $d=14$) and $\pm 2.0\%$ for COBO ($n=2$; $d=2$). Because COBO was only analysed twice, the reported value ($\pm 2.0\%$) refers to the deviation of the two individual measurements from the mean value. Tellurium reproduced within $\pm 0.53\%$ for CANS ($n=4$; $d=4$), $\pm 2.4\%$ for Murchison ($n=5$; $d=5$), $\pm 4.7\%$ for the weathered Allende sample ($n=16$; $d=14$) and $\pm 5.2\%$ for COBO ($n=2$; $d=2$). Since COBO was only analysed twice for Te, the “reproducibility” refers to the deviation from the mean value. For S, Se and Te the reproducibility for chondrite samples from different aliquots measured in different sessions is generally better than the reproducibility based on repeated digestions. Thus the overall reproducibility including repeated digestions is clearly compromised by sample heterogeneity between powder aliquots. For the

CANS powder, heterogeneity was not evident. Procedure blanks for S, Se and Te were always <90 ng, <0.6 ng for Se and <0.4 ng for Te. These blanks contribute no more than 1 ‰ for S and Se and 6 ‰ for Te to either CANS or COBO. Thus blanks are considered negligible.

2.3.3 Additional analysis by Q-ICP-MS, EMS, INAA, XRF, and Karl Fischer titration

Karl Fischer titration: Additional measurements were carried out, in order to evaluate and complement the data sets on CANS and COBO (Tables 2.2 and 2.3). Water contents were determined by Karl-Fischer Titration in Bochum, Germany which is based on the quantitative reaction of water with iodine and offers a precision of about 5% (c.f. Behrens et al. 1996). CANS was analysed twice (6.66 and 6.67 wt. %) and COBO once, consuming about 5-10 mg sample powder.

Quadrupole (Q) ICP-MS: One powder aliquot for CANS and COBO, respectively, was externally analysed by Q-ICP-MS at the Montanuniversität Leoben in Austria.

Instrumental neutron activation analysis (INAA): About 70 mg and 100 mg of CANS and COBO respectively were analysed by INAA at the Universität zu Köln, following irradiation of the samples for 6h with a neutron dose of $7 \cdot 10^{11} \text{ N cm}^{-2} \text{ s}^{-1}$ at a reactor in Mainz, Germany. Analytical procedures are outlined in Weckwerth (2014).

X-ray fluorescence (XRF): Elemental abundances in CANS were also determined using a Philipps PW 2400 sequential wavelength dispersive XRF at the Universität zu Köln, Germany (Wolf & Palme 2001). The uncertainty given in Table 2.2 is obtained from the relative 2 standard deviation determined from eight analyses from two fusion disks for the Allende chondrite (cf. Stracke et al. 2012).

Electron microprobe analysis: Fifteen elements (Si, Al, Fe, Mn, Mg, Ca, Na, P, S, Ti, Ni, Cr, Co, Zn, Cu) were analysed in a CANS powder tablet using wavelength dispersive x-ray spectroscopy at the JEOL JXA-8900 RL electron microprobe at the University of Göttingen/Germany. Peak counting times were 15 s for Na, Mg, Fe, Si, Al, and 30 s for K, S, Ca, Ni, Cr, and 60 s for Co, P, Mn, Zn, Ti, 120 s for Cu and about half of the peak counting time was spend for the determination of background values. For calibration and sample analyses an

accelerating voltage of 20 keV and a beam current of 15 nA was applied. The CANS powder tablet was analysed with a defocused beam of $\sim 10 \mu\text{m}$. The following natural and synthetic standards were used for calibration: albite (Na), San-Carlos olivine (Mg, Si), sanidin (K), hematite (Fe), cobalt-metal (Co), baryte (S), wollastonite (Ca), nickel oxide (Ni), Cu_2O (Cu), apatite (P), anorthite (Al), Cr_2O_3 (Cr), rhodonite (Mn), zinc-metal (Zn) and TiO_2 (Ti). To ensure accurate calibration, standard analyses were performed prior and after sample analyses. The structural difference between the porous pressed nanoparticle powder pellet and the crystalline structure of the standards used for calibration can result in substantial matrix effects (*e.g.* Reed, 2005). To correct for such effects the phi-rho-Z correction method was applied.

2.4 RESULTS AND DISCUSSION

2.4.1 Composition of CANS

The successful application of CANS as external calibration material for LA-ICP-MS analysis requires that its elemental composition is well constrained. Thus, major and minor element and Se and Te abundances were determined by several methods and a set of preferred values is now defined and given as oxides in wt. % and as elemental abundances in $\mu\text{g/g}$ in Table 2.2. Isotope dilution analysis is generally highly precise and accurate and therefore the SO_3 , Se and Te abundances obtained by isotope dilution are chosen. The isotope dilution data obtained agrees within 2% with the results obtained by SF-ICP-MS. The very good agreement between the isotope dilution and SF-ICP-MS data underscores the quality of the reported SF-ICP-MS data. Furthermore, reproducibility (2 sd) for the SF-ICP-MS session #1 are better than 2% for most elements except ZnO, Se and Te (2 sd of 3 to 6%) and SiO_2 (10%).

High precision and accuracy of the SF-ICP-MS data results from the careful matrix-matched calibration specifically designed for the quantification of CANS, the limited set of elements measured and the high signal intensities for the major and minor elements analysed. Therefore, apart from SiO_2 and the elements determined by isotope dilution (SO_3 , Se and Te), the SF-ICP-MS session #1 data is chosen to define the reference composition (the preferred values in Table

2.2). The SiO₂ data obtained by SF-ICP-MS for CANS samples that were not taken to dryness after digestion, however, display inferior reproducibility of about 10% for SF-ICP-MS session #1 and also for the ICP-OES analysis from the same digestions (40%; 2 sd). Both SiO₂ data display lower average values than determined by Q-ICP-MS, electron microprobe (EMP) and XRF which suggests that Si was partially volatilized from the sample solutions. The SiO₂ data from Q-ICP-MS, EMP and XRF, however, agree within $\pm 2\%$ with the calculated average. This average is therefore chosen as the preferred Si value for CANS.

With the exception of SiO₂ that was partially lost and ZnO that was too low for accurate ICP-OES analysis, the results from ICP-OES and SF-ICP-MS session #1 deviate by no more than 1.1%. This constrains the high quality obtained by both methods, but not necessarily the accuracy as both data sets are obtained from the same set of sample and calibration solutions and could therefore be subject to systematic biases. To evaluate the accuracy the SF-ICP-MS #1 data chosen as preferred values, will be compared with results from independent analysis. First, CANS was again analysed by SF-ICP-MS (sessions #2a and b) using a method that is purpose-build for chondrite samples and utilizes a different set of calibration solutions. Data obtained in both sessions all agree within better than 5%. Elements determined by Q-ICP-MS, INAA and electron microprobe agree with the preferred SF-ICP-MS #1 data within $\pm 8\%$ and usually much better, with the following exceptions: CaO differs by +22% (Q-ICP-MS) and -13% (INAA), Na₂O by -17% (EMP), TiO₂ by +10% (Q-ICP-MS) and +12% (EMP), Cr₂O₃ by +9.5% (EMP) and Se by +11% (INAA). The data by EMP and INAA, however, is either within the stated uncertainties or close (TiO₂ and Se), thus only the CaO and TiO₂ data by Q-ICP-MS are clearly different outside the stated uncertainties. Most XRF data agrees with the chosen SF-ICP-MS data within 9% and usually much better, but NiO, Na₂O, MnO₂, ZnO and Cr₂O₃ differ by -11, -13, -15, -16 and -53%. The Na₂O data, however, agrees within uncertainty and ZnO data is only slightly outside uncertainties.

In summary, the preferred values for the CANS composition are well constrained, with SiO₂ data that agrees within $\pm 2\%$ for three independent methods, consistent isotope dilution and SF-ICP-MS data for SO₃, Se and Te and with SF-ICP-MS session #1 data for all other elements chosen. The SF-ICP-MS data agrees with at least two independent (one for Cr₂O₃ and Na₂O) methods (Q-ICP-MS, INAA, EMP, XRF) within at least 5%. Titanium data, agrees within $\pm 3\%$

for the two SF-ICP-MS sessions and ICP-OES, but is systematically lower than XRF, EMPA and Q-ICP-MS by +8 to +12%. Nevertheless, the TiO₂ data from SF-ICP-MS session #1 have been chosen. This is because, for the data discussed below for COBO, the TiO₂ from SF-ICP-MS session #2 also agrees well with the result from Q-ICP-MS and literature values. Thus, while most elements are certainly well constrained in CANS, i.e. within better than $\pm 5\%$, Cr₂O₃ and Na₂O data are perhaps less certain and TiO₂ data could potentially be too low by about 10%.

Karl-Fischer titration showed that CANS contains an appreciable amount of H₂O that is most likely adsorbed at the surface of the nanoparticles. The sum of the oxides and water yields a total of 100.6%, suggesting that no major component is significantly biased.

The target elemental composition of CANS was planned to be in approximately CI chondritic abundance for major and minor elements and Se and Te. After production, the nanoparticle powder was delivered with information values from Nano SRM Ltd. only (Table 2.2). The sum of the information values corresponds to 100%. If a water content of 6.66% is considered, almost exactly 90% of the sulphur are missing and must have been lost during the production by flame spray synthesis. The presence of water diluted the abundance of the other elements, while the missing S, a major element in CI chondrites, leads to a systematic positive shift in the concentration of other elements. If the Nanograde information values are recalculated considering the water content and a 90% S loss all other elements agree with the preferred values within 5% except, ZnO that is by 13% too high and Te, Se and CuO that are by -12, -15 and -46% too low and were probably partially lost along with S during the production process. Trace element quantification during SF-ICP-MS session #2 revealed that CANS is contaminated by a few trace elements that were above the detection limit, including Mo, In and several REE (Table 2.2 caption). This contamination most likely results from the production process of the nanoparticle powder.

Table 2.2 CANS – major element, Se and Te abundances

information	SF-ICP-MS #1		SF-ICP-MS #2a, b [§]		ICP-OES		Q-ICP-MS n=2		INAA		EMPA		XRF		preferred values			µg/g elemental	
	values	n=12; 6 Si, Zn, Se	mean	±2 sd	mean	±2 sd	mean	±2 sd	mean	±2 sd	±2 sd	mean	±2 sd	±2 sd*	wt% oxides	2 sd oxides	2 rsd [%]		
[wt%]																			
SiO ₂	27	27.7	2.8				22.7	9.1	30.49	0.74		31.42	0.69	30.57	0.52	30.8	1.0	3.4	144108
Al ₂ O ₃	2.0	2.229	0.033	2.26	0.23	2.25	0.10	2.319	0.043			2.343	0.066	2.22	0.14	2.229	0.033	1.5	11796
Fe ₂ O ₃	31	32.25	0.42	32.0	1.6	32.4	1.6	32.08	0.60	31.5	1.5	32.8	1.1	33.71	0.62	32.25	0.42	1.3	225531
MnO ₂	0.30	0.3299	0.0028	0.321	0.019	0.330	0.016	0.321	0.051	0.316	0.025	0.350	0.020	0.281	0.015	0.3299	0.0028	0.86	2085
MgO	19	21.50	0.27	21.2	1.1	21.6	1.0	20.88	0.50			22.18	0.59	22.38	0.54	21.50	0.27	1.3	129652
CaO	1.5	1.613	0.019	1.574	0.094	1.621	0.057	1.976	0.036	1.40	0.28	1.646	0.053	1.66	0.12	1.613	0.019	1.2	11529
Na ₂ O	0.80	0.893	0.015	0.86	0.043	0.898	0.041			0.876	0.040	0.739	0.159	0.78	0.23	0.893	0.015	1.7	6625
P ₂ O ₅	0.22	0.2571	0.0033	0.245	0.015	0.258	0.013	0.255	0.016			0.267	0.019	0.276	0.017	0.2571	0.0033	1.3	1122
SO ₃	16	1.530	0.023	1.52	0.20	1.534	0.083	1.522	0.036			1.55	0.66			1.522	0.036	2.3	6096
TiO ₂	0.10	0.1135	0.0013	0.1101	0.0066	0.1131	0.0055	0.1246	0.0031			0.127	0.012	0.1230	0.0065	0.1135	0.0013	1.2	680
NiO	1.5	1.685	0.012	1.655	0.083	1.689	0.085	1.645	0.024	1.65	0.17	1.669	0.070	1.50	0.11	1.685	0.012	0.70	13241
Cr ₂ O ₃	0.50	0.5544	0.0070	0.536	0.048	0.555	0.027	0.543	0.018	0.512	0.041	0.61	0.23	0.2602	0.0026	0.5544	0.0070	1.3	3793
CoO	0.093	0.1040	0.0012	0.1035	0.0052	0.1043	0.0043	0.1075	0.0018	0.0990	0.0050	0.108	0.012	0.113	0.010	0.1040	0.0012	1.1	818
ZnO	0.050	0.0617	0.0016	0.0609	0.0043	0.0617	0.0043	0.0574	0.0007	0.0597	0.0030	0.061	0.017	0.0517	0.0066	0.0617	0.0016	2.6	496
CuO	0.020	0.0117	0.00018	0.01139	0.00068	0.0114	0.0006	0.01191	0.00002	0.0125	0.0050	0.0111	0.0031			0.01170	0.00018	1.6	93.5
H ₂ O																6.66	0.33	5.0	
sum [%]																100.6			
[µg/g]																elemental (µg/g)			
Se	43	39.2	2.3					39.72	0.25	44	4					39.72 ID	0.25	0.63	39.72
Te	5	4.69	0.20	4.85	0.17			4.787	0.025							4.79 ID	0.025	0.53	4.787

n = number of analyses

[§] trace elements detected during SF-ICP-MS#3: Mo: 0.2±0.1; In: 0.45±0.04; La 1.7±0.1; Ce: 0.17±0.03; Pr: 0.016±0.003; Nd 0.10±0.01; Gd: 0.02±0.01 µg/g, n=12. detectable trace elements by SF-ICP-MS (LOD see Table 3) and INAA .

* estimated from the relative 2 sd of 8 repeated analysis of a Allende chondrite sample

2.4.2 Composition of COBO

Application of COBO as a quality control material for LA-ICP-MS analysis or as an alternative calibration material requires that its elemental composition is well constrained. Thus, major, minor and trace element abundances were determined by SF-ICP-MS, Q-ICP-MS, INAA and isotope dilution analysis and a set of preferred values is defined and given as elemental abundances in $\mu\text{g/g}$ in Table 2.3. Isotope dilution data for S, Se and Te are chosen as preferred values. The S and Te data by SF-ICP-MS deviates from the isotope dilution data by -5 ± 14 and -3 ± 6 %, respectively; the Se data obtained by INAA differs by -2 ± 8 %. Generally, the SF-ICP-MS data offers better reproducibility than Q-ICP-MS (median for 2 rsd is 5% for SF-ICP-MS vs. 10% for Q-ICP-MS) and INAA, where the conservatively stated reproducibility correspond to 5% or worse. However, the major and minor element data from SF-ICP-MS session #2 is less precise than that from SF-ICP-MS session #1 for CANS. For the same set of major and minor elements, the median of the double relative standard deviation equals ± 1.3 % for CANS in session #1, but ± 6 % for both, CANS and COBO in session #2.

In addition, several obvious outliers had to be removed for COBO, especially for the sample digestion including HClO_4 , but none for CANS. Thus, the determination of (major and minor elements) in COBO is not as good as for CANS in session #1 and further improvements may be possible regarding this newly developed procedure for chondrite analysis.

Where available and apart from the isotope dilution data, the more precise SF-ICP-MS data are chosen to define a set of preferred values for COBO. (see Table 2.3). Else INAA or Q-ICP-MS data are chosen, e.g. for Si only Q-ICP-MS data is available. For Sc, Ga and Cs INAA and Q-ICP-MS data were available. For Cs, the more precise Q-ICP-MS value was chosen, for Sc the INAA value was chosen. Admittedly both values were chosen also because they fit better with the literature data in Table 2.3. For Ga the INAA value was chosen, but the Q-ICP-MS data is very similar. Of the 42 elements that were measured by SF-ICP-MS and Q-ICP-MS and/or INAA, the data agrees within stated uncertainties for 25 elements, including most major, minor and rare earth elements. Although in agreement within uncertainty, Cu, Lu and Hf by INAA as well as As and La by Q-ICP-MS deviate from SF-ICP-MS data by more than 20%. The data for 18 elements disagrees between SF-ICP-MS/Q-ICP-MS/INAA outside uncertainty. Of these, Ni

and Co Q-ICP-MS data differ from SF-ICP-MS data by -11 and -21%, but SF-ICP-MS and INAA data agree within 3%. Neodymium, Sm and Ir SF-ICP-MS data does not differ by more than 21% from either Q-ICP-MS or INAA data. Terbium Q-ICP-MS and INAA data deviate from SF-ICP-MS data by +35 and -18 %. The Ga data by Q-ICP-MS and INAA is 41 and 50 % higher than the SF-ICP-MS data. Apart from Ga, no INAA data deviated from SF-ICP-MS data by more than 21 %. However, results from Q-ICP-MS for As, Rb, Sr, Zr, Nb, Sn, La, Tb, W, Pb Th and U differ by 35% or more from the SF-ICP-MS data. Scandium was only obtained by INAA and Q-ICP-MS, with the result from the latter method being 43% higher.

For comparison, Table 2.3 also contains published average data for CM2 chondrites taken from Lodders and Fegley (1998), except for highly siderophile elements (PGEs, Re, Au) that are those of Fischer-Gödde et al. (2010). Table 3 also contains previously published data for the Cold Bokkeveld CM2 chondrite (see citations in Table caption). Preferred data for Zn, Ag, Cd, In, Au and Tl agrees reasonably well within ± 16 % with that of Wolf et al. (1980), but differs from their Se, Rb, Te, Re, Os, Ir and U data by 34 to 90 %. Since the Wolf et al. (1980) data for the latter elements also differs substantially from the other published data, is not included in the discussion below.

By far most major and minor element data agrees within 10% with the published data, but Ca, Na and Cr fall systematically below the published values by -9 to -26 %, -46 to -53 % and -8 to -25 %. However, Ca, Na and Cr data determined within this study by SF and Q-ICP-MS and by INAA agree well (2sd relative of 11, 7 and 4 %, respectively). Thus it can be concluded that the preferred values given here, reflect the true values of the used Cold Bokkeveld powder rather accurately. Mid mass range elements from V to Mo often agree with the published data within 10 % or better with the following exceptions: Vanadium differs by -13 % from the only other V data, the CM2 chondrite reference data of Lodders and Fegley (1998). The Ga data is 16% higher than that of Zolensky et al. (1997), while the two other published Ga data differ by no more than 7 %. The Zr value is 34 % lower than the CM2 chondrite reference value of Lodders and Fegley (1998), but is only 4 % lower than the Zr isotope dilution data reported for Cold Bokkeveld by Münker et al. (2003). For Sr and Mo, the SF-ICP-MS data is by 41 and 58 % lower than the reference value provided by Lodders and Fegley (1998). The Sr data from Q-ICP-MS, however, would be 53 % higher than the data from Lodders and Fegley (1998). Thus, no preferred value

was defined for Sr and Mo. Concerning highly siderophile elements, the INAA data differs from the CM2 reference and published Cold Bokkeveld data by -10 and -14 for Ru, +24 for Os and by -2 % for Au. The highly siderophile elements determined by SF-ICP-MS (Rh, Pd, Re, Ir and Pt) tend to display systematically lower values than those given for CM2 chondrites or Cold Bokkeveld by 11 to 29 %. For W, the data are also 32% lower than the CM2 reference value provided by Lodders and Fegley (1998), but only 7% lower than the reference data from Kleine et al. (2002). Many of the chalcophile and lithophile trace elements from Ag to U do not differ by more than -15 to +9% from any reference data. However, the value obtained for Ag is lower than any reference value by -7 to -29%. Ce, Tl and Th values are lower by up to -18%, -17 and -21%, respectively. The literature values for Hf are by 15 to 26% lower, but only 6% lower than the isotope dilution data by Münker et al. (2003). The preferred Pb value is 23% higher than the CM2 reference.

Components of major elements are also given in wt. % (Table 2.3). A H₂O content of 13.51 wt. % was determined by Karl-Fischer titration. Since CM2 chondrites contain about 2.2 wt. % C on average (Lodders and Fegley 1998), a combined C and H₂O content of 15.7% is given in Table 2.3. In order to calculate the total from the measurement, it has to take into account that Fe, S, and Mn coexist with different oxidation states which leads to different atomic weights of their compounds. While the uncertainty of the calculated total due to the different oxidation states of Mn is negligible due to the low Mn abundance, different oxidation states of Fe and S will be significant. According to Orthous-Daunay et al. (2010), 41 % of the total sulfur in Cold Bokkeveld is sulfidic, i.e. bond to iron, three percent of the S is oxidized in CaSO₄, and 56 % is bond to organics. Sulfur reported as SO_{0.09} in Table 2.3 refers to 97% of S bond to Fe and organics and three percent as SO₃. Howard et al. (2011) suggests that 47 % of the Fe in oxides and silicates in Cold Bokkeveld is in the 3+ oxidation state. The FeO_{1.17} reported in Table 2.3 refers to this distribution of Fe²⁺ and Fe³⁺ in silicates and oxides, while 5.5 % of the Fe resides in FeS. The calculated total then amounts to 95.7 %. The missing 4.7% cannot be explained by N or missing trace elements. Either Fe and/or S in Cold Bokkeveld are more oxidized or some major elements determined in this study have been underestimated. If for example all Fe and S in Cold Bokkeveld that is not in FeS is recalculated as Fe₂O₃ and SO₃, the total corresponds to 99.5 %. Thus stronger oxidation of the used Cold Bokkeveld sample is a possible explanation for the low total and also consistent with the comparatively high water content of 13.51 wt. % which is

higher than the typical 9.50 wt.% for CM2 chondrites and the typical 11 wt. % for CI chondrites (Lodders and Fegley 1998). A rather high water content of the used sample aliquot from Cold Bokkeveld may also explain the frequently observed lower elemental abundances compared to published values with a median of -5.8 %. Alternatively, the low yield of 95.7 % given in Table 2.3 is not explained by high oxidation states of Fe and S, but by systematic differences due to an underestimation of some major elements.

Table 2.3 COBO – major and trace element abundances

	SF-ICP-MS #2 a, b n = 12			Q-ICP-MS n=2		INAA n=1		preferred values incl. ID (MC)-ICP-MS n=2; n=18 for S			literature values					wt %		
	LOD			mean	±2sd	mean	±2sd	μg/g	±2sd	±2sd [%]	Cold Bokkeveld							
	mean	±2sd	[μg/g]								CM2 [*]	I	II	III	IV			
Si				119384	12173			119384 Q	12173	10	127000		126000		127600	SiO ₂	25.5	
Al	11129	869	1E-03	10844	711			11129	869	7.8	11300	11300	11000		12100	Al ₂ O ₃	2.1	
Fe	204697	1959	2E-02	192108	15038	200000	10000	204697	1959	1.0	213000	197000	200700	206000	208500	FeO _{1.17} *	27.3	
Mn	1619	40	3E-05	1603	125	1600	80	1619	40	2.5	1650	1570	1710		1500	MnO ₂	0.3	
Mg	107661	7528	3E-02	106236	5697			107661	7528	7.0	115000	110000	112200		112900	MgO	17.9	
Ca	10055	1242	2E-03	11140	1169	11000	2200	10055	1242	12	12900	12200	11900	13600	11100	CaO	1.4	
Na	2096	62	2E-02			2200	110	2096	62	3.0	3900	3910	4430	3990	4500	Na ₂ O	0.3	
K	377	11	1E-03	411	101	420	42	377	11	3.0	370				330	420	K ₂ O	0.0
P	1018	198	2E-04	903	94			1018	198	19	1030		970				P ₂ O ₅	0.2
S	26148	3784	5E-03					27589 ID	754	2.7	27000		30200		29800	SO _{0.09} [*]	2.9	
Ti	572	42	5E-05	583	61			572	42	7.3	550		620		500	TiO ₂	0.1	
Ni	11974	518	1E-04	10598	978	12000	1200	11974	518	4.3	12300	10900	11900	12800	11700	NiO	1.5	
Cr	2606	196	7E-05	2594	244	2700	270	2606	196	7.5	3050	2820	3490	3100	2900	Cr ₂ O ₃	0.4	
Co	555	23	9E-06	440	42	540	27	555	23	4.1	560		473	585	600	CoO	0.1	
Zn	174.2	6.2	3E-05	168	15	180	14	174	6.2	3.6	180	170	209		204	ZnO	0.0	
Cu	127.0	7.0	9E-06	116	12	100	30	127	7.0	5.5	130					CuO	0.0	
																C + H ₂ O ^S	15.7	
																sum ^S	95.7	
V	65.1	4.3	5E-06	63.3	6.7			65.1	4.3	6.6	75.00							
Sc				11.41	0.85	8.0	1.6	8 NA	1.6	20	8.20				8.64			
Ga	5.33	0.74	2E-06	7.52	0.63	8.0	0.8	8.00 NA	0.80	10.0	7.60	6.90	8.57					
As	1.85	0.34	2E-06	2.50	0.33	2.2	0.3	1.85	0.34	18	1.80	1.97			1.83			
Se						12	1	12.24 ID	0.25 ^S	2.0	12.00				13.5	8.58		
Rb	1.52	0.11	7E-05	2.12	0.25			1.52	0.11	7.1	1.60		1.55		1.07			
Sr	5.92	0.37	3E-05	15.3	1.6			uncertain			10.00							
Y				2.08	0.25			2.08 Q	0.25	12.0	2.00							
Zr	4.64	0.12	1E-05	8.0	2.7			4.64	0.12	2.5	7.00		4.828					
Nb	0.378	0.088	2E-07	0.08	0.10			0.378	0.088	23.3	0.40		0.359					
Mo	0.582	0.035	7E-06					uncertain			1.40							
Ru						0.735	0.147	0.735 NA	0.15	20	0.817	0.850						
Rh	0.1329	0.0034	3E-07					0.1329	0.0034	2.6	0.149							
Pd	0.466	0.087	4E-06					0.466	0.087	19	0.606					0.660		
Ag	0.114	0.023	2E-06					0.114	0.023	20	0.160		0.146		0.122			
Cd	0.356	0.012	3E-06	0.348	0.052			0.356	0.012	3.5	0.420	0.387	0.404		0.395			
In	0.0444	0.0013	2E-07					0.0444	0.0013	2.9	0.050		0.048		0.047			
Sn	0.75	0.24	1E-05	6.4	2.2			0.75	0.24	32	0.790							
Te	1.391	0.079						1.435 ID	0.075 ^S	5.2	1.300		1.33		1.07			
Cs				0.1137	0.0014	0.06	0.02	0.1137 Q	0.0014	1.2	0.110		0.129					
Ba	3.4	1.1	2E-06					3.4	1.1	34	3.100							
La	0.302	0.013	3E-07	0.49	0.20	0.30	0.03	0.302	0.013	4.2	0.320	0.319	0.352	0.286	0.352			
Ce	0.774	0.024	4E-07					0.774	0.024	3.1	0.940		0.916		0.916			
Pr	0.1211	0.0045	2E-07	0.131	0.011			0.1211	0.0045	3.8	0.137							
Nd	0.611	0.029	4E-07	0.679	0.053			0.611	0.029	4.7	0.626		0.638		0.638			
Sm	0.198	0.014	4E-07	0.213	0.019	0.24	0.02	0.198	0.014	7.0	0.204	0.193	0.217	0.211	0.217			
Eu	0.0737	0.0039	1E-07	0.0796	0.0049	0.070	0.007	0.0737	0.0039	5.3	0.078	0.077	0.084	0.081	0.084			
Gd	0.263	0.013	5E-07	0.300	0.031			0.263	0.013	5.1	0.290		0.283		0.283			
Tb	0.0491	0.0032	1E-07	0.0663	0.0084	0.04	0.02	0.0491	0.0032	6.6	0.051							
Dy	0.335	0.017	4E-07	0.375	0.040			0.335	0.017	5.2	0.332		0.337		0.337			
Er	0.2115	0.0034	6E-07	0.225	0.029			0.2115	0.0034	1.6	0.221		0.228		0.228			
Tm	0.0334	0.0013	8E-08	0.0359	0.0032			0.0334	0.0013	3.8	0.035							
Yb	0.2224	0.0066	4E-07	0.226	0.013	0.19	0.05	0.2224	0.0066	3.0	0.215	0.227	0.225	0.225	0.225			
Lu	0.0333	0.0012	1E-07	0.0366	0.0054	0.04	0.01	0.0333	0.0012	3.7	0.033	0.033		0.037				
Hf	0.1326	0.0048	1E-06	0.139	0.036	0.16	0.04	0.1326	0.0048	3.6	0.180	0.164	0.1408	0.156				
W	0.108	0.049	2E-06	0.1731	0.0064			0.108	0.049	45	0.160	0.116						
Re	0.0424	0.0016	9E-08					0.0424	0.0016	3.8	0.046				0.0687			
Os						0.7	0.1	0.70 NA	0.11	15	0.563				1.30			

Table 2.3 continued

	SF-ICP-MS #2 a, b n = 12			Q-ICP-MS n=2		INAA n=1		preferred values incl. ID (MC)-ICP-MS			literature values					wt %
	LOD			mean	±2sd	mean	±2sd	n=2; n=18 for S			Cold Bokkeveld					
	mean	±2sd	[µg/g]					µg/g	±2sd	±2sd [%]	CM2 ^{&}	I	II	III	IV	
Ir	0.473	0.048	3E-07			0.57	0.03	0.473	0.048	10	0.554	0.597		0.584	1.19	
Pt	0.952	0.044	8E-07					0.952	0.044	4.7	1.087					
Au						0.17	0.01	0.1700 NA	0.0085	5.0	0.173			0.173	0.146	
Tl	0.0767	0.0021	7E-07	0.069	0.011			0.0767	0.0021	2.7	0.092				0.088	
Pb	1.97	0.11	1E-06	3.541	1.237			1.97	0.11	5.4	1.600					
Th	0.0325	0.0019	8E-07	0.063	0.027			0.0325	0.0019	5.9	0.041					
U	0.0088	0.0005	3E-08	0.0148	0.0040			0.0118	0.0023	19	0.012				0.0062	

* all S reported as FeS; remaining Fe as FeO, see text for discussion

§ uncertainty given as the deviation from the mean of two measurements

Cold Bokkeveld literature data: I: Kallemeyn and Wasson (1981), Hf + W Kleine et al. (2002); II: Wolf & Palme (2001), Na, S Dreibus et al. (1993),

Co, Zn, Ga, Rb, Ag, Cd, In, Te, Cs Zolensky et al. (1997), REE: Evensen et al. (1978), HFSE: Münker et al. 2003; III: Middlefehldt (2002),

IV: Wiik (1969), REE: Dreibus et al. (1993), Wolf et al. (1980) other trace elements incl. Zn

& CM2 average from Lodders and Fegley (1998), except highly siderophile elements from Fischer-Gödde et al. (2010)

Chapter 3

Quantification of trace elements in chondritic components using femtosecond LA-ICP-MS

3.1 INTRODUCTION

Microanalysis using laser ablation - inductively coupled plasma - mass spectrometry (LA-ICP-MS) provides a quantitative technique, able to resolve the spatial distribution of elemental abundances at the tenth of μm scale and sub-ppm level (*e.g.* Gao et al. 2002, Jochum et al., 2007, Liu et al. 2008). Previous applications of LA-ICP-MS to chondritic materials focussed on the analysis of specific components, such as metal (*e.g.* Campbell et al. 2001; Horstmann et al. 2014), matrix and chondrules (Bland et al. 2005; Grossman et al. 2007; Hewins et al. 2014, Pack et al. 2004) or bulk compositions after preparation of fused spheres (Pack et al. 2007) or powder tablets (Andronikov et al. 2013). Using chondrite thick sections, the approach taken here aims at the elemental microdistribution among major components like chondrules, matrix, CAIs as well as for minor constituents like chondrule rims and less well defined interstitial matrices.

Trace element profiles and elemental maps from chondrite sections were previously reported by Dyl et al. (2014) using synchrotron X-ray fluorescence. Their method offers much better and variable spatial resolution down to 2 μm , but a more limited set of accessible trace elements, higher detection limits and inferior accuracy. Secondary ion mass spectrometry (SIMS), especially time of flight-SIMS and nanoSIMS also offer higher resolution, but worse multi-element capabilities and in part higher detection limits (*e.g.* Bland et al. 2007). Thus, LA-ICP-MS provides a complementary method with superior detection limits and multi element capabilities, but lower spatial resolution.

Accurate LA-ICP-MS analysis generally requires matrix-matched external calibration materials (*e.g.* Guillong et al. 2005, Kroslakova & Günther 2007). So far there is no calibration material available for chondrites and thus non-matrix matched calibration is commonly applied, *e.g.* using NIST SRM 61x glass or USGS natural basalt glasses such as BCR-2G and BIR-1G (Pack et al. 2004; Bland et al. 2004, 2005; Grossman et al. 2007, Andronikov et al. 2013, Hewins

et al. 2014 and references therein). While the best calibration material for LA-ICP-MS should be similar to bulk chondrite material, perfect matrix matching is utterly impossible simply due to the variability of compositions and phases in chondrites. Thus variable elemental fractionation effects are expected, depending on the actual material ablated at the time. Femtosecond (fs) lasers diminish the difficulty of variable elemental fractionation for different phases, as they offer an enhanced generation of particles for different materials such as metals, semi- and non-conductors, and therefore optimized transport conditions and reduced fractionation effects within the plasma and ablation site (Bian et al. 2006, Liu et al. 2004, Günther & Hattendorf 2005, Koch & Günther 2011). Compared to nanosecond lasers, the very short interaction time between fs-laser pulses and the sample generates only minimal heat in the sampling region and provides reduced or even negligible vaporisation of more volatile elements during sampling (Koch et al. 2006, Liu et al. 2004). Thus fs-laser ablation is not perfect, but most suited for the determination of volatile elements in different chondritic components and phases.

As a consequence of different local physical properties of chondritic matter, highly variable amounts of ablated material are delivered to the plasma. To correct for such variable ablation yields, internal standardisation to an element of known concentration in the sample is commonly used (Longerich et al. 1996). However, the accurate determination of such an internal standard element e.g. by electron microprobe is extremely time-consuming. Furthermore, the accurate spatial matching of internal standard values from an external method (e.g. electron microprobe) with laser spots is generally not feasible for heterogeneous chondritic materials. In particular electron microprobe analysis only captures the sample surface, while laser ablation liberates particles from depths of several tens of micrometers.

This chapter evaluates a novel approach for the quantification of the micro-distribution of elements among chondritic components with a special emphasis on the moderately volatile chalcogene elements S, Se, and Te. It takes advantage from (i) femtosecond LA-ICP-MS, (ii) the use of yield correction factors (AYCF) based on the sum of major element compounds (Hoffmann et al. 1997; Leach & Hieftje 2000; Halicz & Günther 2004; Liu et al. 2008), and (iii) two innovative external calibration materials, a custom-tailored chondrite analog nanoparticle standard (CANS), and one that has been prepared from the CM2 chondrite Cold Bokkeveld (COBO). The latter will be used for quality control purposes. The preparation of CANS and

COBO and the determination of their chemical compositions by several analytical methods are presented in chapter 2 of the thesis.

3.2 EXPERIMENTAL

3.2.1 Femtosecond LA-ICP-MS

Femtosecond (fs) LA-ICP-MS measurements were performed with chirped pulse amplification (CPA)-type Ti: Sapphire-based laser system (Legend, Coherent, USA), generating pulse durations < 150 fs, operated in near infrared (NIR, $\lambda \sim 800$ nm) to obtain a better ablation yield for trace element analysis. The output energy was about 1 mJ, and a repetition rate of 10 Hz was applied. Sampling from NIST SRM 612, CANS and COBO powder tablets and the chondrite thick sections was performed by line scans with a travel speed of $10 \mu\text{m/s}$ and a laser spot size of about $80 \mu\text{m}$. It has been shown by Bian et al. (2006) that the accuracy of quantification for optically transparent materials (e.g. NIST SRM 612 – 616 glasses) ablated by fs-LA-ICP-MS in near infrared, strongly depends on the laser fluency. The same authors demonstrated that a high fluency has to be applied to obtain accurate results. Since the optically transparent NIST SRM 612 glass is used for external calibration of trace elements a high fluency of about 20 J/cm^2 was applied. For optical control, a CCD camera equipped with a macro-objective of variable magnification ($0.8 - 4.0 \times$) was used. To adjust the vertical sample position and spot size independently, the optical path and the beam delivery system are separated. Samples and calibration materials were fixed to the bottom of a small volume cylindrical ablation cell ($V = 15 \text{ cm}^3$). Helium was used as the carrier gas and Ar was added as a make-up gas before entering the ICP. A ThermoScientific Element2 sector field ICP-MS was used for data acquisition in low mass resolution with mass windows corresponding to 1 or 5% peak width. The following isotopes were measured: ^{23}Na , ^{25}Mg , ^{27}Al , ^{29}Si , ^{31}P , ^{34}S , ^{43}Ca , ^{44}Ca , ^{49}Ti , ^{53}Cr , ^{55}Mn , ^{57}Fe , ^{59}Co , ^{60}Ni , ^{62}Ni , ^{65}Cu , ^{66}Zn , ^{67}Zn , ^{69}Ga , ^{71}Ga , ^{75}As , ^{77}Se , ^{82}Se , ^{85}Rb , ^{86}Sr , ^{88}Sr , ^{89}Y , ^{90}Zr , ^{91}Zr , ^{93}Nb , ^{95}Mo , ^{101}Ru , ^{105}Pd , ^{108}Pd , ^{107}Ag , ^{109}Ag , ^{111}Cd , ^{115}In , ^{118}Sn , ^{119}Sn , ^{121}Sb , ^{125}Te , ^{128}Te , ^{137}Ba , ^{143}Nd , ^{146}Nd , ^{147}Sm , ^{177}Hf , ^{182}W , ^{195}Pt , ^{202}Hg , ^{205}Tl , ^{208}Pb , ^{209}Bi , ^{232}Th , ^{238}U . Where possible, masses without or negligible contribution of interferences were chosen. For some elements, two isotopes were

selected to test for isobaric interferences. Atomic isobaric interferences of ^{108}Cd and ^{115}Sn were stripped from ^{108}Pd and ^{115}In offline. The 44 elements (56 different masses) were measured with sample times of 1 - 10 ms depending on the elemental and isotopic abundances. The analog detector mode was used for major and minor elements, while the both or counting mode was chosen for trace elements. A complete standard analysis took two minutes, commencing with ~30s of background determination with the laser beam path blocked and including washout. For line scans on chondrite samples the acquisition time was dependent on the length of the line ablation profile and was individually adjusted by varying the number of runs (mass scan cycles). Mass offsets were determined daily using the COBO powder pellet. Gas flows, torch position, and lens settings were optimized prior to every session and after sample change by ablating NIST SRM 612 to obtain maximum signal intensities while keeping oxide interferences low (0.4 to 0.5 % ThO/Th) and assuring complete atomization and ionization as testified by the ^{238}U - ^{232}Th ion-signal intensity ratio close to one for NIST SRM 612 (e.g. Günther und Hattendorf, 2005). For external calibration and quality control CANS, NIST SRM 612 and COBO are analyzed twice prior and twice after chondrite sample data acquisition in order to monitor drift in sensitivity and mass discrimination.

3.2.2 Data treatment and ablation yield correction

Selection and integration of background and analyte signals and background correction was performed following the protocol of Longerich et al. 1996. Spikes in the background signals were extremely rare and if they occurred they were either removed manually or filtered if their intensity exceeded the average signal intensity plus three times the standard deviation. Due to the intrinsic heterogeneity of chondrite samples, removal of signal spikes cannot follow a general procedure. Spikes were removed if the following arguments suggested that the spikes were analytical artefacts: (i) when the spike is not observed for two isotopes of the same element, (ii) when no spike is observed for at least one more element with the same chemical affinity (siderophile, chalcophile, lithophile) as the “spike element” and, (iii) when spikes occur in one mass scan only. The presence of occasional spikes during gas blank analyses constrains that spikes can be artefacts. On the other hand, occasional spikes could be caused by micro-phases (e.g. small sulfide or oxide grains). Since it is impossible to unambiguously state whether signal

spikes resulting from sampled micro-phases, interpretation of such spikes is simply impossible. Thus, for “cosmetic” reasons occasional spikes within the sample were removed manually and replaced by the average of the acquisition points prior and after the spike. After spike correction, the average background signal was subtracted from each individual mass scan of the respective sample or standard measurement.

The different material properties of samples and calibration materials result in highly variable amounts of material being ablated (e.g. Horn et al. 2001). In the heterogeneous mix of materials that make up chondrites, the ablation yield will significantly vary locally. The most common strategy to correct for variable ablation yields is internal standardization to an element of known concentration in the sample (Longerich et al. 1996). For chondrite samples such an internal standard element would need to be determined prior to LA-ICP-MS analyses by an independent method such as electron microprobe. As discussed in the introduction, the application of such an internal standard element, i.e. the spatial fit between electron microprobe and laser data, cannot be accurately achieved for heterogeneous chondritic matter. Alternatively, the sum of major element signals from the ablated material itself can be applied as an internal standard (Hofmann et al. 1997; Leach and Hieftje 2000; Halicz and Günther 2004; Liu et al. 2008). This strategy however, requires that all major and minor elements that contribute significantly to the total are accurately determined. For this purpose, we determine all major and minor elements from Na to Zn, with the exception of K and V that contribute <0.1 and <0.01 wt. % to *bulk* chondrite samples and oxygen. Oxygen however contributes between 28 and 46 wt. % to the chondrite mass. Therefore, all the analyzed elements have to be recalculated as oxides, sulfides and metals based on reasonable assumptions about their importance. Finally carbon and H₂O can be abundant in the matrices of at least some chondrite groups where C and H₂O can contribute up to 3.5 and more than 10 wt.% (Cold Bokkeveld is highly hydrated and contains 13.5 wt. % water (Chapter 2) and 2.16 wt. % C (Pearson. et al. 2006), respectively. Since H₂O cannot and C is not analyzed by the method employed here, all data reported for chondrite thick sections will be reported on a dry and carbon-free basis. This may as well be viewed as an advantage as elemental concentrations for example between chondrules and hydrated matrix are compared based on their “mineral content” rather than being diluted by water and carbonaceous components.

The custom-designed calibration material CANS contains only two well determined trace elements, Se and Te (Table 2.2 in Chapter 2). Thus, NIST SRM 612 is employed for trace element calibration. To combine the use of CANS and NIST SRM 612 for the external calibration of major, minor and trace elements, an ablation yield correction is applied, using internal standardization to an element of about similar concentration C in both calibration materials. Here, Al is chosen to calculate the ablation yield correction factor (AYCF) and it is shown below that many other elements are consistent with this choice:

$$AYCF_{\text{NIST-CANS}} = (\text{cps}_{\text{Al}} / C_{\text{Al}})_{\text{NIST SRM 612}} / (\text{cps}_{\text{Al}} / C_{\text{Al}})_{\text{CANS}} \quad (1)$$

Average signal intensities obtained for NIST SRM 612 trace elements are then divided by $AYCF_{\text{NIST-CANS}}$ in order to provide a consistent CANS (major and minor elements and Se, Te) - NIST SRM 612 (trace element) set of intensities for the quantification of COBO or chondrite samples. A comparison of possible internal standard elements is given below. Once the NIST SRM 612 signal intensities are in line with those for CANS, the elemental concentrations in the sample (C_{spl}) are calculated by multiplying the concentration in the calibration materials (C_{calib} ; CANS-NIST SRM 612) with the ratio of the signal intensities of the sample (cps_{spl}) to that for the calibration materials ($\text{cps}_{\text{calib}}$).

$$C_{\text{spl}} = C_{\text{calib}} \times \text{cps}_{\text{spl}} / \text{cps}_{\text{calib}} \quad (2)$$

The abundances obtained are not yet corrected for variable ablation yields between CANS-NIST SRM 612 on one hand and COBO on the other. For this purpose, the major and minor element abundances in the sample are converted into compound abundances (e.g. as SiO_2 , FeO , FeS) in wt. % and summed up. After recalculation of elemental concentrations into compounds the ablation yield correction factor ($AYCF_{\text{sum}}$) is calculated by dividing the expected sum, e.g. 100 (%) by the sum of the wt. % of major and minor element compounds in the sample ($C_{\text{comp. sample}}$):

$$AYCF_{\text{sum}} = 100 / \sum C_{\text{comp. sample}} \quad (3)$$

The $AYCF_{\text{sum}}$ is then multiplied with the abundances C_{spl} of major, minor and trace elements (in $\mu\text{g/g}$) for every acquisition point along the COBO or chondrite sample profile. Note that if “100” is used in Eq. 3, the elemental abundances are essentially calculated on a H_2O and carbon free basis.

3.3 RESULTS AND DISCUSSION

3.3.1 Homogeneity of CANS, COBO and NIST SRM 612

The homogeneity of the calibration materials was compared by laser ablation line scans on CANS and COBO powder tablets and NIST SRM 612 glass using $\sim 80 \mu\text{m}$ laser spot sizes. To evaluate the signal stability and hence homogeneity in more detail the median of the relative standard deviation (RSD in %) of the ion beam signals over ten 60 s line scans was calculated (Figure 3.1). CANS shows a median RSD of about 5% for all major and minor elements up to Zn, and slightly higher for the trace elements Se and Te. In contrast the median RSD observed for the same major and minor elements in NIST SRM 612 glass is often higher, in particular for Fe and Ti. Trace elements vary typically between 4 and 12 % (Figure 3.1). Signal stability over time within the COBO powder tablet shows that major and minor elements are as homogeneously distributed as in CANS, with the exception of P, Ca and Ti with median RSD of 9 to 19%, which could be a consequence of heterogeneously distributed trace phases like apatite and titanite. In COBO, signal intensities versus time for Ca and to a lesser extent S display correlated fluctuations (not shown). This might be a hint towards CaSO_4 precipitation related to the preparation of the COBO powder by wet milling. For other elements, this implies a fairly homogeneous distribution at the beam diameter (and the 1 mm length) scale. Trace elements in COBO tend to display larger fluctuations than in NIST SRM 612, exceeding 15% for W, Th and U. This could also relate to heterogeneously distributed trace phases, but more likely reflects low concentrations or heterogeneous contamination, as suggested for W below.

Taken together, homogeneity of CANS is considered suitable for the use as external calibration material and in fact it is superior or equal to NIST SRM 612 for most of the elements incorporated. In terms of homogeneity the COBO powder tablet is also considered to be suitable

for many but not all elements as a quality control or external calibration material. At least for Ca and S some improvement in the preparation of powder tablets from natural chondrite materials is required. Because of the low concentration of Fe and the large scatter associated NIST SRM 612 appears to be not well suitable as external calibration for Fe rich materials such as chondrites if 100% standardization is required.

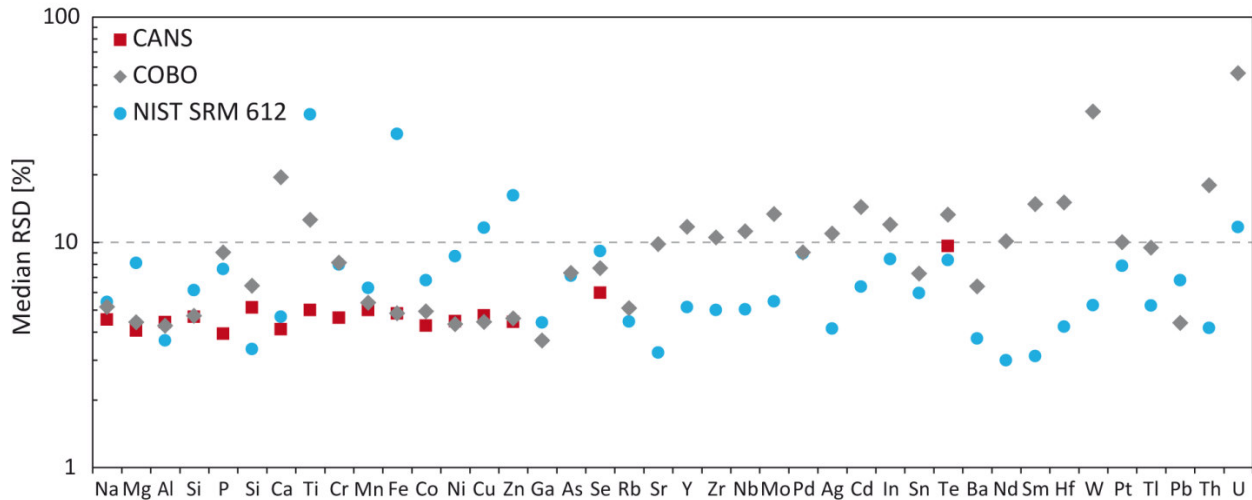


Figure 3.1 LA-ICP-MS signal stability (median of RSD in %; $n = 10s$) for CANS (red square) and COBO (gray diamond) powder pellets and NIST SRM 612 glass (blue circle).

3.3.2 Comparison of ablation yields for NIST SRM 612, CANS and COBO

General sources of uncertainties in LA-ICP-MS analysis are imperfect reference materials for external calibration, instrumental drift, and interferences like oxides and doubly charged ions. Interferences induced by oxides and doubly charged ions (e.g., $^{39}\text{K}^{16}\text{O}$ and $^{38}\text{Ar}^{16}\text{OH}$ on ^{55}Mn or $^{50}\text{Ti}^{2+}$ on ^{25}Mg) were minimized by optimizing the carrier and make-up gas flows to suppress the oxide formation while interferences caused by gas based polyatomic ions such as $^{36}\text{Ar}^{40}\text{ArH}^+$ were simply corrected by subtracting the count rates of the gas blank that was measured prior to every measured standard or sample. Additional sources of uncertainty in the present method are variable oxidation states of major elements and the consideration of compounds (H_2O , C mainly as graphite, carbonate and organics, and K) that were not measurable or analyzed but may be (locally) present in chondrite samples in significant amounts.

The present method employs two different external calibration materials, CANS for major and minor elements, Se and Te and NIST SRM 612 for trace element calibration. Prior to data evaluation CANS and the NIST glass need to be connected. For this purpose, the measured counts for NIST SRM 612 are adjusted to the counts obtained for CANS by internal normalization to an element of similar concentration in both calibrants (Eq. 1). Different internal standard elements could result in different ablation yield correction factors (AYCF) due to matrix dependent element fractionation effects, especially for elements with different properties (first ionization potential, mass, volatility) (e.g. Gaboardi & Humayun 2009), or if the accurate analysis of the element is hampered by low concentration or heterogeneous distribution in (one of) the calibration materials. Aluminum was chosen for ablation yield correction, but for comparison the AYCF was first calculated for all elements present in both CANS and NIST SRM 612 (and COBO, see below) (Figure 3.2 a). For example, $\text{AYCF}_{\text{NIST-CANS}}$ of one means that NIST SRM 612 and CANS were ablated to the same extent while a factor >1 mean that NIST SRM 612 was ablated to a greater extent. For Al, the average ablation yield calculated from ten pairs of line scans obtained on two different days of NIST SRM 612 and CANS is equal to 1 ± 0.5 . Thus on average the same amount of matter was ablated for both calibration materials. In detail, $\text{AYCF}_{\text{NIST-CANS}}$ changed progressively from 1.3 at the beginning to 0.8 at the end of the second day, possibly due to drift in the laser conditions. $\text{AYCF}_{\text{CANS-COBO}}$ and $\text{AYCF}_{\text{NIST-COBO}}$ were 0.56

± 0.12 and 0.54 ± 0.16 , respectively which mean that much more material was ablated from the COBO powder pellet than from CANS or NIST SRM 612.

In Figure 3.2, the ablation yields are plotted for different elements relative to that of Al for comparison. The combined uncertainties plotted in Figure 3.2 include the 2sd from the ten pairs of analysis and the uncertainties stated for the preferred values for CANS and COBO in Chapter 2. In Figure 3.2a ablation yields for the NIST SRM 612 – CANS pair agree for most elements with that for Al within uncertainty or are at least very close (Ca and Si). Furthermore, there is no systematic fractionation between light and heavy mass elements from Na to Se or Nd (the latter is a contaminant in CANS that may not be as reliably quantified; see Chapter 2). However, ablation yields calculated from Fe, Mg and P which are of low concentration in NIST SRM 612 compared to CANS apparently suggest that NIST SRM 612 was ablated with about 40% higher efficiency. These inconsistent results for Fe, Mg and P show that these elements in NIST SRM 612 cannot be used for accurate quantification. Zinc, In (another contaminate element in CANS) and Te, three volatile elements, display lower values for the ablation yield. Surprisingly, S and Se agree well with an ablation yield of Al and most other elements. These observations suggest possible matrix dependent elemental fractionation effects for some volatile elements (e.g. Koch & Günther 2007). When calculated ablation yields for different elements are compared to that of Al for the CANS-COBO pair in Figure 3.2b, again most data agree within uncertainty with that of Al and no systematic dependence on mass is observed. However, some elements like S, Ca and Ti appear to show systematic deviations. These deviations are still within uncertainty (except for Ti) but only because of the large variations in the 10 analysis of COBO. The apparent ablation yield for the volatile elements Se and Te are about 20% higher which may again indicate matrix dependent elemental fractionation for volatile elements.

When the Al normalized ablation yields are compared for NIST SRM 612 and COBO, it becomes apparent that the ablation yield for only about half of the elements agrees with that of Al within uncertainty. For Mg, P and Fe this again relates to the low abundance in NIST, and S and Ca probably deviate due to their loss as CaSO_4 during the wet preparation of the COBO powder. As with the CANS-COBO pair, the Se ablation yield for NIST SRM 612 - COBO is by about 20 % to high. We suggest without further proof that Se was partially lost along with S and Ca during the powder preparation. Strontium and Y are the other two elements that display an about 20% higher apparent ablation yield. It seems likely the COBO reference values are not accurate

enough. This is especially conceivable for Sr, since we used the Sr (and Mo) CM2 reference value of Lodders and Fegley (1998) as representative for COBO. Tungsten falls way below the apparent ablation yields for any other element. This large discrepancy can only be explained by contamination during the preparation of the powder tablet. In fact, the CANS tablet contains similar amounts of W and Pb than COBO although these elements were not detectable in the CANS powder during solution analysis, which suggests that W and Pb became contaminated during preparation of the powder tablets. Apart from W and Pb, other trace elements such as Zn, Ga, As, Rb, Pd, Ag, Cd, In, Tl and Th display lower apparent ablation yields by about 20 to 50 %, (the latter value for Cd). With the exception of Th and Pd, these are rather volatile elements. Thus some matrix effects seem likely, but contamination during powder preparation, occasional systematic errors in some reference values and interferences cannot be excluded. The observation that the heavy refractory trace elements Zr, Nd, Sm, Hf display the same ablation yield than light and medium elements like Na, Al and Co, Ni, Cu show that matrix dependent mass discrimination effects are insignificant.

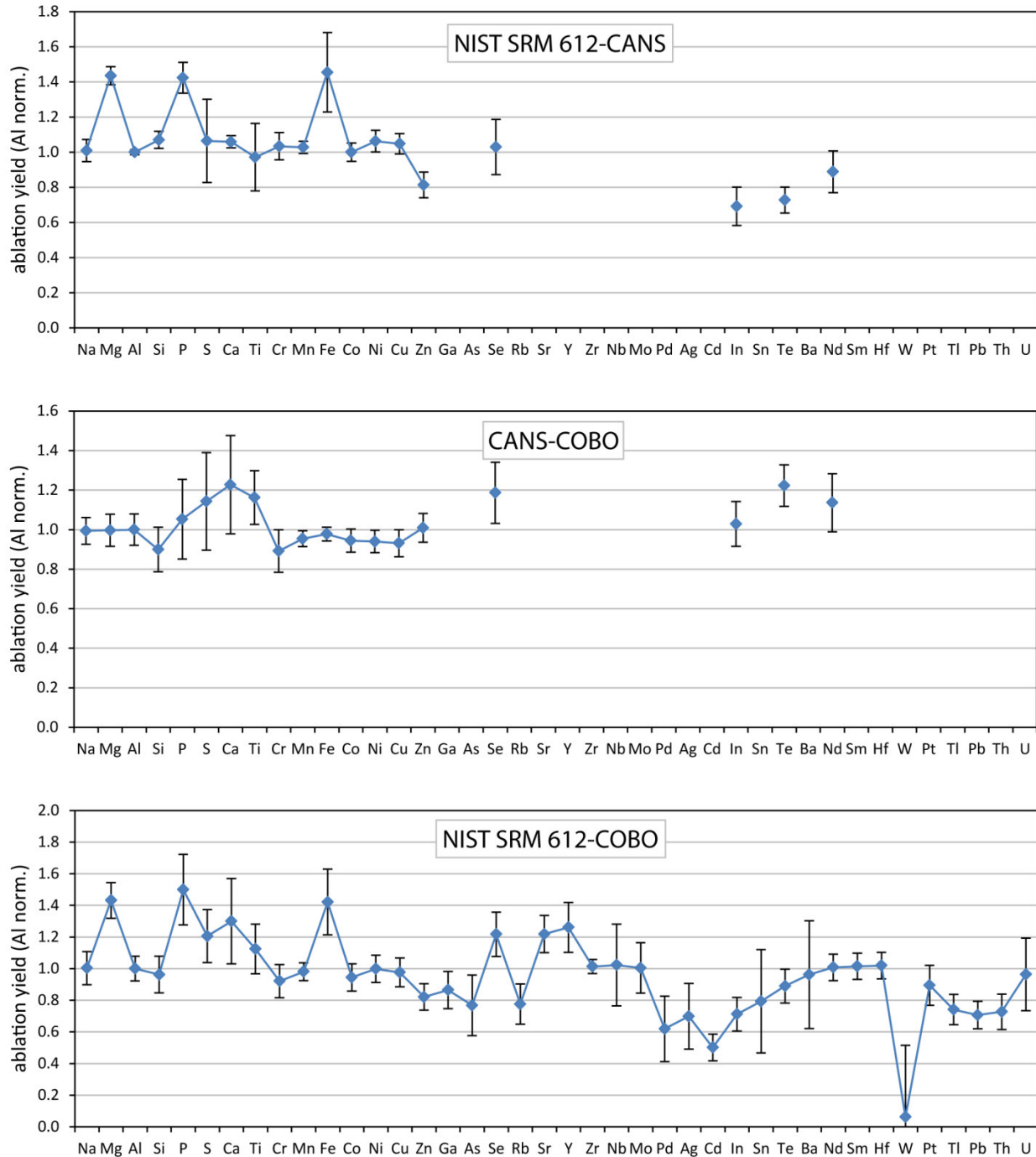


Figure 3.2 Comparison of ablation yields (e.g. cps per $\mu\text{g/g}$ element in CANS / cps per $\mu\text{g/g}$ element in NIST SRM 612) calculated from different elements relative to the ablation yield for Al. a) CANS relative to NIST SRM 612; b) CANS relative to COBO and c) NIST SRM 612 relative to COBO. Uncertainties include 2 sd from 10 pairs of line scans and the uncertainties stated for CANS and COBO in Tables 2.2 and 2.3 (Chapter 2). Abundances for NIST SRM 612 are taken from the GeoReM database (Jochum et al. 1997, 2011), for CANS and COBO, the preferred values given in Chapter 2 are used, except for Mo and Sr that are taken from the CM2 chondrite reference in Lodders & Fegley (1998).

3.3.3 Evaluation by 100% sum standardization with external CANS-NIST calibration using COBO as a test sample

Figure 3.3 shows LA-ICP-MS data obtained for COBO relative to the preferred values that were mainly determined by solution nebulization ICP-MS (Chapter 2). For this comparison, the COBO reference data were first recalculated on a dry basis by dividing the $\mu\text{g/g}$ abundances by 0.8 based on the observed sum of major element components (as given in Table 2.3, Chapter 2, minus H_2O and carbon). The laser ablation data for COBO are first calculated from the background corrected intensities without yield correction using Eq. 2 and the combination of CANS-NIST SRM 612 linked by Al (Eq. 1).

For the yield correction, the 100% sum standardization was applied. All analyzed major and minor elements up to the mass of Zn were recalculated as wt. % oxide components (as specified in Table 2.3, Chapter 2). The sum of these components then provides the AYCF_{sum} , which is applied for the yield correction of the $\mu\text{g/g}$ abundances (Eq.3).

Many major, minor, and trace element data (Na, Mg, Al, Mn, Fe, Co, Ni, Cu, Zn, Zr, Mo, Ba, Nd, Sm, Hf and U) match the reference values within 5% relative deviation. Silicon, P, Cr, Nb and Pt agree within 10%. The major elements S, Ca and the minor element Ti deviate by 15 to 21 %, and some trace elements by up to 30% or more for Pd, Ag, Cd, In, Pb and Th, with W deviating by 1600 % due to contamination. As already discussed above for apparent yield correction factors, deviations may be caused by several processes, including interferences, contamination, inaccurate reference values, matrix effects and losses during wet COBO powder preparation. Figure 3.3 also reports data for COBO with calibration based on NIST SRM 612 only. In this case concentrations for Mg, P and Fe are more than 20% lower than the reference values. Because of the systematic error in the determination of the major element components of Mg and Fe other elements determined by LA-ICP-MS are systematically displaced to higher values, typically by 16 %.

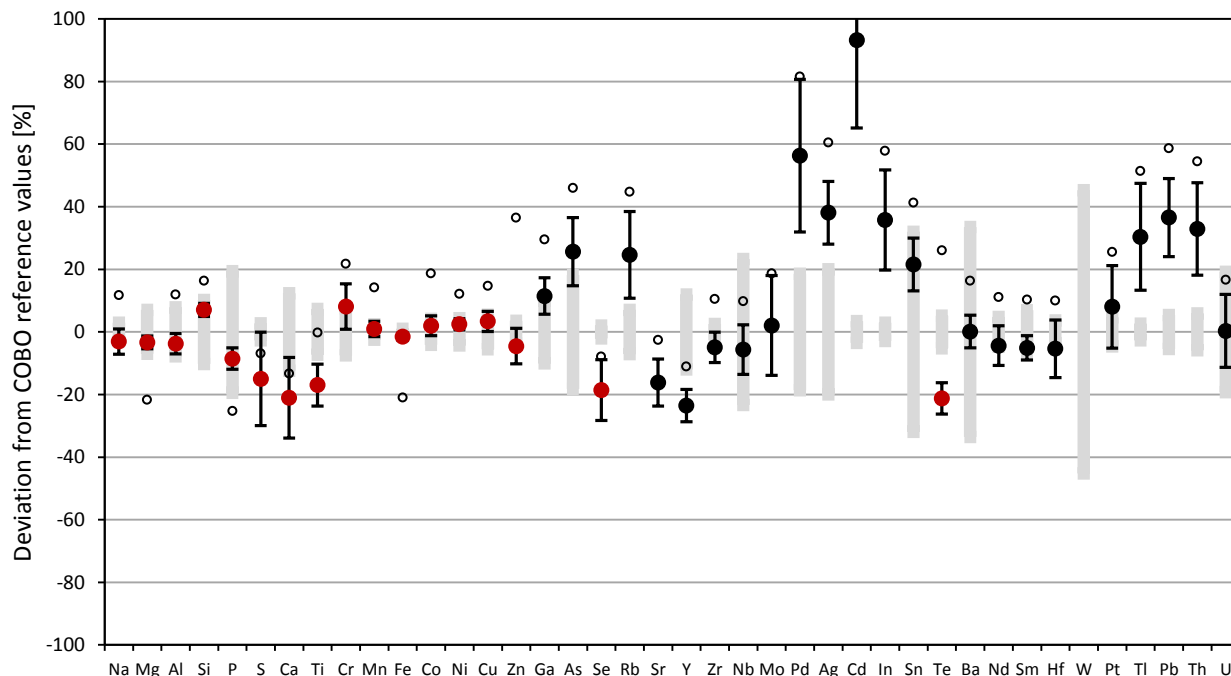


Figure 3.3 Percent deviation for COBO analyzed by fs-LA-ICP-MS with 100% sum standardization, relative to COBO reference data scaled to 100% (preferred values in Table 2.3, Chapter 2; Mo and Sr from CM2 reference Lodders & Fegley, 1998). Large filled circles: 100% sum standardization to CANS; red circles analyzed relative to CANS; black circles analyzed relative to NIST SRM 612 linked to CANS via Al (see text). Small black open circles: 100% sum standardization and analysis based on NIST SRM 612 only. Uncertainties: Thin bars refer to 2 sd from 10 pairs of COBO and linked CANS-NIST SRM 612 line scans. Wide light grey bars represent uncertainties for preferred COBO values (Table 3.3, Chapter 2).

3.4 CONCLUSION

The use of CANS allows much better yield corrections based on the sum of major element components, while the use of NIST SRM 612 alone would result in systematic errors of typically 16%. The use of CANS combined with NIST SRM 612 allowed a rather accurate quantification of many major, minor and trace elements. However, for several elements, especially for As, Rb, Pd, Ag, Cd, In, W, Tl, Pb and Th that deviate by > 25%, the applicability of the method is difficult to assess at this stage as the exact cause of the deviations is presently unknown. If these deviations result from contamination or inaccurate reference values for COBO, data for real

samples may be accurate. However, if these deviations are caused by interferences reasonable quantification may not be achieved. For some of the critical elements this can be further tested with additional isotopes.

Powder tablets prepared from natural chondrite samples such as COBO may serve as alternatives to the calibration using CANS-NIST SRM 612 for in-situ analysis of chondrite thick sections. However, some problems observed here should be overcome: The heterogeneity of S, Ca and Ti and contamination e.g. for W introduced by the preparation. Also the elemental abundances in such a chondrite powder reference material need to be known with high confidence to avoid systematic errors. Furthermore, the low average abundance of some trace elements in chondrite powders will result in some error magnification.

There are more things to consider if the method discussed here is applied to chondrite thick sections. In natural chondrite samples Fe, S, and Mn coexist with different oxidation states which leads to different weights of compounds, depending on the number of oxygen atoms bond to the elements. These different weights lead to different totals and therefore to different ablation yield correction factors, if 100% sum standardization is applied as in the present method. The extent of the uncertainties caused by different oxidation states largely depend on the concentration of the element in the sample. While the uncertainty produced by the different oxidation states of Mn is negligible caused by its low concentration, different oxidation states of the highly abundant elements Fe and S can result in seriously different totals depending on the expression as oxide or elemental compounds (e.g. Fe^0 , FeO, Fe_2O_3 ; S^0 , SO_3). The different weight of Fe and S compounds then affect the total wt. % that is used to calculate the AYCF. Mass balance calculations based on data by Howard et al. 2011 suggest that 47% of the Fe in oxides and silicates (olivine, cronstedtite, and magnetite) in Cold Bokkeveld (COBO) is in the 3+ state. According to Orthous-Daunay et al. (2010) 41% of the total sulfur within the CM2 chondrite Cold Bokkeveld is bond to iron (as sulfides), 3 % is oxidized in CaSO_4 , and 56 % is bond to organics. These data formed the basis for the ablation yield calculated above (cf. Chapter 2) with the sulfur bond to organics being simply treated as elemental S. A second case was evaluated were the different oxidation states of S and Fe were simply ignored and all S was calculated as FeS, while the remaining Fe was calculated as FeO. This results in deviations in concentrations by about 1 % only for single elements and can therefore be considered as negligible. However, in extreme cases, where perhaps locally all Fe and S would be reduced or oxidized as Fe_2O_3 and

SO₄²⁻ the systematic deviations will amount to -6 and +9% in these extreme cases. This may be relevant if chondrite components are analyzed that differ substantially from the bulk composition, e.g. sulfide/metal assemblages in otherwise oxidized chondrites. In most applications, this will not be critical. However, matrix dependent element fractionations may be more different from e.g. the CANS-NIST SRM 612 standard used for the calibration even with fs-laser ablation. These issues need to be kept in mind if such data is interpreted.

LA-ICP-MS offers a rapid opportunity to monitor the distribution of a large set of trace elements among chondritic components compared to the time consuming data generation by solution nebulization ICP-MS which requires handpicking of components and acid digestion. Furthermore, in-situ analysis by laser ablation offers a better control of the material analyzed than handpicking, where for example chondrule rims and matrix are difficult to distinguish.

Chapter 4

Sulfur, selenium and tellurium abundances and distributions in chondrites and their components

4.1 INTRODUCTION

The formation of the solar system, including the formation of chondritic components, planetesimals, and planets involved various stages of thermal processing during which volatile elements were fractionated from the initial solar system elemental abundance. The fractionation patterns, especially in carbonaceous chondrites are generally a smooth function of the half-mass condensation temperature ($50\%T_c$). The process that could have caused these patterns is still under debate (see Chapter 1.5), but the main models are based on fractional evaporation (*e.g.* Anders 1964; Larimer & Anders 1967; Alexander 2004; Alexander et al. 2008; Grossman et al. 2007; Huss et al. 2003; Huss 2004; Yin 2005) or incomplete condensation (*e.g.* Wasson & Chou 1974; Wai & Wasson 1977; Cassen 1996, 2001). In addition to the primary (pre-accretion) depletion of volatiles, further depletion and or redistribution of highly volatile elements can occur on the parent body due to thermal metamorphism (*e.g.* Wombacher et al. 2008; Schaefer & Fegley 2010; Schönbachler et al. 2008; Luck et al. 2005). Volatile element abundances may also be affected by aqueous alteration (*e.g.* Lodders et al. 2009; Morlok et al. 2006; Barrat et al. 2012), and terrestrial weathering (*e.g.* Dreibus et al. 1995).

Different chondrite classes display different abundances and ratios of the moderately volatile elements S, Se and Te (*e.g.* Funk et al. 2012a, b; Wang & Becker 2013b, Kadlag et al. 2014c). Elemental abundances in unequilibrated chondritic meteorites are largely controlled by the host phases contained in their major components - chondrules and matrix. To understand the elemental fractionation in bulk chondrites it is thus essential to study the elemental abundances and distributions among different chondritic components.

Sulfur, Se and Te are well suited to study the various chemical processes involved in the formation of inner solar system materials. The major element sulfur, and the trace elements Se

and Te belong to the moderately volatile elements and have very similar equilibrium 50% condensation temperatures (50% T_c : S ~ 664 K; Se ~ 697 K; Te ~ 709 K) at 10^{-4} bar total pressure (Lodders 2003). The relatively low condensation temperatures, makes these elements sensitive to thermal processes and one would expect that all three elements behave similarly during evaporation and or condensation under nebula conditions. However, theoretical calculations (Lodders 2003), heating experiments (Ikramuddin et al. 1977), and metal-silicate partitioning experiments (Rose-Weston et al. 2009) imply that Te tends to be more sensitive to changes in pressure and temperature than S and Se in different environments and is therefore potentially suited as indicator for nebula, parent body, and planetary conditions. Sulfur and to a smaller extent also Se are highly mobile in aqueous fluids and are therefore indicative for parent body aqueous alteration and terrestrial weathering (*e.g.* Dreibus et al. 1995; Gao & Thiemens 1993).

Sulfides are the predominant S-bearing phases in chondrites. Additionally, sulfates form during aqueous alteration and S can be bond to organic molecules (*e.g.* Orthous-Daunay et al. 2010). According to Dreibus et al. (1995) Se is purely chalcophile and condenses exclusively into sulfides. Recent investigations on magnetic and non-magnetic separates of unequilibrated ordinary and enstatite chondrites, however showed that a significant portion of Se may be also contained in the metal. Furthermore, it was shown that most of the Te is incorporated in metals and minor in the sulfides (Kadlag & Becker 2013a, b, 2014; Kadlag et al. 2014). This indicates that Se, and Te have siderophile and chalcophile affinities in ordinary and enstatite chondrites. In the Earth, all three elements become more siderophile with increasing pressure and temperature (Rose-Weston et al. 2009). It is therefore assumed, that S, Se and Te partition into the Earth core during differentiation. The excess of these elements as well as the excess of highly siderophile elements (HSE) in the bulk silicate Earth is therefore assumed to result from the accretion of a chondritic “late veneer” after core formation (*e.g.* Rose-Weston et al. 2009; Wang & Becker 2013b). Because different chondrite classes are characterized by different fractionation patterns of S, Se, and Te – precise data for chondritic meteorites can help to further constrain the type of chondritic material that delivered moderately volatile siderophile and chalcophile elements in the late accretion phase of the Earth.

Here, accurate and precise isotope dilution concentration data for S, Se, and Te from the same sample aliquot from 54 bulk samples of carbonaceous, ordinary, enstatite, and Rumuruti

chondrites are presented. Additionally, a novel femtosecond laser ablation ICP-MS method (Chapter 3) was applied to investigate the distribution and abundances of S, Se, and Te among different components (*e.g.* chondrules, matrix and CAIs) in Allende (CV3), Semarkona (LL3), and Indarch (EH4). This method takes advantage from new and innovative external calibration material based on nanoparticles (*cf.* Tabersky et al. 2014) and internal standard independent ablation yield correction (Haliz & Günther 2004; Liu et al. 2008). From in-situ analyses by laser ablation ICP-MS it was possible to detect the S, Se, and Te carrier that control the S, Se and Te abundances in bulk Allende, Semarkona, and Indarch. The combination of in-situ and bulk analysis allows better constraints on the distribution of the moderately volatile elements S, Se, and Te in different chondritic materials (indicative for different environments) and reasons for their fractionation from solar system abundance ratios.

4.2 ANALYTICAL METHODS

4.2.1 Isotope dilution ICP-MS analysis of S, Se and Te

Sample preparation

Most chondrites used for bulk isotope dilution ICP-MS analysis are falls or Antarctic finds with low weathering grades. The Rumuruti chondrite NWA 753 (R3.9), Acfer 187 (CR2), Acfer 182 (CH2), and the EH3 chondrite Sahara 97072 are desert finds. Fresh chips (typically 300 – 700 mg) were pre-crushed using an agate mortar. Subsequently, coarse grained samples were milled to fine-grained powders with a Fritsch pulverisette 23 agate swing mill. For LA-ICP-MS measurements thick sections of 250 μm thickness were prepared from Allende (CV3), Semarkona (LL3), and Indarch (EH4).

Typically 50 mg aliquots of homogenized sample powders were weighted into 7 ml PFA beakers and mixed with spike solutions enriched in ^{34}S , ^{77}Se and ^{125}Te . Details about spike preparation and calibration are given in Chapter 2.3.2. Sample-spike mixtures were first oxidized with 1 ml 14 M HNO_3 and 0.1 ml H_2O_2 and then dried down at 65°C. Subsequently, 2 ml of each, conc. HNO_3 and conc. HF were added for sample digestion and capped beakers were placed on a

hot plate at 120°C for 48 h. After digestion an aliquot was taken for sulfur analyses. This aliquot was dried down and redissolved in 3 ml of 0.14 M HNO₃ and further diluted to S contents of about 1 µg/g in 0.14 M HNO₃ for analysis. The remaining bulk sample solution used for Se and Te analyses was dried down, taken up in 2 ml 6 M HCl and refluxed for 24 h at 80°C to ensure complete conversion of Se(VI) and Te(VI) to the 4+ oxidation state (*e.g.* Marin et al. 2001; Wang et al. 2013a). This solution is dried down again, taken up in 6 ml 6 M HCl and refluxed for another 24 h at 80°C. After cooling, the sample was diluted with ultrapure water (18.2 MΩ) to achieve 36 ml of 1 M HCl sample solution. Thiol cotton fibers (TCF) were employed for the separation of Se and Te from sample matrices. Preparation of TCF followed the protocols of Yu et al. (2002); Rouxel et al. (2002); Elwaer & Hintelmann (2008); König et al. (2012) and Mitchell et al. (2012). For this purpose, a mixture of 20 ml thioglycolic acid (96-99%), 14 ml acetic anhydride (99.9%), 6.4 ml glacial acetic acid, 0.064 ml sulfuric acid (97.5%) and 2.5 ml 18.2 Ω water is added to 6 g medical grade hydrophilic cotton in a brown wide mouth borosilicate glass bottle. The capped bottle is then placed into a water bath at 40 ± 2°C for 5 days with the mixture slued gently twice a day. The treated cotton was then air dried for two days. While Se(IV) and Te(IV) have a strong affinity for the thiol cotton fibers (Yu et al. 2002), all major elements pass through the columns.

Chemical separation of Se and Te

Following the protocol of Rouxel et al. (2002), diluted sample solutions were loaded onto 5 ml polypropylene columns. The columns were filled with 140 mg of TCF, previously washed with 3 ml H₂O and conditioned with 2 ml of 6 M HCl and 2 ml of 1 M HCl. Both Se and Te are finally eluted together by destruction of the functional groups of the TCF. For destruction the TCF was transferred to 10 ml test tubes and mixed with 0.5 ml 7 M HNO₃. Test tubes were capped and left at room temperature for 20 minutes. Afterwards, the test tubes were put into a boiling water bath for another 20 minutes, and subsequently diluted with 4.6 ml ultrapure water. Samples were centrifuged and filtered through a 0.45-µm filter with a syringe to remove the cotton fibers from the sample solution. For Se and Te analyses the solution was split and mixed with 0.25 ml 10 M HCl to ensure that both, Se and Te are in the reduced 4+ state.

Hydride generation MC-ICP-MS analyses of Se and Te

For Se and Te isotope ratio analysis a Thermo Finnigan Neptune MC-ICP-MS equipped with an ESI SC-2 autosampler and a home-made hydride generator (cf. Wombacher et al. 2009; König et al. 2012) was utilized. Hydride-liquid separation was achieved within a borosilicate glass spray chamber consisting of a cyclonic and Scott type chamber arranged in tandem. Using the built-in peristaltic pump, about 0.7 ml/min of the sample solution (in 0.56 M HNO₃) and the reducing agent (freshly prepared 0.13 M NaBH₄ - 0.05 M NaOH) are fed via capillary tubes through the drain into the cyclonic chamber where both solutions mix at the spray chamber wall. The volatile Se and Te hydrides are carried to the plasma by an Ar gas flow of about 1.1 ml/min provided by a concentric nebulizer with a sealed sample inlet. Using a set of two Y connectors, the waste solution is removed by a second peristaltic pump through the same drain port that is used to introduce the sample solution and reductant. Hydride generation provides an extra separation from remaining matrix elements and, taking the higher uptake rate into account, a 10 – 15 times higher ion yield. The higher sensitivity is probably mainly due to the far more efficient delivery of Se and Te to the plasma. A one ppb solution yields about 20 mV for ⁸²Se and 400 mV for ¹²⁸Te using 10¹¹ Ω resistors. The cup configuration includes ⁷⁶Se, ⁷⁷Se, ⁷⁸Se and ⁸²Se and ¹²⁴Te, ¹²⁵Te, ¹²⁶Te, ¹²⁸Te and ¹³⁰Te. Each analysis comprises 20 cycles with an integration time of 4.2 s. Because Se and especially Te tend to stick to uptake tubing, rinsing with 0.56 M HNO₃ took up to 20 minutes. The background was then determined right prior to every standard and sample analysis. Measured background intensities are subtracted offline from the signal intensities recorded, subtracting both, residual Se and Te signals and contributions from gas blanks, e.g. ⁴⁰Ar³⁶ArH on ⁷⁷Se, ⁸²Kr on ⁸²Se and ¹²⁶Xe on ¹²⁶Te. Instrumental mass bias was monitored externally by repeated analysis of standard solutions and corrected using the natural ⁷⁷Se/⁸²Se of 0.87447 and ¹²⁵Te/¹²⁶Te of 0.376688 (Berglund & Wieser, 2011).

Sector field ICP-MS analyses of sulfur

Sulfur analyses were performed on an ElementXR sector field ICP-MS, using a Scott type PFA spray chamber, a microconcentric PFA nebulizer, medium resolution and counting mode. Sensitivity was ~ 2 x 10⁶ cps for ³²S. Mass, search and integration windows are set to 80, 80 and 40%. Data acquisition consists of 25 runs, 25 passes each, with 12, 60 and 24 ms on ³²S, ³³S and

^{34}S peaks. After rinsing for 2 minutes, the background, typically about 1 % of the intensities, is determined, the sample solution taken up and the measurement started. The background was always subtracted.

4.2.2 Femtosecond laser ablation ICP-MS analysis

A detailed protocol about the instrumental setup, data evaluation and assessment is given in Chapter 3. Relevant, additional information about the data and their usage is given here. Due to the rather large laser spot size of about 80 μm , which is necessary to detect trace elements and the depth of the laser track, the ablated sample material often consist of a mixture of silicates, metals, and sulfides so that we cannot expect stoichiometric concentrations and an identification of the Se and Te host phases is not always possible and is in most cases based on indirect observations. To identify metal for example, which is the expected host phase for Te, highly siderophile elements like Pt and Pd were included in the routine. For element plots (Figures 4.4, 4.5, 4.7, and 4.8) the element concentrations were carefully selected from regions in which the laser sampled well defined chondrules, fine-grained matrix, CAIs, an amoeboid olivine aggregate (AOA), and metal and sulfide rich components. For such plots, transitional acquisition points between components were avoided, so that the concentrations are mainly based on the signal intensities from the different components measured. Laser data are provided in the form of an electronic annex (CD-ROM). This study includes analysis for the carbonaceous chondrite Allende, the ordinary chondrite Semarkona, and the enstatite chondrite Indarch. Thus, the three major chondrite classes are included, but the individual samples cannot represent the three different chondrite classes in all respects.

4.3 RESULTS

4.3.1 Reproducibility and accuracy

The external reproducibility is evaluated from two relative standard deviations of repeated measurements (n = number of measurements) of different digestions (d = number of digestions) from Murchison (CM2), Cold Bokkeveld (CM2), the Allende (CV3) Smithsonian reference powder, and samples of other carbonaceous, ordinary, enstatite and Rumuruti chondrites (Tables 4.1 and 4.2). Additionally, a powder prepared from a weathered piece of the Allende CV3 chondrite was used as in-house standard and processed and analyzed by default together with every set of chondritic samples (Table 4.1). Sulfur reproduced within $\pm 1.5\%$ for Murchison ($n=12$; $d=5$), $\pm 2.7\%$ for Cold Bokkeveld ($n=18$; $d=6$), $\pm 2.4\%$ ($n=8$; $d=3$) for the Allende reference powder (Smithsonian Institute), and within $\pm 4.0\%$ for the weathered piece of Allende ($n=20$; $d=8$). For selenium the external reproducibility is $\pm 1.5\%$ for Murchison ($n=5$; $d=5$), $\pm 0.9\%$ for Allende ($n=3$; $d=3$), and $\pm 2.9\%$ for weathered Allende ($n=16$; $d=14$). Because Se and Te were only measured twice in Cold Bokkeveld, the reported values of $\pm 2.0\%$ for Se and $\pm 5.2\%$ for Te refers to the %-deviation of the two values from the average. For tellurium, we obtained $\pm 2.4\%$ for Murchison ($n=5$; $d=5$), $\pm 2.2\%$ for Allende ($n=3$; $d=3$), and $\pm 4.9\%$ for the weathered piece of Allende ($n=16$; $d=14$). Repeated digestions from the weathered Allende sample result in comparatively high deviations (2.9 to 4.9%). In contrast, the precision obtained from single digestions that were measured in triplicate and quadruplicate in repeated sessions offer reproducibilities of 0.4 and 1.1% for S, 0.5% for Se and 1.3% for Te. According to this, high deviations from individual digestions might be affected by sample powder heterogeneity. Comparing the S and Se concentrations of the Smithsonian reference powder from Allende with the concentrations of the weathered Allende sample show that the latter is depleted in S (-70%), and Se (-50%) while Te concentrations are in agreement with the Smithsonian powder and appear to be unaffected by terrestrial weathering.

Duplicates (in most cases different digestions) from further individual carbonaceous, ordinary, enstatite and Rumuruti chondrites are shown in Table 4.2. Since these samples were only analyzed twice, the “reproducibility” refers to the %-deviation from the mean value.

Selenium and Te concentrations for the CI chondrites Orgueil and Y-980115 were reproduced within 0.5%, while duplicates from the CM2 chondrites Mighei and Cold Bokkeveld and the CR2 chondrite GRA 95229 show %-deviations up to 5.2% for Te. Selenium and Te concentrations of most ordinary, enstatite and Rumuruti chondrites could be reproduced within 1%. Larger deviations of >2% were found for individual digestions from the ordinary chondrites ALH 77299 (H3), Bovedy (L3), GRO 95544 (L3), A-881567 (LL3), the enstatite chondrite Indarch (EH4), and the Rumuruti chondrite NWA 753. Such large deviations most likely result from sample heterogeneity (*e.g.* Wolf & Lipschutz 1995; Friedrich et al. 2002, 2003; Fehr et al. 2005; Wang & Becker 2013a) which is also supported by the observation that replicates from other samples which were processed and measured together, reproduced within 1%. Procedure blanks for S, Se and Te were always <90 ng for S, <0.4 ng for Se and <0.2 ng for Te and therefore considered negligible.

The accuracy was assessed by comparison of mean concentrations from this study with literature data from well examined chondrites like Orgueil (CI), Ivuna (CI), Murchison (CM2), and Allende (CV3) (Table 4.1). Sulfur, Se and Te concentrations for Orgueil and Ivuna deviate less than 4% from mean literature values. An exception is the conspicuously low sulfur concentration (-16 % deviation from literature mean) obtained for Orgueil, which most likely reflects sample heterogeneity. As mentioned by Lodders (2003) CI chondrites underwent extensive parent body aqueous alteration at which water soluble elements like S (*e.g.* Gao & Thiemens 1993) as well as Ca and Mn were heterogeneously redistributed by aqueous fluids and precipitated as sulfates and carbonates in cracks and pore spaces. According to this it is possible that different sample aliquots of Orgueil contain different concentrations of such water soluble elements. Selenium concentrations for Orgueil agree within 4% with data from Dreibus et al. (1995), Mittlefehld (2002), and Kallemeyn & Wasson (1981). The obtained Te abundance agree within 0.5% with data from Wang & Becker (2013b), Wang et al. (2014b), Lodders (2003), Anders & Grevesse (1989), Smith et al. (1977), and Loss et al. (1984). Sulfur, Se, and Te concentrations for Ivuna are in good agreement (< 2.2% deviation) with data from Lodders (2003), Dreibus et al. (1995), Loss et al. (1984), Burnett et al. (1989), Case et al. (1973). Sulfur and Se concentrations from Murchison are in excellent agreement (< 3.1%) with concentrations given by Makishima et al. (2009), Wolf et al. (2005), Wang & Lipschutz (2005), Dreibus et al. (1995), and Xiao & Lipschutz (1992). Te concentrations are in general agreement with data from

Makishima et al. (2009) and within uncertainty of Te concentrations given by Smith et al. (1977) but on average 9% lower when compared to ICP-MS data from Wang & Becker (2013b), Wang et al. (2014b), Wolf et al. (2005), Fehr et al. (2005), and Friedrich et al. (2002). As replicate analyses of five individual digestions yield good reproducibility (2RSD = 2.4%), lower Te concentrations might reflect heterogeneous distribution of Te bearing phases in Murchison. With deviations 2.6% for S, 1.8% for Se, and 3.4% for Te from average literature values, concentrations obtained for the Allende CV3 chondrite (Smithsonian reference powder) are in excellent agreement with literature values from Wang & Becker (2013b), Wang et al. (2014b), Makishima et al. (2009), Fehr et al. (2005), Dreibus et al. (1995), Yanai et al. (1995), Paul and Lipschutz (1990), Kaczaral et al. (1989), Loss et al. (1984), Kallemeyn & Wasson (1981), Fitzgerald (1979), Smith et al. (1977), and Clarke et al. (1970).

Table 4.1 Reproducibility of isotope dilution ICP-MS data and comparison with literature data

Sample	S		Se		Te		S/Se		Se/Te		
	[$\mu\text{g/g}$]	2 s.d.	2 RSD [%]	[$\mu\text{g/g}$]	2 s.d.	2 RSD [%]	[$\mu\text{g/g}$]	2 s.d.	2 RSD [%]		
Orgueil (CI) mean	45297			21.4		0.4"	2.29		0.2"	2116	9.4
Digestion 1				21.5			2.29				9.4
Digestion 2	45297			21.3			2.28			2125	9.4
<i>Wang and Becker (2013a)</i>				20.9	0.3		2.31	0.02			9.1
<i>Wang et al. (2014b)</i>	53900	400		20.4	0.2		2.34	0.04		2642	8.7
<i>Anders and Grevesse (1989)</i>	52500			18.2			2.27			2885	8.0
<i>Dreibus et al. (1995)</i>	54400	1414	2.6	21.4						2542	
<i>Lodders et al. (2009)</i>	53500	2675		20.3	1.4		2.28	0.16		2635	8.9
<i>Loss et al. (1984)</i>							2.24	0.09	4.2		
<i>Smith et al. (1977)</i>							2.34	0.35	15.2		
<i>Kallemeyn and Wasson (1981)</i>				21.5	1.8	8.4					
<i>Mittlefehldt et al. (2002)</i>				21.3							
<i>Wiik H. B. (1969)</i>	54900										
Mean literature:	53840			20.6			2.3			2616	9.0
Deviation from literature [%]:	-16			4.0			-0.5				
Ivuna (CI) mean	51001		0.4"	20.6			2.26			2481	9.1
Digestion 1	50802										
replicate	51200										
<i>Lodders (2003)</i>	50820	10100	19.9	20.0	2.2	11.0	2.34	0.44	18.8	2541	8.5
<i>Dreibus et al. (1995)</i>	53500			21.1						2536	
<i>Loss et al. (1984)</i>							2.27	0.04	1.8		
<i>Burnett et al. (1989)</i>				20.7							
<i>Case et al. (1973)</i>				20.5							
Mean literature:	52160			20.6			2.28			2535	9.0
Deviation from literature [%]:	-2.2			-0.07			1.1				
Murchison (CM2) mean	29171	439	1.5	12.5	0.19	1.5	1.37	0.03	2.4	2336	9.1
Digestion 1				12.5			1.35				9.2
<u>Digestion 2 (mean)</u>	29216	164	0.6								
replicate	29226										
replicate	29129										
replicate	29292										
<u>Digestion 3 (mean)</u>	29382	134	0.5	12.6			1.38			2332	9.1
replicate	29401										
replicate	29437										
replicate	29307										
<u>Digestion 4 (mean)</u>	29164	292	1.0	12.5			1.36			2335	9.2
replicate	29002										
replicate	29286										
replicate	29204										
Digestion 5	29782 #			12.5			1.38			2375	9.1
Digestion 6	28799			12.4			1.39			2332	8.9
replicate	28799										
<i>Wang and Becker (2013b)</i>				14.1			1.56				9.0
<i>Wang et al. (2014b)</i>	30400	300	1.0	13.8	0.1	0.7	1.58	0.02	1.3	2203	8.7
<i>Makishima et al. (2009)</i>	27000	2646	9.8	12.3	0.7	5.7	1.32	0.07	5.3	2195	9.3
<i>Wolf et al. (2005)</i>				12.5			1.52				8.2
<i>Wang and Lipschutz (2005)</i>				12.6			1.60				7.9
<i>Dreibus et al. (1995)</i>	30300			12.8						2367	

Table 4.1 continued

Sample	S		Se		Te		S/Se		Se/Te		
	[µg/g]	2 s.d.	2 RSD [%]	[µg/g]	2 s.d.	2 RSD [%]	[µg/g]	2 s.d.	2 RSD [%]		
<i>Xiao and Lipschutz (1992)</i>				12.6	0.8		1.66				7.6
<i>Kallemeyn and Wasson (1981)</i>				13.2	1.7	12.9					
<i>Smith et al. (1977)</i>							1.53	0.01	0.9		
Mean Murchison literature:	29233			13.0			1.54			2251	8.4
Deviation from literature [%]:	-0.2			3.1			8.8				
<u>Cold Bokkeveld (CM2) mean</u>	27589	754	2.7	12.3	2.0"		1.44	5.2"		2252	8.5
Digestion 1				12.0			1.36				8.8
<u>Digestion 2 (mean)</u>	27013	330	1.2								
replicate	27237										
replicate	26859										
replicate	27029										
replicate	26926										
Digestion 3	28145										
replicate	27829										
<u>Digestion 4 (mean)</u>	27840	124	0.4								
replicate	27810										
replicate	27825										
replicate	27762										
replicate	27917										
replicate	27888										
<u>Digestion 5 (mean)</u>	27506	200	0.7	12.5			1.51			2200	8.3
replicate	27462										
replicate	27493										
replicate	27649										
Digestion 6	27557										
replicate	27367										
<u>Digestion 7 (mean)</u>	27923	147	0.5								
replicate	27975										
replicate	27871										
<i>Dreibus et al. (1995)</i>	30200			12.2							
<i>Kallemeyn & Wasson (1981)</i>				11.6	1.3	10.9					
<i>Mittlefehldt et al. 2002</i>				13.3							
<i>Wiik, H. B. (1980)</i>	29800										
<i>Zolensky et al. (1997)</i>				12.9			1.33				9.7
Mean Cold Bokkeveld literature:	30000			12.5			1.33			2400	9.4
Deviation from literature [%]:	8.7			2.0			-7.3				
<u>Allende (CV3) mean</u>	19755	473	2.4	8.5	0.08	0.9	0.92	0.02	2.2	2321	9.3
Digestion 1				8.5			0.93				
<u>Digestion 2 (mean)</u>	19855	66	0.3								
replicate	19875			8.6			0.91				
replicate	19817										
replicate	19873										
<u>Digestion 3 (mean)</u>	19907	112	0.6								
replicate	19967			8.5			0.92				
replicate	19899										
replicate	19856										
Digestion 4	19376										
replicate	19380										
<i>Wang and Becker (2013b)</i>	20500			8.7	0.2	1.8	1.02	0.24	23.6	2359	8.6
<i>Wang et al. (2014b)</i>	20100	200	1.0	8.25	0.02	0.2	0.94	0.01	1.1	2436	8.8

Table 4.1 continued

Sample	S		Se		Te		S/Se		Se/Te		
	[µg/g]	2 s.d.	2 RSD [%]	[µg/g]	2 s.d.	2 RSD [%]	[µg/g]	2 s.d.	2 RSD [%]	S/Se	Se/Te
<i>Makishima et al. (2009)</i>	20666	2540	12.3	7.9	0.7	8.6	0.86	0.10	11.6	2603	9.2
<i>Fehr et al. (2005)</i>							1.02	0.13	12.8		
<i>Dreibus et al. (1995)</i>	20600			9.1						2264	
<i>Yanai et al. (1995)</i>	20300										
<i>Paul and Lipschutz (1990)</i>				8.4			0.96				8.8
<i>Kaczaral et al. (1989)</i>				8.5			0.96				8.9
<i>Loss et al. (1984)</i>							0.96	0.03	2.9		
<i>Kallemeyn and Wasson (1981)</i>				8.2	0.2	2.2					
<i>Fitzgerald M. J. (1979)</i>	19700										
<i>Smith et al. (1977)</i>							1.02	0.27	26.5		
<i>Clarke et al. (1970)</i>	20000										
Mean Allende literature:	20267			8.5			0.97			2397	8.8
Deviation from literature [%]:	2.6			1.8			3.4				
<u>Allende CV3 (weathered) mean</u>	6159	246	4.0	4.50	0.13	2.9	0.95	0.05	4.9	1369	4.7
Digestion 1				4.49			0.95				4.7
Digestion 2				4.50			0.95				4.8
Digestion 3				4.47			0.95				4.7
Digestion 4				4.57			0.95				4.8
<u>Digestion 5 (mean)</u>				4.55	0.02	0.5	0.96	0.01	1.3		4.7
replicate				4.54			0.95				4.8
replicate				4.56			0.96				4.8
replicate				4.54			0.97				4.7
Digestion 8				4.55			0.95				4.8
Digestion 9				4.44			0.95				4.7
Digestion 10				4.51			0.91				4.9
Digestion 11				4.47			0.95				4.7
Digestion 12				4.58			0.99				4.6
<u>Digestion 13 (mean)</u>	6100	26	0.4	4.31			0.89			1414	4.9
replicate	6100										
replicate	6113										
replicate	6087										
Digestion 14	6061			4.51			0.96				4.7
replicate	6049										
Digestion 15	6351			4.50			0.96				4.7
replicate	6325										
Digestion 16	6065			4.44			0.95			1367	4.7
replicate	6072										
<u>Digestion 17 (mean)</u>	6197	67	1.1								
replicate	6197										
replicate	6156										
replicate	6228										
replicate	6232										
replicate	6173										
Digestion 18	6395										
replicate	6384										
Digestion 19	5988										
replicate	6029										
Digestion 20	6089										
replicate	6084										

" deviation from average [%]

measured with a MC-ICP-MS

Table 4.2 Sulfur, Se and Te data from isotope dilution ICP-MS analyses

Sample	Group	S		Se		Te		S/Se	Se/Te	sample source
		[$\mu\text{g/g}$]	dev. [%]	[$\mu\text{g/g}$]	dev. [%]	[$\mu\text{g/g}$]	dev. [%]			
<u>Carbonaceous chondrites</u>										
Orgueil	CI			21.5	0.4	2.29	0.2		9.4	[1]
replicate*		45297		21.3		2.28		2125	9.4	
Ivuna	CI	50802	0.4	20.6		2.26		2471	9.1	[2]
replicate		51200								
Y-980115	CI			24.2	0.3	2.40	0.2		10.1	[3]
replicate*		61057	0.4	24.0		2.41		2543	10.0	
replicate		61488								
Tagish Lake	C ungr.	33759	0.1	15.2		1.61		2220	9.4	[1]
replicate		33811								
Paris	CM	32448	0.6	12.8		1.44		2545	8.9	[2]
replicate		32825								
SCO 06043	CM1	32365	0.2	13.3		1.34		2441	9.9	[4]
replicate*		32209								
MET 01070.28	CM1			13.6		1.43			9.5	[4]
Murchison (mean)	CM2	29171		12.5		1.34		2336	9.3	[5]
Mighei	CM2			13.1	0.6	1.48	1.7		8.9	[5]
replicate*		31939		13.0		1.43		2461	9.1	
Murray	CM2	26065		12.5		1.44		2090	8.7	[5]
Cold Bokkeveld	CM2			12.0	2.0	1.36	5.2		8.8	[6]
replicate*		27506		12.5		1.51		2200	8.3	
Nogoya	CM2	31513	0.1	11.2		1.26		2826	8.8	[5]
replicate		31457								
Allende (mean)	CV3	19755		8.5		0.92		2322	9.2	[5]
Vigarano	CV3			7.4		0.86			8.6	[7]
A-881317	CV3	15448								[3]
ALHA 77307	CO3.0	17161		8.8		0.96		1950	9.2	[4]
ALH 82101	CO3	16357		7.6		0.83		2152	9.2	[4]
Lancé	CO3.5			7.6		0.84			9.1	[8]
Moss	CO3.6			7.7		0.87			8.8	[1]
Kainsaz	CO3.2			7.5		0.88			8.5	[5]
Acfer 187	CR2			5.0		0.54			9.3	[1]
GRA 95229	CR2			4.6	2.6	0.47	2.6		9.7	[4]
replicate*		10143		4.3		0.45		2338	9.7	
LAP 02342	CR2	10062		5.1		0.50		1989	10.2	[4]
Acfer 182	CH2	4829		3.6		0.40		1341	9.0	[1]
Karoonda	CK4	15106		7.7		0.80		1964	9.6	[5]
Ninuiang	C3 ungr.			12.0		0.92			13.0	[5]
<u>Ordinary chondrites</u>										
A 881641	H3			9.3	0.02	2.62	0.8		3.6	[3]
replicate*		6912		9.3		2.58		741	3.6	

Table 4.2 continued

Sample	Group	S		Se		Te		S/Se	Se/Te	sample source	
		[$\mu\text{g/g}$]	dev. [%]	[$\mu\text{g/g}$]	dev. [%]	[$\mu\text{g/g}$]	dev. [%]				
A 881298	H3			8.8	0.2	0.63	1.0		14.1	[3]	
replicate*		15804		8.8		0.64		1802	13.7		
WSG 95300	H3.3			8.3	0.2	0.42	0.4		19.7	[4]	
replicate*		12226		8.4		0.42		1464	19.7		
Florence	H3			8.7	0.2	0.50	1.9		17.2	[7]	
replicate*		17191		8.6		0.48		1994	17.8		
ALH 77299	H3			8.4	0.5	0.46	3.3		18.0	[3]	
replicate*		12997		8.3		0.43		1572	19.1		
Bremervörde	H/L3.9			8.1		0.42			19.5	[5]	
QUE 97008.42	L3.05			10.2	0.3	0.43	0.6		23.4	[4]	
replicate*		23193		10.1		0.44		2301	23.0		
Bovedy	L3			9.9	0.5	0.22	2.3		45.9	[7]	
replicate*		21062		9.8		0.23		2158	43.4		
GRO 95544	L3.2			9.9	0.2	0.37	2.1		26.6	[4]	
replicate*		23437		9.9		0.39		2359	25.6		
Y-74191	L3			8.3		0.16		1762	51.7	[3]	
A-881092	L3			10.0		0.33			30.2		
LEW 86505	L3.4			10.2		0.61		2298	16.6	[4]	
Bishunpur	LL3.1									[9]	
ALHA 76004	LL3.2/3.4			11.1		1.09			10.2	[4]	
GRO 95658	LL3.3			8.4	0.3	0.93	0.01		9.0	[4]	
replicate*		18988		8.3		0.93		2281	8.9		
A-881567	LL3			8.9	1.6	0.43	4.6		20.7	[3]	
replicate*		20062		9.2		0.47		2184	19.5		
A-881146	LL3			8.4		0.29			29.5	[3]	
<u>Enstatite chondrites</u>											
Qingzhen	EH3			24.0	0.2	1.72	0.4		14.0	[7]	
replicate*		39263		24.1		1.70		1631	14.1		
Sahara 97072	EH3			25.3	0.2	1.98	0.3		12.8	[5]	
replicate*		22958		25.4		1.99		903	12.8		
KLE 98300	EH3	#	29583	22.3		1.87		1330	11.9	[4]	
<u>Indarch (mean)</u>	EH4		25662	13.1	29.2	2.3"	2.49	3.0"	880	11.7	[5]
Digestion 1				29.5		2.52			11.7		
replicate*		#	27343	28.8		2.51		949	11.5		
replicate*			23981	29.2		2.45		822	11.9		
Abee	EH4			32.2	1.8	2.75	0.2		11.7	[7]	
replicate*			39902	31.1		2.74		1285	11.3		
EET96341	EH4/5			25.9		1.81		1750	14.3	[4]	
MAC 02839.8	EL3			16.5	0.5	1.29	0.2		12.8	[4]	
replicate*			34943	16.4		1.29		2135	12.7		
MAC 88136	EL3	#	41223	18.0		1.54		2288	11.7	[4]	
ALHA 81021	EL6	#	26430	13.4		0.15		1968	92.0	[4]	

Table 4.2 continued

Sample	Group	S		Se		Te		S/Se	Se/Te	sample source
		[$\mu\text{g/g}$]	dev. [%]	[$\mu\text{g/g}$]	dev. [%]	[$\mu\text{g/g}$]	dev. [%]			
<u>Rumuruti chondrites</u>										
NWA 753	R3.9			14.5	0.8	1.05	2.5		13.8	[1]
replicate*		22672		14.3		1.11		1585	12.9	
PRE 95404	R3	37124		14.9		1.08		2498	13.8	[4]
EET 96026.44	R3			5.6		0.11			51.3	[4]

* different digestion

preliminary S data (measured with a MC-ICP-MS)

" 2RSD [%]

[1] = Institute of Planetology, University of Münster/ Germany;

[2] = Natural History Museum, Paris/ France;

[3] = National Institute of Polar Research/ Japan

[4] = ANSMET/MWG

[5] = Institute of Geochemistry, FU Berlin/ Germany;

[6] = Natural History Museum, London/ Great Britain

[7] = Mineralogisches Museum, University of Hamburg/ Germany

[8] = Mineralogisches Museum, University of Bonn/ Germany

[9] = Smithsonian NMNH, Washington, USA

4.3.2 Sulfur, selenium, and tellurium concentrations in bulk chondrites

Carbonaceous chondrites

Because CI chondrites inherent non-atmophile element abundances almost indistinguishable from the solar photosphere their composition is widely used for reference purposes. As discussed in the previous section, Se and Te concentrations obtained for Ivuna and Orgueil are in excellent agreement with the literature while S concentration obtained for Orgueil is lower than expected. The Antarctic CI chondrite Y-980115 shows unusual high concentrations in S (6.1 mg/g), Se (24 $\mu\text{g/g}$) and Te (2.4 $\mu\text{g/g}$) when compared to Orgueil, Ivuna and to the literature data for other CIs. Furthermore, Y-980115 shows enrichment in S and Se relative to Te and Ivuna. Ivuna and Y-980115 have S/Se of about 2500 which is in agreement with the ratio given in the latest compilation of CI chondritic abundances given by Palme et al. (2014). In contrast, the ratio for Orgueil (S/Se = 2125) is lower due to the low S concentration. The Se/Te ratios are 9.1 (Ivuna), 9.4 (Orgueil) and 10.0 for Y-980115. High Se/Te for Y-980115 may result from low Te abundance relative to Se which is also typical for ordinary, enstatite and Rumuruti chondrites, or from enrichment due to redistribution of aqueous mobile S and Se relative to Te. Due to the fractionation of S from Se and Te in Orgueil and the fractionation of Te from S and Se in Y-

980115, only S, Se and Te concentrations from Ivuna (in the following sections also referred to as CI) are used for normalization in the present study.

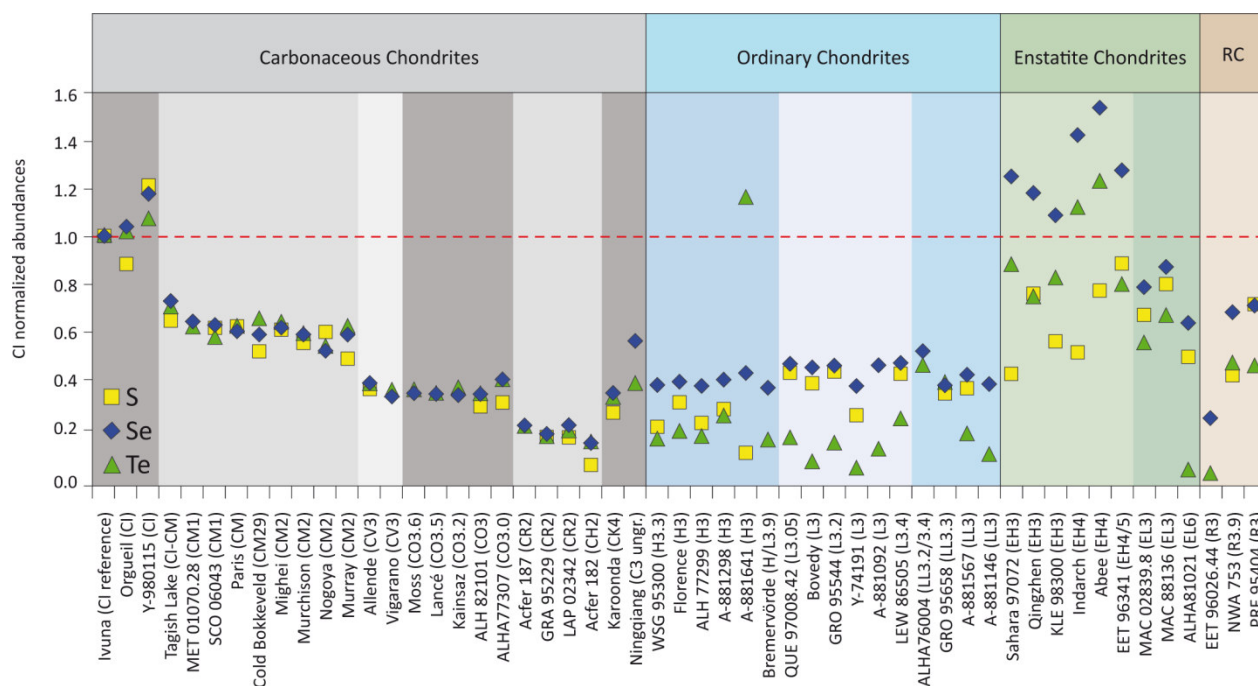


Figure 4.1 Abundances of S (square), selenium (diamond) and tellurium (triangle) for measured carbonaceous, ordinary, enstatite and Rumuruti chondrites normalized to the CI chondrite Ivuna.

An overview of S, Se and Te abundances relative to Ivuna is given in Figure 4.1. The Antarctic CI chondrite Y-980115 has unusual high S, Se, and Te abundances when compared to Ivuna and Orgueil. While S and Se are enriched to the same extent over our reference Ivuna, Te is depleted relative to S and Se but still enriched over Ivuna. An explanation might be again the redistribution of water-soluble elements either on the parent body and/or on Earth. (Antarctic CIs are not collected right after their fall). A hint from this study comes from the used in-house-standard, a weathered piece of the Allende CV3 chondrite where by about 70% of the S and 50% of Se was removed due to terrestrial weathering while Te is unaffected. Thus, S and Se may be heterogeneously enriched or depleted relative to Te in different sample portions.

In carbonaceous chondrites S, Se and Te are increasingly depleted relative to CI in the following order: Tagish Lake (C2 ungr.) < CM < CO = CV < CR < CH. Furthermore, all three elements are commonly depleted to the same extent relative to CI (Figure 4.1 and Table 4.2). CM

chondrites show generally CI chondritic Se/Te, but somewhat more variable S as displayed in vertical trends in Figure 4.2 c. The CV3 chondrites Allende (oxidized subgroup) and Vigarano (reduced subgroup) differ slightly in Se and Te concentrations. Both show variable Se and Te concentrations and ratios. Allende shows the same depletions in S, Se and Te and therefore CI chondritic S/Se, S/Te and Se/Te (Figure 4.1 and 4.2). The reduced CV3 chondrite Vigarano is slightly more depleted in both Se and Te relative to Allende and CI with a Se/Te of 8.5 which implies that Te is slightly less depleted relative to Se. Four of five CO3 chondrites display only little variation in Se and Te concentrations. Se/Te range from 8.5 – 9.2 which implies that Se and Te are generally depleted to the same extent. Sulfur concentrations were only determined for two Antarctic CO3 chondrites. Both are slightly more depleted in S relative to Se and Te. Both CR2 and CH2 chondrites analyzed in the present study lost by about 80% of their S, Se and Te when compared to Ivuna and are therefore the most depleted samples of carbonaceous chondrites. From the three CR2 chondrites analyzed only LAP 02342 is slightly more depleted in S and Te relative to Se, which results in an elevated Se/Te and lower S/Se relative to CI. Acfer 182 (CH2) is evenly depleted in Se and Te while S has much lower abundances compared to Se and Te. The CK4 chondrite Karoonda has Se and Te abundances similar to CO chondrites with Se and Te being depleted to the same extent while S is slightly more depleted relative to Se and Te. The ungrouped C3 chondrite Ningqiang shows Se depletion similar to CM chondrites and a more pronounced Te depletion relative to Se, which is rather uncommon for carbonaceous chondrites.

Ordinary chondrites

Measured S, Se and Te concentrations are compiled in Table 4.2. Compared to carbonaceous chondrites chalcogene element fractionation in ordinary chondrites appears to be more complex. In general and independent of the group (H, L, LL) ordinary chondrites experienced a more pronounced Te depletion relative to Se and S. Selenium depletions were found to be rather constant among all groups (H, L, and LL) at a level similar to CM, CV and CO chondrites. However, there is a tendency for L chondrites in having slightly higher Se concentrations relative to H and LL (Figures 4.1 and 4.2 a). In contrast to the constant Se, Te depletions are highly variable and govern the large variations in Se/Te which increase with decreasing Te concentrations relative to Se (Figure 4.2 b). In most L and LL samples Se depletion is accompanied with S depletion as reflected by almost constant but slightly lower than CI

chondritic S/Se (Figures 4.1 and 4.2 c). In contrast, H chondrites display a tendency of accompanied S and Te depletions (Figures 4.1 and 4.2 d). Noticeably high and supra-chondritic Te concentration (2.6 $\mu\text{g/g}$) was found for one H chondrite (A-881641) while Se is only slightly higher when compared to the mean Se concentrations in H chondrites. Furthermore, two L3 chondrites (ALHA 76004 and GRO 95658) display equal depletions in both Se and Te. GRO 95658 additionally shows the same depletion in S (no S data for ALHA76004).

Enstatite chondrites

Sulfur, Se and Te concentrations from six high iron (EH), and three low iron (EL) enstatite chondrites are listed in Table 4.2. Bulk data from EH chondrites display highly variable S, Se and Te abundances relative to CI. Selenium is consistently enriched over CI while Te overabundance only occurs within the EH4 chondrites Abee and Indarch. Similar to ordinary chondrites, Se/Te are elevated when compared to the CI chondritic ratio (Figures 4.1 and 4.2 a). Sulfur abundances are always below CI and Se and display unsystematic scatter relative to Te (Figures 4.1 and 4.2 c, d). Different to EH chondrites, unequilibrated EL chondrites (MAC 02839, MAC 88136) are neither enriched over CI in Se nor in Te or S. Equal to ordinary and EH chondrites Te depletion is more pronounced relative to Se. Sulfur depletion is intermediate to Se and Te as reflected by low S/Se and high S/Te relative to CI (Figures 4.1 and 4.2 c, d). The metamorphosed EL6 chondrite ALHA81021 shows that Se and S are only slightly more depleted when compared to unmetamorphosed EL3 samples, while Te is almost entirely lost.

Rumuruti chondrites

Sulfur, Se and Te concentrations for three Rumuruti chondrites from Antarctica and North West Africa were determined (Table 4.2). Selenium depletion is similar to Tagish Lake (C2 ungr.) and CM chondrites. The Antarctic R3 chondrite EET 96026 is much more depleted in Se and Te when compared to the other two samples. Sulfur depletion appears to be more variable relative to Se, Te, and CI. The Antarctic R3 chondrite PRE 95404 displays CI-like S/Se while the R3.9 chondrite NWA 753 from the hot desert has low S/Se indicating higher S depletion relative to Se. Similar to ordinary and enstatite chondrites Te depletion is more pronounced relative to Se (high Se/Te relative to the CI ratio). Interesting to note is the observation that Te depletion is

consistently by about 20% more pronounced relative to Se independent of the Se concentration indicating that Se and Te were depleted when the decoupling of Te from Se was already present (Figure 4.1).

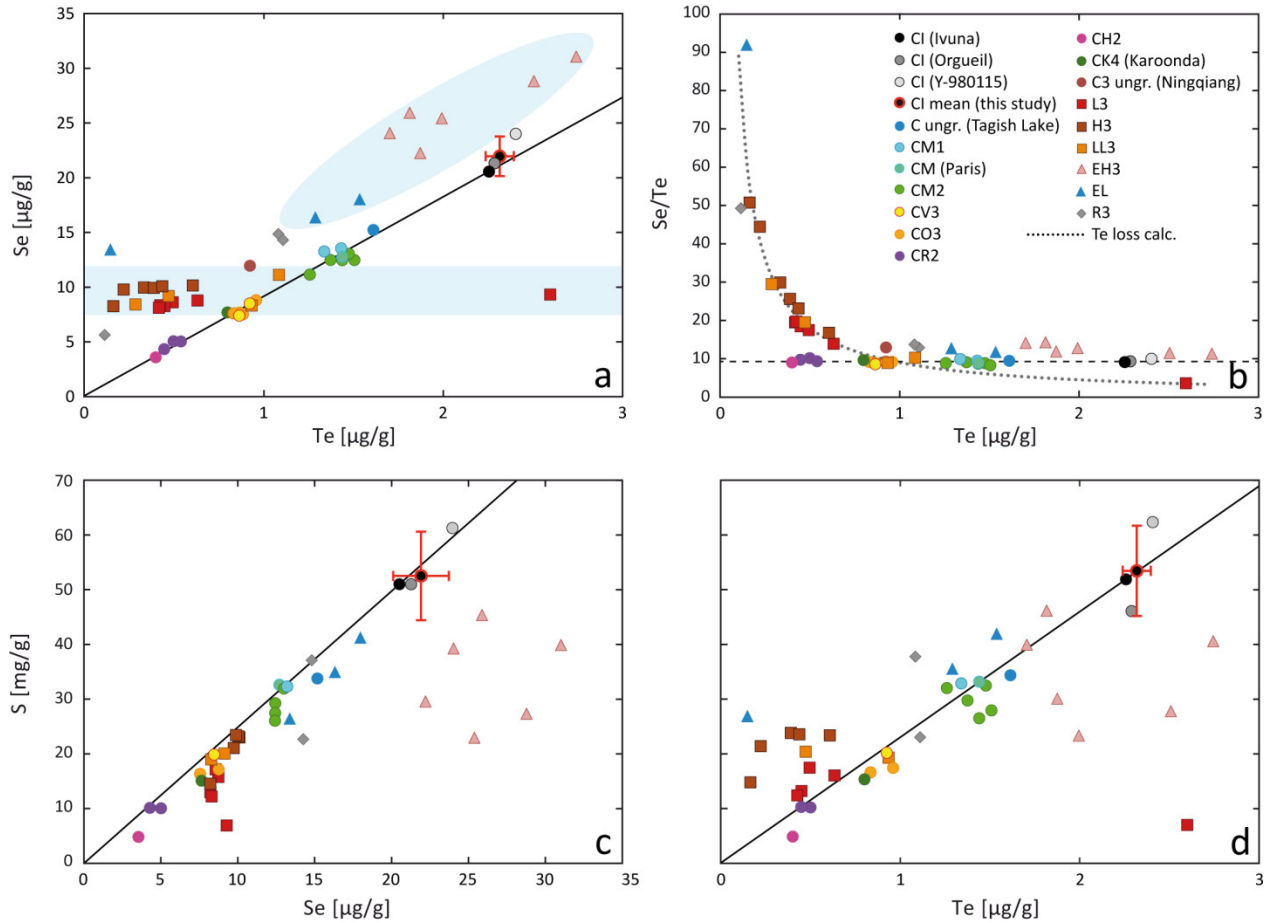


Figure 4.2 Element plots of S, Se and Te for different chondrite classes and groups. (a) Se vs. Te for different chondrites. Carbonaceous chondrites have CI-like Se/Te and plot along the reference line defined by the CI chondrite Ivuna, while ordinary, enstatite and Rumuruti chondrites lie significantly above CI. (b) Shows the dependence of the Se/Te from the Te concentration. (c) Sulfur and Se concentrations correlate in almost all groups, except in EH and H chondrites. Chondrites show a general tendency towards low S/Se relative to CI. (d) Variable S/Te in ordinary and enstatite chondrites.

4.3.3 Abundances and distribution of S, Se and Te in chondritic components

Data obtained from laser ablation ICP-MS provide additional information for the interpretation of bulk analyses, taking advantage of the spatial resolution and optical control of the material analyzed. Laser data yield reliable information about the (relative) abundances of S, Se and Te which allows insight into the nature of the different S, Se and Te carrier phases and components and thus implications for processes that could have produced the different S, Se and Te fractionation patterns in different chondrite classes relative to CI. Figures 4.3 and 4.6 show the CI normalized abundances of S, Se and Te for Allende CV3, Semarkona LL3, and Indarch EH4 along the laser line tracks that are shown as red lines in back scattered electron (BSE) images. Element plots in Figures 4.4, 4.5, 4.7, and 4.8 results from carefully selected element abundances for different chondritic components (cf. Chapter 4.2.2 and electronic annex) in Allende, Semarkona, and Indarch.

Laser line scans measured in the *Allende* CV3 chondrite are shown in Figures 4.3 a, b, and c. Here the laser sampled material from different components such as fine-grained matrix (mx), chondrules (ch), and CAIs which partly contain sulfide-rich blebs or grains (srm = sulfide-rich materials), an amoeboid olivine aggregate (AOA) (Figure 4.3 b), and a chondrule like rounded object surrounded by a broad sulfide/magnetite/metal-rich rim (srr = sulfide-rich rim) (Figure 4.3 a). As expected, high-temperature components such as chondrules, CAIs, and the AOA are depleted in S, Se and Te, except when the laser samples material which includes blebs or grains consisting of sulfide, magnetite and metal, located in chondrules and the CAI (Figure 4.3 c).

Allende matrix is enriched in S, Se and Te relative to high-temperature components and bulk Allende, but depleted relative to CI (Figures 4.4 a, b). While Se and Te show in average CI-like ratios within the matrix, S/Se and S/Te are predominantly low (Figures 4.4 c, d) indicating that S depletion is more pronounced relative to Se and Te depletion (see also Figure 4.3 b). The same decoupling of S from Se and Te is observable in some opaque blebs (most likely magnetite/metal-sulfide associations) within the chondrule in Figure 4.3 c. Compared to bulk Allende where S depletion relative to Se is only about 7%, S depletion in the matrix observed in the laser profiles may be somewhat more pronounced. There are three possible explanations for this observation: First, the line scans are simply not representative for bulk Allende. Second, S

could have been redistributed during aqueous alteration on the parent body, because it is highly mobile in aqueous fluids and Allende underwent extensive aqueous alteration (*e.g.* Krot et al. 1995). In this regard, the Smithsonian Allende powder that was analyzed for the bulk composition may not be perfectly similar to the piece of Allende from which the thick section was prepared. Note that S was also preferentially removed from the weathered Allende test sample. Third, analytical issues related to matrix dependent elemental fractionation of sulfur from Se and Te during laser sampling, transport to the plasma, and at the plasma interface might be another possible explanation.

Relative abundances of S, Se, and Te in the thick sulfide-rich rim around the chondrule-like rounded object on the right-hand side of the profile in Figure 4.3 a, and the sulfide inclusion within the CAI in Figure 4.3 c, reveal that Allende contains components in which Te is more depleted relative to Se and S. Complementary, constituents with enrichment of Te relative to Se and S are present (*e.g.* metal-inclusion in chondrule pyroxene in Figures 4.3 c and 4.4 a, b). Mass balance calculations indicate that the scarce occurrence of such components with non-CI-like Se/Te can be blurred by high modal abundance of material with CI-like Se/Te (fine-grained matrix) and are therefore not detectable in bulk analyses. However, small differences in S, Se and Te depletion detected in other bulk carbonaceous chondrites (Figure 4.1) implies that those constituents are also present in other carbonaceous chondrites and can affect the bulk chemistry or at least result in heterogeneities at the sample scale.

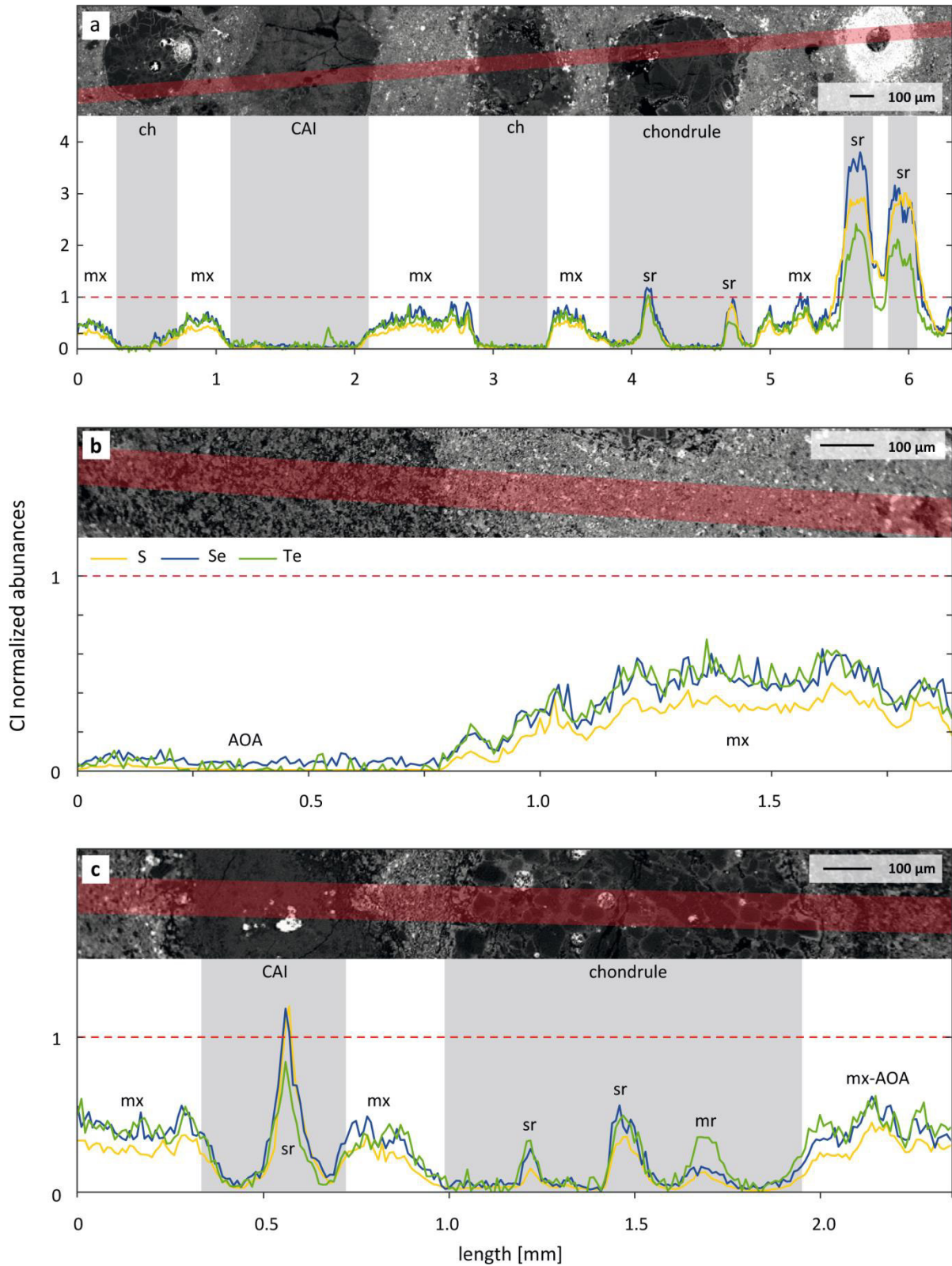


Figure 4.3 CI normalized S, Se and Te abundances in different components of Allende (CV3) measured by laser ablation ICP-MS. ch = chondrule; mx = matrix; CAI = Ca, Al-rich inclusion; sr = sulfide-rich ablation region; mr = metal-rich ablation region; AOA = amoeboid olivine aggregate

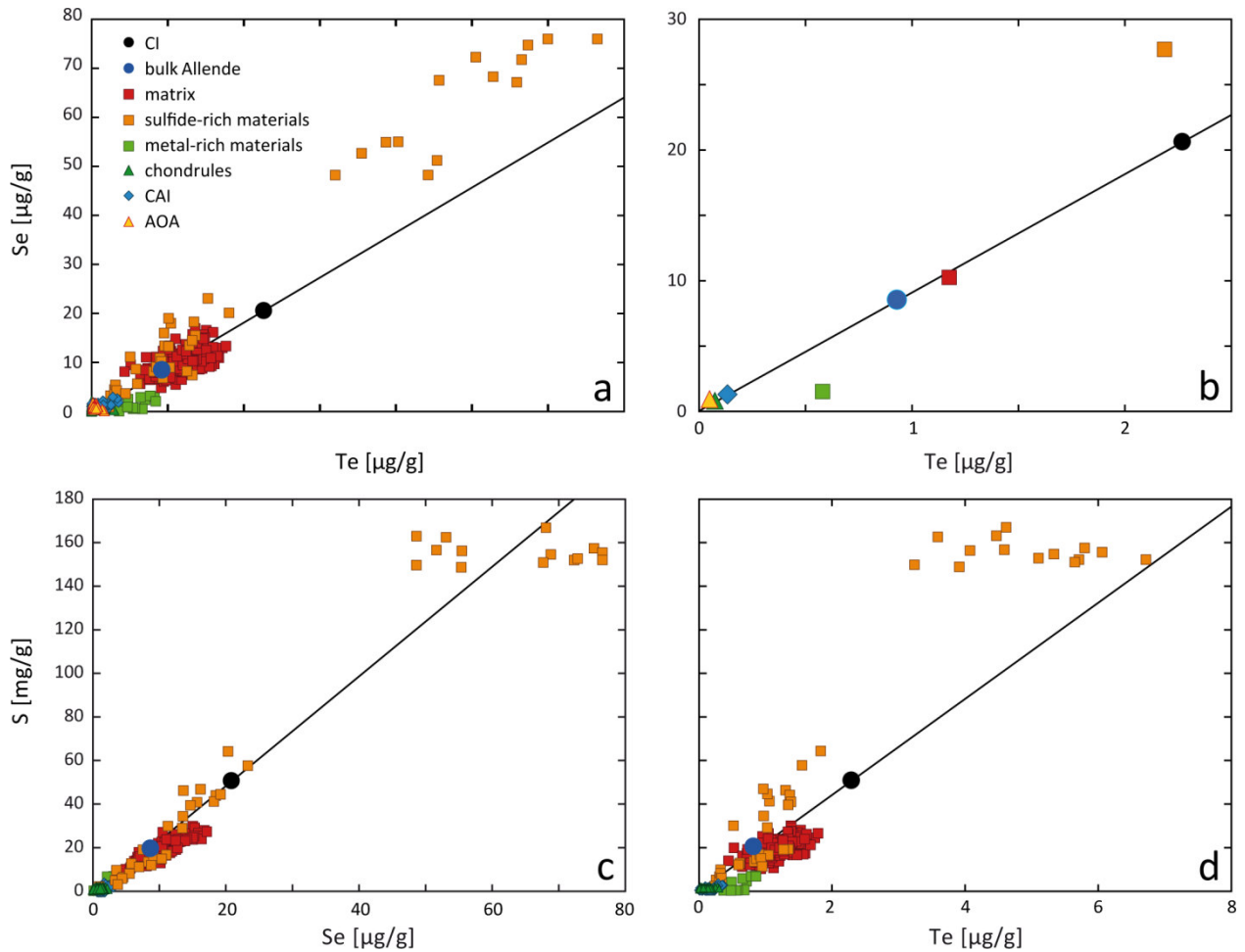


Figure 4.4 Element plots of S, Se and Te from different components in the CV3 chondrite Allende determined by laser ablation ICP-MS. (a) Se vs. Te for different components; (b) average Se and Te concentrations for different components; a, and b, shows that most Allende constituents have CI-like Se/Te. High Se/Te (orange square on top of b) refer to a broad sulfide-rich rim (see also Fig. 4.3 a). Low Se/Te refers to metal-rich material (mr) (see also Fig. 4.3 c). (c) S vs. Se and (d) S vs. Te. Both, Se and Te display a general correlation with S for most components. Outliers with high S, Se and Te concentrations display data from the broad sulfide-rich rim in Fig. 4.3 a.

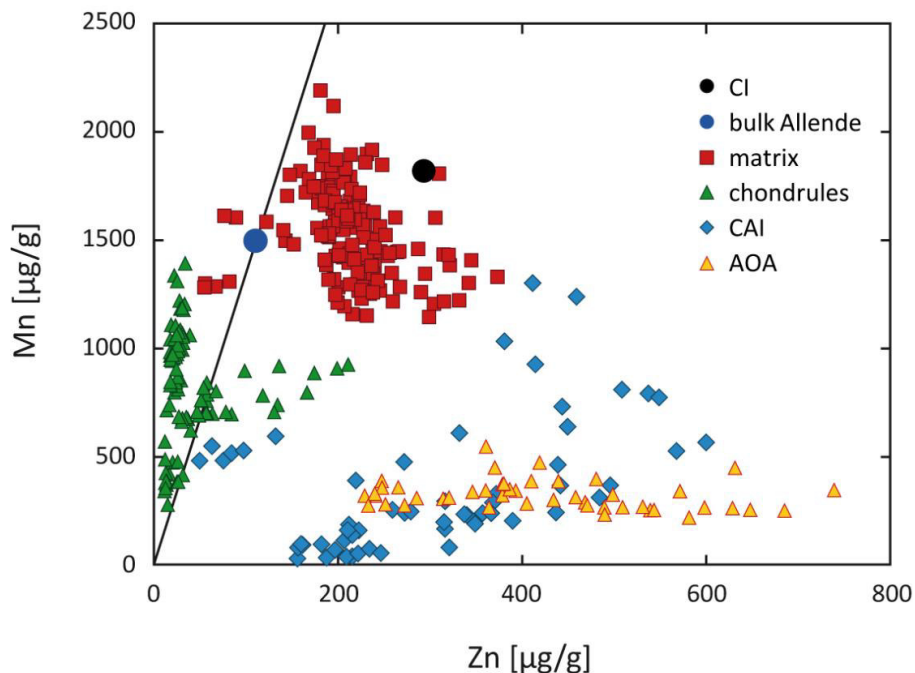


Figure 4.5 Manganese vs. Zn abundances for different components of the Allende CV3 chondrite measured by LA-ICP-MS. Both, Mn and Zn show a tendency of complementary distribution between chondrules and matrix. While matrix is enriched over bulk Allende (blue circle) in Mn and Zn, chondrules are complementary depleted.

Semarkona (LL3) belongs to the least altered ordinary chondrite samples available for studies and is therefore most suitable for the investigation of the S, Se and Te distribution among chondritic components. In the first of two profiles (Figure 4.6 a), the laser sampled material from a porphyritic chondrule (ch) surrounded by a thin sulfide-rich rim (srr), fragments of porphyritic chondrules (ch), sulfide-metal assemblages (sma) interstitial to chondrules, small areas of fine-grained matrix (mx), and a xenolith (xth). The second profile includes two porphyritic chondrules and chondrule fragments (ch), a cryptocrystalline chondrule (cch), small areas of fine-grained matrix (mx), and sulfide-metal assemblages (sma) interstitial to chondrules.

High-temperature components such as chondrules and chondrule fragments are depleted in all three elements. Only the cryptocrystalline chondrule (Figure 4.6 b) contains some S and Se with the same relative abundances to CI, hosted in finely dispersed sulfide grains, while Te is far more depleted. In line with their chemical affinity S, Se and Te are generally concentrated within sulfides (mainly S and Se, minor Te) and in metals (mainly Te, minor Se) which occur as

irregularly shaped metal-sulfide assemblages interstitial to chondrules and at chondrule rims, finely dispersed within fine-grained matrix, and in the form of blebs within chondrules. In all those constituents S, Se and Te abundances are highly variable relative to CI and show different relative enrichment and depletion pattern (Figures 4.6 a, b; 4.7 a - d). Sulfide-metal assemblages interstitial to chondrules and on chondrule edges as well as sulfide/metal-rich rims around chondrule fragments display similar properties to bulk ordinary chondrites with high Se/Te, low S/Se and variable S/Te (Figures 4.1). Metal-sulfide associations (outside chondrules) are the main carrier of S, Se and Te and therefore control the depletion pattern of the bulk chondrite (Figures 4.7 a, b).

Scarce regions of interstitial fine-grained matrix show enrichment in Se and Te relative to bulk Semarkona but depletion when compared to CI (Figures 4.7 a, b). On average it appears that fine-grained matrix is evenly depleted in both, Se and Te (Figure 4.7 b), while S depletion is generally more pronounced (Figure 4.7 c). In all other components S is either more depleted or at the same level than Se (Figures 4.7 c and 4.6 a, b). In contrast S/Te ratios are highly variable in all sulfide-metal assemblages indicating that Te abundance is not controlled by sulfides. In fact, the good general correlation between Te and the highly siderophile element Pt suggests a dominant control of metal over Te abundances (Figures 4.7 d, e).

Indarch is classified as a high iron enstatite chondrite of petrologic type four. It contains abundant Fe, Ni-metal and exotic sulfides. Figure 4.6 c shows the sampling region of the laser which includes fragments of silicates (mostly enstatite) associated with fine-grained metals and sulfides, chondrules (ch), larger sulfide grains (s) (>100 μm), small metal nuggets (m), and sphalerite (sph) in the center of the profile. CI normalized abundances obtained by laser ablation show that all three elements are concentrated in all of the sulfide and metal phases. Unlike Allende and Semarkona, even chondrules and enstatite contain some S, Se, and Te (Figures 4.6 c and 4.8 a). Most likely, their S, Se, and Te are in finely dispersed metals and sulfides enclosed in enstatite within and outside chondrules. High abundances especially for Se and Te are in agreement with the bulk data from Indarch. As demonstrated in Figures 4.6 c and 4.8 a, b almost all components display the same signature of high Se/Te as bulk Indarch, including different chondrules, sulfides, sphalerite, and enstatite within and outside chondrules. Only very few

constituents (most likely metals) are enriched in Te relative to S and Se. The correlation of Te concentrations with Pt, and the large scatter of S/Te again, support the siderophile behavior of Te (Figures 4.8 d, f). Selenium however, appears to be mainly chalcophile and located in sulfides as indicated by highly constant, CI-like S/Se and large variations in Pt/Se.

The constant CI-like S/Se for most laser ablation data points (Figures 4.6 c and 4.8 c) is in contradiction to the low S/Se obtained from isotope dilution bulk analyses for Indarch (Figure 4.1). Decoupling of S from Se as indicated by bulk analyses cannot be explained by admixture of abundant sphalerite as sphalerite addition would move the S towards higher abundances, while the bulk ID data display rather low abundances. Again, the Indarch thick section has been prepared from a different piece of Indarch and contrasting data most likely imply that Indarch is rather heterogeneous in S.

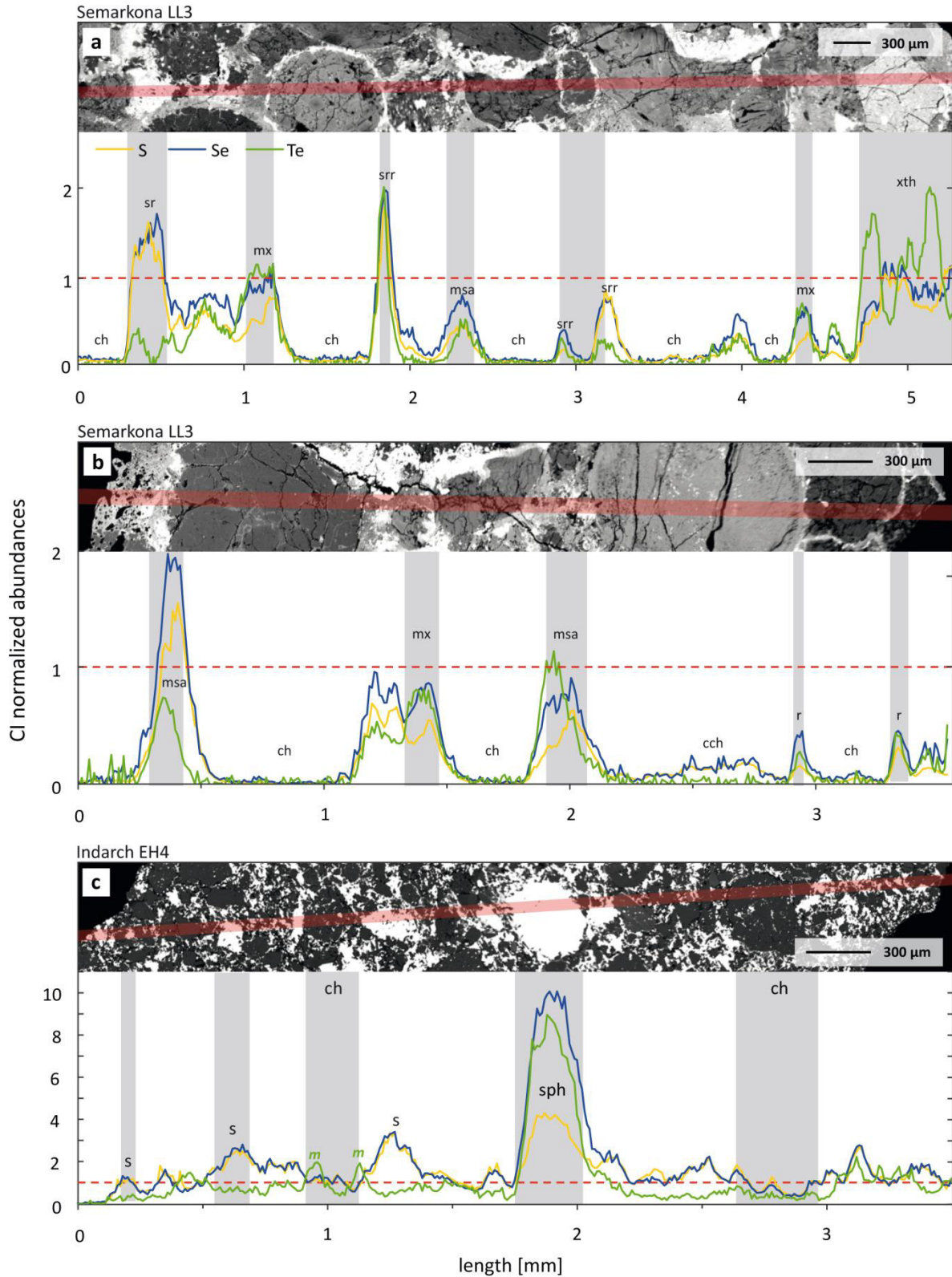


Figure 4.6 CI normalized S, Se and Te abundances in different components of (a, b) Semarkona (LL3) and (c) Indarch (EH4). ch = chondrule; cch = cryptocrystalline chondrule; mx = matrix; srr = sulfide-rich rim; r = rim; msa = metal-sulfide assemblage; xth = xenolith; s = sulfide; m = metal; sph = sphalerite.

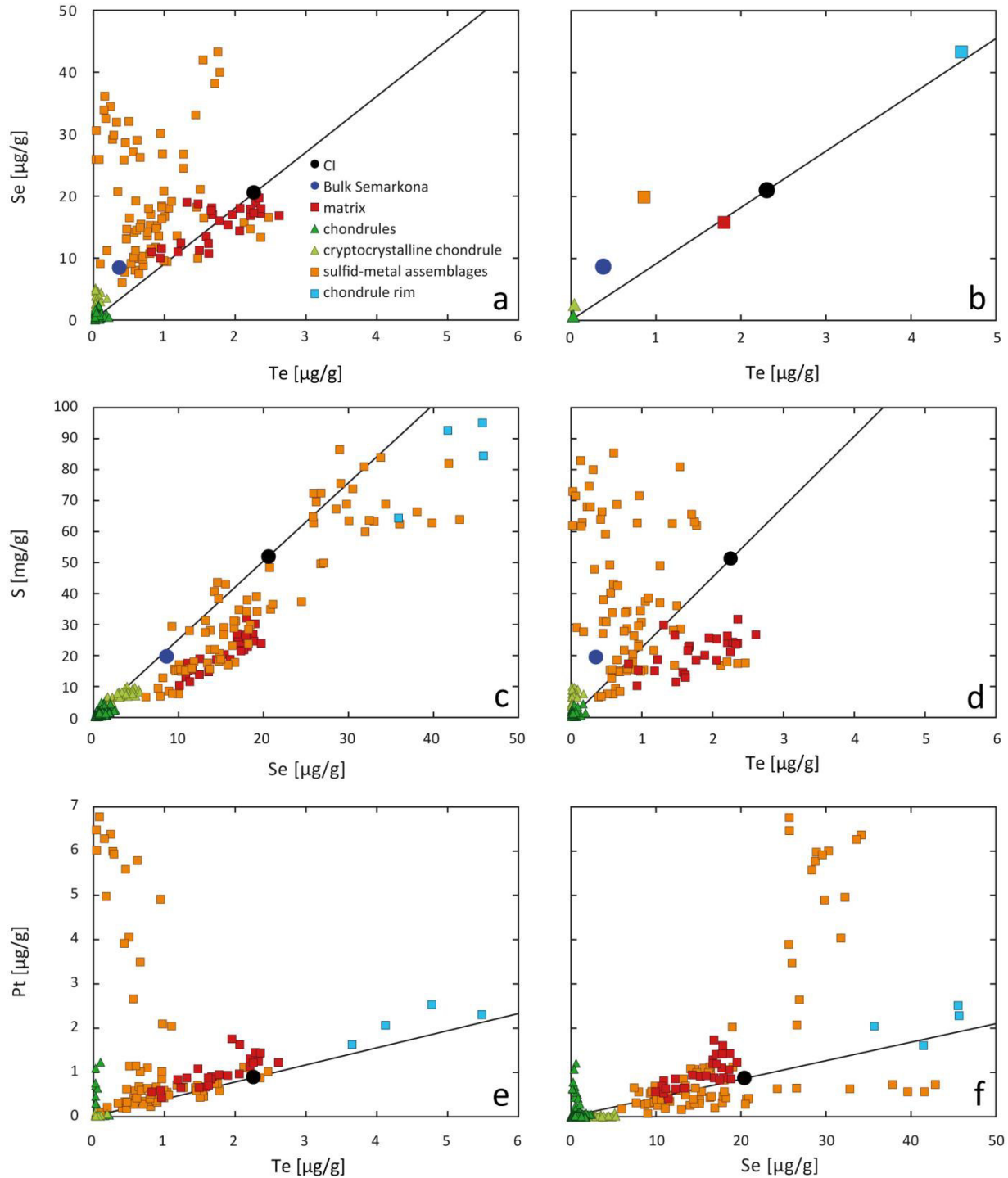


Figure 4.7 Sulfur, Se, Te and Pt abundances in different components of Semarkona (LL3) from laser ablation ICP-MS analyses. (a) Se vs. Te in different components; (b) average Se and Te concentrations for different components; (c) Sulfur and Se abundances correlate but have low S/Se relative to CI. (d) No correlation for S and Te abundances – highly variable S/Te in different components. (e) Correlation between Te and Pt abundances. (f) Variable Pt/Se. Sulfur, Se and Te data for bulk Semarkona are from Jarosewich (1966), Kallemeyn et al. 1989, and Binz et al. 1976 respectively.

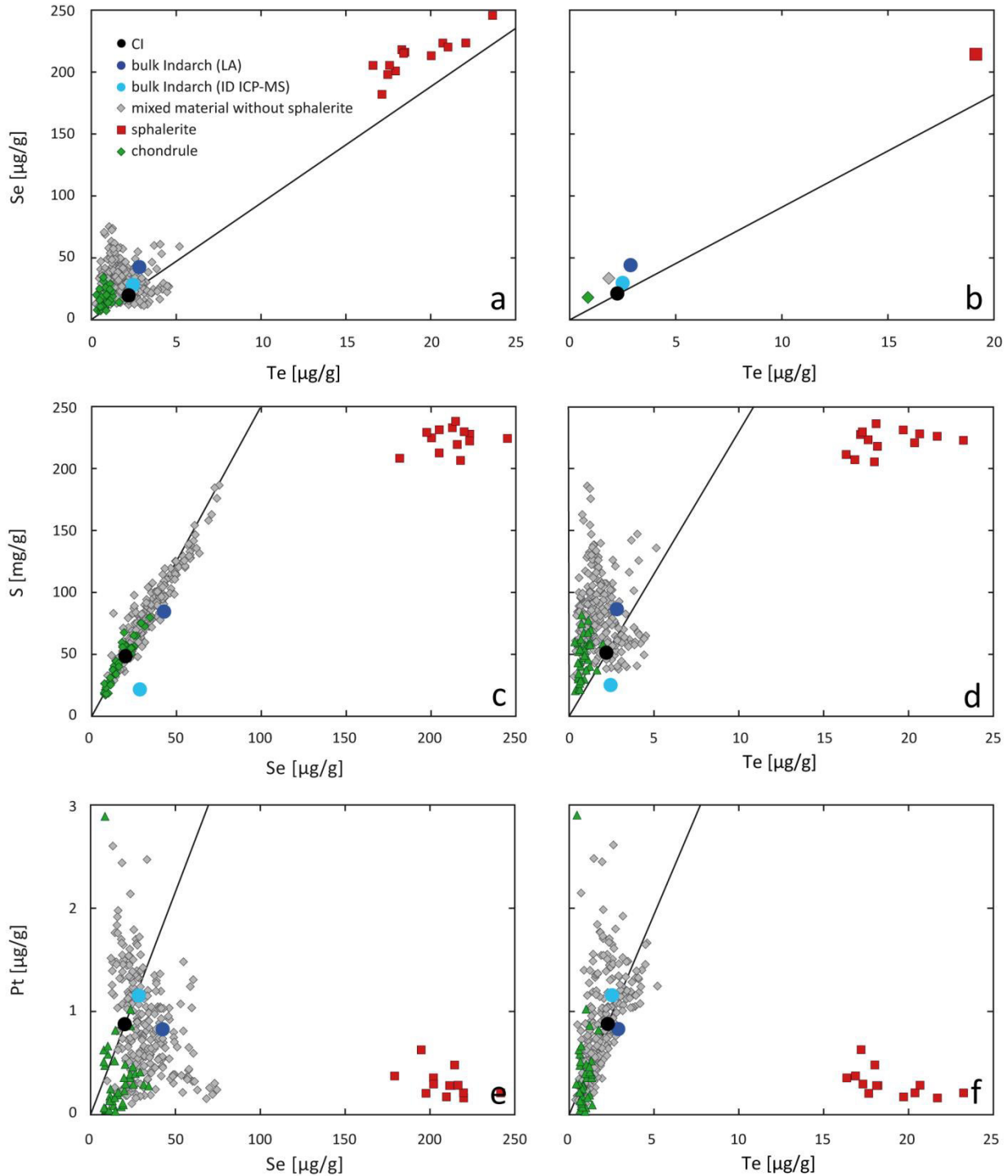


Figure 4.8 Sulfur, Se, Te and Pt abundances in different components of Indarch (EH4) from laser ablation ICP-MS analyses. (a) Se vs. Te in different components; (b) average Se/Te of different components; (c) CI-like S/Se except for sphalerite; (d) variable and commonly high S/Te; (d) highly variable Pt/Se; (f) General correlation of Te and Pt implies that Te is in the metal. Platinum data for bulk Indarch are from Fischer-Gödde et al. 2010.

4.4 DISCUSSION

Different carbonaceous chondrite groups are depleted to different extents in S, Se, and Te relative to CI but display very similar depletions in S, Se and Te relative to CI which indicates that S, Se and Te responded very similar to the depletion process. In contrast ordinary, enstatite and Rumuruti chondrites experienced a more pronounced depletion in Te. In this section possible mechanisms for primary volatile loss will be discussed, based on observations from bulk S, Se, and Te abundances in different chondrites combined with important hints obtained from laser ablation ICP-MS analyses. Based on the present results primary depletion of the moderately volatile elements S, Se, and Te can be attributed to chondrule formation. In ordinary and enstatite chondrites Te depletion could have also been affected by parent body thermal metamorphism.

4.4.1 *Primary (pre-accretionary) depletion during chondrule formation*

Chondrites are a mixture of components with very different compositions (*e.g.* chondrules, matrix, Ca, Al-rich inclusions (CAIs), and metal grains). The bulk chemistry of unequilibrated chondrites is therefore largely controlled by the composition and the modal abundance of these components. The two major components that control the chemical compositions of carbonaceous chondrites are volatile element enriched fine-grained matrix with average modal abundances between 30 – 70 vol. %, and volatile element depleted chondrules (mostly 20 – 70 vol. %). CAIs consist mainly of ultra-refractory elements and contribute no more than 3 vol. % to the bulk compositions of carbonaceous chondrites other than CI (Hezel et al. 2008; Weisberg et al. 2006). Thus, the bulk chemistry of carbonaceous chondrites is predominantly controlled by the two major components, *i.e.* the ratio of volatile enriched matrix and depleted chondrules.

Selenium and Te are naturally hosted in opaque phases like sulfides and metals. Laser data for Allende CV3 shows that Se and Te are mainly located within the fine-grained matrix where they are enriched over bulk Allende but depleted compared to CI. Fine-grained matrix in Allende displays small variation in Se/Te but on average a CI chondritic ratio (Figures 4.3 and 4.4). Further Se and Te rich areas relate to sulfide and/or metal-rich blebs and inclusions located in chondrule mesostasis and pyroxene, in a sulfide-rich inclusion incorporated in a CAI (Figure 4.3

c), and most significantly in a sulfide/metal/magnetite-rich rim (Figure 4.3 a). Bulk carbonaceous chondrites display generally equal S, Se and Te depletions relative to CI (Figure 4.1). However, laser data from Allende show that samples that do not show any decoupling of Te from Se in bulk analyses nevertheless can contain fractionated components with more pronounced Te depletion relative to Se (*e.g.* high Se/Te in an inclusion within a CAI, and the broad sulfide/metal/magnetite-rich rim) or complementary with Te enrichment relative to Se (*e.g.* metal inclusion in chondrule pyroxene, and a Pt,Te-rich nugget within a CAI). Mass balance calculations showed that due to the low modal abundance of such fractionated components, this signature will not systematically affect the Allende bulk composition.

The presence of Se, Te carrier phases with high and low Se/Te could indicate that Se and Te (re)condensed into, or evaporated from metals and sulfides with different efficiency but without any significant fractionation relative to CI in the bulk samples. Evaporation of volatile elements related to chondrule formation is one possible scenario. The broad opaque rim obviously formed after and likely in response to the heating event that formed the rounded chondrule-like object in the center. During this heating, Se and Te and other volatiles may have been evaporated from this material and the differently pronounced smooth depletion patterns for volatile elements in different bulk chondrites may simply display the intensity and/or repetition of short high-temperature events that affected both, chondrules and matrix and resulted in partial loss and complementary redistribution of the remaining volatile elements into the carrier phases in chondrules and matrix which together form the smooth volatility trend of the bulk chondrite.

Evidence for simultaneous chondrule and matrix formation and or processing at which volatile elements were affected was given by Bland et al. (2005). They demonstrated that siderophile and chalcophile volatile elements are complementary distributed between chondrules and matrix in CV3 chondrites and concluded that this originated during chondrule formation and both chondrules and matrix formed from the same chemical reservoir. Because they could not observe such a complementary relationship for lithophile volatile elements they suggested that this complementarity arose due to physical separation of sulfide- and metal melt from chondrules to matrix and that the chondrule forming region was already depleted in volatile elements due to incomplete condensation prior to chondrule formation. However, sulfides and metals separated from the chondrules may be responsible for the separation of volatile siderophile and chalcophile from volatile lithophile elements. The smooth depletion trend may be the combined result of

evaporation from chondrules and associated sulfides/metals and partial recondensation of the vapor into silicate chondrules or the reheated sulfides and metals (cf. Alexander et al. 2005). Some moderately volatile elements may evaporate only partially which should result in stable isotope fractionations for example for K, but stable isotope fractionation is not observed (e.g. Humayun et al. 1995). As suggested by Alexander 2004; Cuzzi & Alexander 2006; Alexander et al. 2008 this argument can be overcome when chondrule formation occurs in dust-enriched environments, where isotopic re-equilibrium between chondrule melts and the surrounding gas is possible.

To test if lithophile volatile elements are affected by chondrule formation and show the same complementary distribution between chondrules and matrix the concentrations of the lithophile volatile elements Mn and Zn obtained from laser ablation ICP-MS analyses were plotted for various components of the Allende CV3 chondrite. Figure 4.5 shows that Allende chondrules are depleted in both, Zn and Mn while the matrix is complementary enriched relative to bulk Allende. Combining the Mn and Zn concentrations of matrix and chondrules could create the (depleted) bulk concentration in Allende.

Matrix-chondrule complementarity was intensively studied in different groups of carbonaceous chondrites and is for example evident by CI-complementary Fe/Mg, Si/Mg, and Ti/Al (e.g. Wood 1963, 1985; Klerner 2001; Hezel & Palme 2008, 2010; Ebel et al. 2009; Palme et al. 2015). Hezel & Palme (2008, 2010) and Palme et al. (2015) pointed out that these complementarities can only be explained when both, chondrules and matrix formed in the same reservoir during short heating events at which the present materials were molten and elements evaporated with an efficiency depending on their condensation temperature. During cooling elements recondensed onto chondrules and fine-grained matrix materials that either evaporated incompletely or recondensed as well as tiny condensation nuclei during cooling. Locally restricted evaporative processes would be also consistent with the observation of Huss et al. (2003) and Huss (2004) that specific assemblages of presolar grains with characteristic thermal and chemical resistance correlate with the volatile element abundance of chondritic matrices in which they are embedded. This suggests a common evaporative process that affected both, volatile elements and presolar grains.

It seems likely that the primary depletion of volatile elements in general could have taken place during chondrule formation and no further processes such as incomplete condensation or evaporation, prior to chondrule formation is needed but cannot be completely excluded. For carbonaceous chondrites it seems that Se and Te were present in the same relative abundance to CI and the depletion event affected both elements to the same extent. In contrast to carbonaceous chondrites, ordinary, enstatite, and Rumuruti chondrites experienced a decoupling of Te from Se with the common characteristic that Te is less abundant relative to Se. Even enstatite chondrites where both elements are partly enriched over CI display the same signature. Since Te and Se have very similar 50% condensation temperatures under nebula conditions (Se = 697 K, Te = 709 K; Lodders 2003), the more pronounced Te depletion in the majority of all known chondritic meteorites might be related to a different behavior of Te under different environmental conditions.

4.4.2 *Decoupling of Te during chondrule formation*

Compared to carbonaceous chondrites ordinary and enstatite chondrites are predominantly composed of chondrules (~80 vol. %). Fine-grained matrix is nearly absent in most enstatite chondrites and constitute about 15 vol. % in ordinary chondrites (*e.g.* Weisberg et al. 2006). Therefore the matrix composition has a smaller effect on the bulk composition of ordinary and enstatite chondrites and chondrules are more significant for the budget of volatile elements of the bulk chondrite. This is in line with the predominant presence of type II chondrules in ordinary chondrites (*e.g.* Huss et al. 2005) that have higher contents in volatile elements (*e.g.* S and Na) than type I chondrules (predominant in carbonaceous chondrites). As demonstrated by Grossman et al. 2007 and Alexander et al. 2008 chondrules are not as depleted in volatiles as previously thought. Furthermore, zoned mesostasis in chondrules from Semarkona (Nagahara et al. 1999) and CR2 chondrites (Krot et al. 2004) with higher volatile element content (*e.g.* Si, Na, K) towards the edge and enstatite formation on the inner edge of chondrules indicate back reactions of a vapor enriched in elements that were previously evaporated from chondrules and/or chondrule precursor. This indicates that chondrules acted as open systems and retained volatile elements to some extent (*e.g.* Tissandier et al. 2002; Grossman et al. 2007; Alexander et al. 2008; Hezel et al. 2010, 2014).

Compared to carbonaceous chondrites like Allende, the occurrence of the S, Se, and Te carrier phases and the distribution of these elements within the components of the ordinary chondrite Semarkona, indicates that metal and sulfide processing of ordinary chondrites occurred under different conditions. Prevalent metal-sulfide associations in the form of isolated grains on chondrule edges and within the matrix, sulfide-metal rims around chondrules, and blebs within chondrules indicate intensive thermal processing including melting, evaporation and recondensation (desulfurization and sulfurization of metals) within and outside chondrules. However, sulfides and metals in both Allende and Semarkona are highly processed by high-temperature events that also formed or at least affected chondrules. Considering the appearance of the constituents that display the decoupled Te abundance relative to Se (e.g. sulfide-rich rims around chondrules and around chondrule fragments in Allende and Semarkona and irregularly shaped metal-sulfide assemblages in Semarkona - Figures 4.3 a and 4.6 a, b), indicate that those constituents were affected by the same heating events that also formed or repeatedly processed chondrules. During these high-temperature processes, Te might behave more volatile than S, and Se due to changes in the ambient p/T conditions, and/or the vapor composition including the oxygen fugacity. The observation that the most oxidized carbonaceous chondrites display the least decoupling of Te from Se might indicate that the oxygen fugacity could have had an effect on the volatility of Te. On the other hand no systematic pattern has been observed between the more reduced (H) to oxidized (LL) ordinary chondrite groups which implies that the oxygen fugacity alone might not have played a substantial role. In the case of ordinary and enstatite chondrites more extensive or lengthy chondrule formation at the cost of fine-grained matrix abundance might have changed the ambient pressure under which Te reacted more volatile than S and Se.

4.4.3 Secondary depletion - Redistribution of Te on the parent body

Depletion of Se was found to be relatively uniform in ordinary chondrites with typical concentrations of 8 - 10 $\mu\text{g/g}$. In contrast Te concentrations display large scatter. While most of the samples show concentrations which are depleted relative to Se, two LL3 chondrites have Te concentrations similar to Se and one H3 sample (A-881641) is highly enriched relative to Se. Based on the well-defined horizontal trend for Se concentrations (Figure 4.2 a) in unequilibrated

ordinary chondrites and the observed large scatter in Te concentrations it seems also likely that Se and Te were first depleted to the same extent and further depletion of Te resulted from a secondary process, possibly thermal metamorphism processes on the parent body. According to Schaefer and Fegley (2010) and Ikramuddin et al. (1977) there are differences in the volatilities of the elements under nebula and parent body conditions due to differences in (gas)compositions, pressure, and oxygen fugacity at a given temperature. Based on heating experiments (Ikramuddin et al., 1977) a volatility sequence for ordinary chondrite parent bodies was determined and it could be shown that Se and S are rather constant over a large temperature range while Te behaves more volatile. Based on this observation open-system parent body metamorphism could be attributed as well for the more pronounced depletion of Te relative to Se in ordinary chondrites. According to Schaefer and Fegley (2010) volatile elements can be mobilized and become depleted relative to their initial abundances in the inner (hot) portions of the parent body (high petrologic types). Pushed by the vapor pressure the volatiles can escape and/or partly recondense in the outer portions (low petrologic type). Mobilization (evaporation and recondensation) due to parent body thermal metamorphism has been suggested to explain the variations in Te stable isotope composition of 6.9 ‰ for $\delta^{130/125}\text{Te}$ in unequilibrated ordinary chondrites (Fehr et al. 2014) as well as for the volatile elements Cd, Zn, Cu, and Ag (*e.g.* Wombacher et al. 2003, 2008; Luck et al. 2005; Schönbächler et al. 2008).

4.4.4 Aqueous alteration

Bulk analyses show that sulfur concentrations scatter in some of the carbonaceous chondrites (*e.g.* Orgueil, Tagish Lake, Murray, Nogoya etc., Figure 4.1). This scatter or decoupling of S might partly result from mobilization of the water soluble S by aqueous fluids on the parent body with subsequent heterogeneous redeposition, generating leached and enriched areas as indicated by higher and lower abundances of S relative to Se and Te. This is a prominent problem for CI chondrites (Lodders et al. 2009; Morlok et al. 2006; Barrat et al. 2011) but should be also relevant for other chondrites that experienced parent body aqueous alteration. Bulk S, Se and Te concentrations obtained from the weathered piece of Allende show that terrestrial weathering affects both S and Se abundances, while aqueous alteration on the parent body appears to affect predominantly S, rather than Se. The decoupling of Te from higher S and Se abundances in the

Antarctic CI chondrite Y-980115 may therefore simply reflect decoupling of S and Se from Te due to terrestrial weathering where S and Se, similar to Allende, became mobile and were heterogeneously redistributed so that the sample aliquot used for bulk analyses might simply reflect enrichment of S and Se relative to Te.

4.4.5 *Sample heterogeneity*

Large scatter in Te concentrations in ordinary chondrites and inferior whole procedure reproducibility for some samples indicate problems with the sample size and the preparation of homogeneous sample powders from chips especially for samples containing abundant metallic iron. In the present study sample powders were mainly prepared from 300 mg chips using an agate swing mill. Carbonaceous chondrites which mostly contain only small amounts of metal could be comminute very quickly. In contrast, samples with high modal abundances of metal like H and EH chondrites, had to be carefully pre-crushed with an agate mortar and several milling steps were necessary to obtain fine-grained powders. It seems that even with accelerated effort, some of these samples could not be sufficiently homogenized to avoid preparation induced heterogeneities. These heterogeneities might be overcome when larger amounts of sample powders are used for analyses. Furthermore, Se and Te bulk concentrations determined for the carbonaceous chondrites Ningqiang, Tagish Lake, and SCO 06043 show that Te is slightly more depleted than Se. In contrast, bulk analyses of Cold Bokkeveld display a slight enrichment in Te relative to Se. This might result from sample powders that contained constituents with higher Se/Te or lower Se/Te than CI, abundant enough to have an effect on bulk analyses.

4.4.6 *Comparison of chondritic ratios with the Earth*

Estimates for carbonaceous chondrites from this study display a mean Se/Te of 9.2 ± 0.5 (1 sd). All other chondrites (ordinary, enstatite and Rumuruti) show consistently higher Se/Te due to the common depletion in Te relative to Se. In contrast, recent estimates of the Se/Te for the bulk silicate earth (BSE) yield a mean of 7.9 ± 1.6 (1 sd) with the tendency to lower ratios (Wang & Becker, 2013b). Comparison of the present data for carbonaceous chondrites and the BSE Se/Te ratio show that the ratio given by Wang and Becker (2013b) agrees within the error with

carbonaceous chondrites even if the determined ratio for carbonaceous chondrites here is higher as the value from Lodders (2003) which was used for comparison by Wang & Becker (2013b). The tendency to lower Se/Te in the BSE compared to chondrites could indicate planetary differentiation or redistribution processes.

4.5 CONCLUSION

Different classes and groups of chondrites display different and often characteristic depletions in S, Se and Te. In carbonaceous chondrites all three elements are commonly depleted to the same extent and therefore corresponded equally to the depletion process. However, first data from LA-ICP-MS show that the carbonaceous chondrite Allende contains constituents with different S-Se-Te signatures when compared to the bulk. An example is the broad sulfide-rich rim around a rounded object with high Se/Te when compared to CI which has no effect on the bulk chemistry because of the scarce occurrence of such objects in bulk Allende. The same signature of high Se/Te as recognized in this single component in Allende, is characteristic for *bulk* ordinary, enstatite, and Rumuruti chondrites.

In-situ LA-ICP-MS analysis in the ordinary chondrite Semarkona reveals that most sulfide-metal assemblages interstitial to chondrules and chondrule rims show this characteristic signature of high Se/Te as observed in bulk ordinary chondrites. Thus, it is obvious that these sulfide-metal assemblages interstitial to chondrules and around chondrules and chondrule fragments control the signature of the bulk ordinary chondrite Semarkona. The appearance of these irregularly shaped sulfide-metal assemblages interstitial to chondrules as well as different sulfide-metal-rich rims around chondrules and chondrule fragments are characteristic for Semarkona (Brearley & Jones 1998; Zanda et al. 2000; Huang et al. 1993) and indicate repeated metal and sulfide thermal processing during chondrule formation (Zanda et al. 2000; Huang et al. 1993). Because the broad sulfide-rich rim around the rounded chondrule-like object in Allende obviously formed after the formation of the rounded object itself that in turn obviously formed due to a high temperature event, the decoupled Te from Se might be attributed as well to thermal processing during or after chondrule formation at which Te behaved more volatile, rather than to processes such as incomplete condensation, removal of Te-bearing metals after condensation, or the inheritance of

this signature from the molecular cloud which would indicate that the decoupled Te abundance from Se occurred prior to chondrule formation. Based on these initial observations and with the awareness that further investigations are necessary I suggest that at least the more pronounced depletion of Te relative to Se from sulfide-rich constituents in Allende and Semarkona occurred due to thermal processing during chondrule formation. In summary, investigations of bulk chondritic S, Se and Te concentrations in combination with investigations on the distribution and relative abundances of these elements by in-situ LA-ICP-MS analysis with the advantage of optical control of the material under investigation, provide advanced and supplementary insights into the distribution and behavior of elements like S, Se and Te in chondritic matter and therefore into the processes that could have been involved.

5. REFERENCES

- Abel T., Bryan G. L., and Norman M. L. (2000). The formation and fragmentation of primordial molecular clouds. *Astrophysical Journal*, 540: 39 – 44.
- Abel T., Bryan G. L., and Norman M. L. (2002). The formation of the first star in the universe. *Science*, 295: 93 – 98.
- Ackerman L., Rohovec J., and Sebek O. (2012). Determination of total sulfur in fifteen geological materials using inductively coupled plasma-optical emission spectrometry (ICP-OES) and combustion/infrared spectrometry. *Geostandards and Geoanalytical Research*, 36: 407 – 414.
- Alexander C. M. O'D. (2004). Chemical equilibrium and kinetic constraints for chondrule and CAI formation conditions. *Geochimica et Cosmochimica Acta*, 68: 3943–3969.
- Alexander C. M. O'D. and Grossman J. N. (2005). Alkali elemental and potassium isotopic compositions of Semarkona chondrules. *Meteoritics & Planetary Science* 40: 541 – 556.
- Alexander C. M. O'D., Grossman J. N., Ebel D. S., and Ciesla F. J. (2008). The formation conditions of chondrules and chondrites. *Science*, 320: 1617 – 1619.
- Alexander C. M. O'D., Grossman J. N., Wang J., Zanda B., Bourot-Denise M., and Hewins R. H. (2000). The lack of potassium-isotopic fractionation in Bishunpur chondrules. *Meteoritics & Planetary Science*, 35: 859 – 868.
- Amelin Y., Krot A. N., Hutcheon I. D., and Ulyanov A. A. (2002). Lead isotopic ages of chondrules and calcium-aluminum-rich inclusions. *Science*, 297: 1678 – 1683.
- Anders E. (1964). Origin, age and composition of meteorites. *Space Science Review*, 3: 583 - 714
- Anders E. and Grevesse N. (1989). Abundances of the elements – meteoritic and solar. *Geochimica et Cosmochimica Acta*, 53: 197 – 214.
- Andronikov A. V., Lauretta D. S., Connolly H. C., and Andronikova I. E. (2013). Determination of Trace-Element Bulk Composition of Equilibrated Ordinary Chondrite Meteorite Samples by LA-ICP-MS Using Various Reference Materials. *Lunar & Planetary Science Conference*, A1719: 1603.
- Asphaug E., Jutzi M., Movshovitz M. (2011). Chondrule formation during planetesimal accretion. *Earth & Planetary Science Letters*, 308: 369 – 379.
- Athanassiou E., Grass R., and Stark W. (2010). Chemical Aerosol Engineering as a Novel Tool for Material Science: From Oxides to Salt and Metal Nanoparticles. *Aerosol Science and Technology*, 44/2: 161 – 172.
-

-
- Barrat J. A., Zanda B., Moynier F., Bollinger C., Liorzou C., and Bayon G. (2012). Geochemistry of CI chondrites revisited: Major and trace elements, and Cu and Zn isotopes. *Geochimica et Cosmochimica Acta*, 83: 79 – 92.
- Behrens H., Romano C., Nowak M., Holtz F., and Dingwell D. B. (1996). Near-Infrared Spectroscopic Determination of Water Species in Glasses of the System MAISi₃O₈ (M = Li, Na, K): An Interlaboratory Study. *Chemical Geology, 5TH Silicate Melt Workshop*, 128/1: 41 – 63.
- Berglund M. and Wieser M. E. (2011). Isotopic compositions of the elements (IUPAC Technical Report). *Pure and Applied Chemistry* 83/2: 397 – 410.
- Bevan A. W. R. and Axon H. J. (1980). Metallography and thermal history of the Tieschitz unequilibrated meteorite – metallic chondrules and the origin of polycrystalline taenite. *Earth & Planetary Science Letters*, 47: 353 – 360.
- Bian Q., Garcia C. C., Koch J., and Niemax K. (2006). Non-matrix matched calibration of major and minor concentrations of Zn and Cu in brass, aluminium and silicate glass using NIR femtosecond laser ablation inductively coupled plasma mass spectrometry. *Journal of Analytical Atomic Spectroscopy*, 21: 187 – 191.
- Bischoff A., Vogel N., and Roszjar J. (2011). The Rumuruti chondrite group. *Chemie der Erde*, 71: 101 – 133.
- Bischoff A. (1989). Mineralogische und chemische Untersuchungen an chondritischen Meteoriten: Folgerungen für die Entstehung fester Materie im Solarnebel und die Entwicklung der Meteoritenmutterkörper, habilitation thesis.
- Binz C. M., Kurimoto R. K. & Lipschutz M. E. (1974). Trace elements in primitive meteorites— V. Abundance patterns of thirteen trace elements and interelement relationships in enstatite chondrites. *Geochimica et Cosmochimica Acta*, 38: 1579 – 1606.
- Binz C. M., Ikramuddin M., Rey P., and Lipschutz M. E. (1976). Trace-Elements in Primitive Meteorites .6. Abundance Patterns of 13 Trace-Elements and Interelement Relationships in Unequilibrated Ordinary Chondrites. *Geochimica et Cosmochimica Acta*, 40: 59 - 71.
- Bland P. A., Alard O., Gounelle M., Benedix G. K., Kearsley A. T., and Rogers N. W. (2004). Volatile and moderately volatile trace element composition of chondrules and matrix from CM chondrites: Implications for chondrule formation. *Lunar & Planetary Science Conference*. A1737.
- Bland P. A., Alard O., Benedix G. K., Kearsley A. T., Menzies O. N., Watt L. E., Rogers N. W. (2005). Volatile fractionation in the early solar system and chondrule/matrix complementarity. *Proc. Natl. Acad. Sci.* 102: 13755 – 13760.
-

-
- Bland P. A., Stadermann F. J., Floss C., Rost D., Vicenzi E. P., Kearsley A. T., Benedix G. K. (2007). The cornucopia of presolar and early solar system materials at the micrometer size range in primitive chondrite matrix. *Meteoritics & Planetary Science* 42: 1417 – 1427.
- Boynton W. V. (1975). Fractionation in the solar nebula: Condensation of yttrium and the rare earth elements. *Geochimica et Cosmochimica Acta*, 37: 1119 – 1140.
- Brearly A. J. and Jones R. H. (1998). Chondritic meteorites. In: Papike, J. J. (ed.) Planetary Materials. Reviews in Mineralogy, vol. 36: 3-1 – 3-398. Washington, DC: Mineralogical Society of America.
- Bromm V., Coppi P. S., and Larson R. B. (1999). Forming the first stars in the universe: The fragmentation of primordial gas. *The Astrophysical Journal*, 527: L5 – L8.
- Bromm V. and Larson R. B. (2004). The first stars. *Annu. Rev. Astron. Astrophys.*, 42: 79 – 118.
- Brown P. G., Hildebrand A. R., Zolensky M. E., Grady M., Clayton R. N., Mayeda T. K., Tagliaferri E., Spalding R., MacRae N. D., Hoffman E. L., Mittlefehldt D. W., Wacker J. F., Bird J. A., Campbell M. D., Carpenter R., Gingerich H., Glatiotis M., Greiner E., Mazur M. J., McCausland P. J. A., Plotkin H., Mazur T. R. (2000). The fall, recovery, orbit, and composition of the Tagish Lake meteorite: A new type of carbonaceous chondrite. *Science*, 290: 320 – 324.
- Burbidge E.M., Burbidge G.R., Fowler W.A. and Hoyle F. (1957). Synthesis of the elements in stars. *Reviews of Modern Physics*, 29: 547 - 650.
- Burnett D. S., Woolum D. S., Benjamin T. M., Rogers P. S. Z., Duffy C. J., Maggiore C. (1989). A test of the smoothness of the elemental abundances of carbonaceous chondrites. *Geochimica et Cosmochimica Acta*, 53: 471 - 481.
- Cameron A. G. W. (1962). The formation of the Sun and planets. *Icarus* 1: 13 – 69.
- Cameron A. G. W. (1963). Formation of the solar nebula. *Icarus* 1: 339 – 342.
- Cameron A. G. W. and Pine M. R. (1973). Numerical models of the primitive solar nebula. *Icarus* 18: 377 – 406.
- Cassen P. (1996). Models for the fractionation of moderately volatile elements in the solar nebula. *Meteoritics & Planetary Science* 31: 793 – 806.
- Cassen P. (2001). Nebular thermal evolution and the properties of primitive materials. *Meteoritics & Planetary Science* 36: 671 – 700.
- Campbell A. J., Humayun M., Meibom A., Krot A. N., and Keil K. (2001). Origin of zoned metal grains in the QUE94411 chondrite. *Geochimica et Cosmochimica Acta*, 65: 163 – 180.
-

-
- Case D. R., Laul J. C., Pelly I. Z., Wechter M. A., Schmidt-Bleek F., Lipschutz M. E. (1973). Abundance patterns of thirteen trace elements in primitive carbonaceous and unequilibrated ordinary chondrites. *Geochimica et Cosmochimica Acta*, 37: 19 - 33.
- Chizmadia L. J., Rubin A. E., and Wasson T. J. (2002). Mineralogy and petrology of amoeboid olivine inclusions in CO3 chondrites: relationship to parent-body aqueous alteration. *Meteoritics & Planetary Science*, 37: 1781 – 1796.
- Ciesla F. J. (2005) Chondrule-forming processes – An overview. In: Krot AN, Scott ERD, and Reipurth B (eds.) Chondrites and the Protoplanetary Disk, Astronomical Society of the Pacific Conference Series, vol. 341: 811 – 820.
- Clarke R. S. Jr., Jarosewich E., Mason B., Nelen J., Gómez M., and Hyde J. R. (1970). The Allende, Mexico, Meteorite Shower. *Smithson. Contrib. Earth Sci.*, 5: 1 - 55.
- Connelly J. N., Bizzarro M., Ivanova M., and Krot A. N. (2011). Towards a new absolute chronology for the early solar system. LPI contribution No. 1639: 9056, In: *Workshop on Formation of the first solids in the solar system*, November 7 – 9, Kauai, Hawaii.
- Connolly H. C., Jr. and Love S. G. (1998). The formation of chondrules: petrologic tests of the shock wave model. *Science* 280: 62 – 67.
- Cuzzi J. N. and Alexander C. M. O'D (2006). Chondrule formation in particle-rich nebular regions at least hundreds of kilometres across. *Nature* 441: 483 – 485.
- Dauphas N., Marty B., and Reisberg L. (2002). Molybdenum evidence for inherited planetary scale isotope heterogeneity of the protosolar nebula. *Astrophys. J.*, 565: 640 – 644.
- Davis A. M., and Richter F. M. (2003). Condensation and evaporation of solar system materials. In: *Treatise on Geochemistry*, Vol.1. (eds.) A.M. Davis, Elsevier-Pergamon, Oxford: 407 - 430.
- Davis A. M. (2006). Volatile evolution and loss. In: *Meteorites and the Early Solar System II*, D. S. Lauretta and H. Y. McSween Jr. (eds.), University of Arizona Press, Tucson: 295 – 307.
- Desch S. J. and Connolly H. C., Jr. (2002). A model of the thermal processing of particles in solar nebula shocks: application to the cooling rates of chondrules. *Meteoritics & Planetary Science*, 37: 183 – 207.
- Desch S. J., Ciesla F. J., Hood L. L., Nakamoto T. (2005). Heating of chondritic materials in solar nebula shocks. In: Krot, A.N., Scott, E.R.D., Reipurth, B. (Eds.), *Chondrites and the Protoplanetary Disk*. Astronomical Society of the Pacific, San Francisco, pp. 849 – 872.
- Dodd R. T. (1981). *Meteorites: A Petrologic-Chemical Synthesis*. Cambridge: Cambridge University Press: 368.
-

- Dreibus G., Palme H., Spettel B. and Wänke H. (1993). Sulfur and selenium in chondritic meteorites. *Meteoritics* 28: 343 (abs.).
- Dreibus G., Palme H., Spettel B., Zipfel J., and Wänke H. (1995). Sulfur and selenium in chondritic meteorites. *Meteoritics*, 30: 439 – 445.
- Dyl K. A., Cleverley J. S., Bland P. A., Ryan C. G., Fisher L. A., and Hough R. M. (2014). Quantified, whole section trace element mapping of carbonaceous chondrites by Synchrotron X-ray Fluorescence Microscopy: 1. CV meteorites. *Geochimica et Cosmochimica Acta*, 134: 100 – 119.
- Ebel D. S and Grossman L. (2000). Condensation in dust-enriched systems. *Geochimica et Cosmochimica Acta*, 64: 339 – 366.
- Ebel D. S., Leftwich K., Brunner C. E., and Weisberg M. K. (2009). Abundance and size distribution of inclusions in CV3 chondrites by X-ray image analysis. *40th Lunar & Planetary Science Conference*: A2065.
- El Goresy A., Nagel K., and Ramdohr P. (1979). Spinel framboids and fremdlinge in Allende inclusions: Possible sequential markers in the early history of the solar system. *Proc. Lunar & Planetary Science Conference*, 10th: 833 – 850.
- El Goresy A., Palme H., Yabuki H., Nagel K., Herrwerth I., and Ramdohr P. (1984). A calcium-aluminum-rich inclusion from the Essebi (CM2) chondrite: Evidence for captured spinelhibonitepherules and for an ultra-refractory rimming sequence. *Geochimica et Cosmochimica Acta*, 48: 2283 – 2298.
- El Goresy A., Ramdohr P., and Rambaldi E. R. (1981). Sulfide-rich chondrule rims in Bishunpur (L3) chondrite: types, textures, mineralogy and genetic implications. *Lunar and Planetary Science XII* (abstract): 254 – 256.
- Elwaer N. and Hintelmann H. (2008). Precise selenium isotope ratios measurement using a multimode sample introduction system (MSIS) coupled with multicollector inductively coupled plasma mass spectrometry (MC-ICP-MS). *Journal of Analytical Atomic Spectroscopy* 23: 1392 – 1396.
- Evensen N. M., Hamilton P. J., and O’Nions R. K. (1978). Rare-Earth Abundances in Chondritic Meteorites. *Geochimica et Cosmochimica Acta*, 42: 1199 – 1212.
- Fegley B. Jr. (2000). Kinetics of gas-grain reactions in the solar nebula. *Space Science Reviews* 92: 177 – 200.
- Fegley B. Jr. and Palme H. (1985). Evidence for oxidizing conditions in the solar nebula from Mo and W depletions in refractory inclusions in carbonaceous chondrites. *Earth & Planetary Science Letters*, 72: 311 – 326.
-

- Fehr M. A., Rehkaemper M., Halliday A. N., Wiechert U., Hattendorf B., Guenther D., Ono S., Eigenbrode J. L., and Rumble D. (2005) Tellurium isotopic composition of the early solar system - A search for effects resulting from stellar nucleosynthesis, ^{126}Sn decay, and mass-independent fractionation. *Geochimica et Cosmochimica Acta*, 69: 5099 - 5112.
- Fehr M. A., Hammond S. J., and Parkinson I. J. (2014). Tellurium stable isotope fractionation in chondritic meteorites. *77th Annual Meteoritical Society Meeting*: #5290.
- Friedrich J. M., Wang M.-S., and Lipschutz M. E. (2002). Comparison of the trace element composition of Tagish Lake with other primitive carbonaceous chondrites. *Meteoritics & Planetary Science*, 37: 677 – 686.
- Friedrich J. M., Wang M.-S., and Lipschutz M. E. (2003). Chemical studies of L chondrites. V.: Compositional patterns for 49 trace elements in 14 L4–6 and 7 LL4–6 falls. *Geochimica et Cosmochimica Acta*, 67: 2467 – 2479.
- Fitzgerald M. J. (1979). The chemical composition and classification of the Karoonda meteorite. *Meteoritics*, 14: 109 - 115.
- Funk C., Wombacher F., Becker H., and Bischoff A. (2012a). Isotope dilution analyses of Se and Te in chondritic meteorites. *Mineralogical Magazine* 76/6: 1692 – 1728.
- Funk C., Wombacher F., Becker H., and Bischoff A. (2012b). Isotope dilution analyses of Se and Te in chondrites. *European Mineralogical Conference Vol.1*, EMC2012-642.
- Gaboardi M. and Humayun M. (2009). Elemental fractionation during LA-ICP-MS analysis of silicate glasses: implications for matrix-independent standardization. *Journal of Analytical and Atomic Spectrometry*, 24: 1188 – 1197.
- Gao X. and Thiemens M. H. (1993). Isotopic composition and concentration of sulfur in carbonaceous chondrites. *Geochimica et Cosmochimica Acta*, 57: 3159 - 3169.
- Gao S., Liu X., Yua H., Hattendorf B., Günther D., Chen L., Hu S. (2002). Determination of forty two major and trace elements in USGS and NIST SRM glasses by laser ablation-inductively coupled plasma-mass spectrometry. *The Journal of Geostandards and Geoanalysis*, 26/2: 181–196.
- Garbe-Schönberg D. and Müller S. (2014). Nano-particulate pressed powder tablets for LA-ICP-MS. *Journal of Analytical Atomic Spectrometry*, 29: 990 – 1000.
- Goldschmidt V. M. (1937a). Geochemische Verteilungsgesetze der Elemente, IX. *Skrifter Norske Videnskaps-Akad. Oslo. I. Mat. Kl. No. 4*.
- Goldschmidt V. M. (1937b). The principles of distribution of chemical elements in minerals and rocks. *Journal of the Chemical Society*: 655 – 673.
-

-
- Grevesse N. and Sauval A. J. (1998). Standard solar composition. *Space Science Reviews*, 85: 161 – 174.
- Grossman J. N., Alexander C. M. O'D, Ash R. D., Luong M., and McDonough W. F. (2007). Volatile element abundances in chondrules revisited: An LA-ICP-MS study of QUE 97008 (LL3.05). *Planetary Science Conference* 38: A2000.
- Grossman L. (1972). Condensation in the primitive solar nebula. *Geochimica et Cosmochimica Acta*, 36: 597 – 619.
- Grossman L. and Larimer J. W. (1974). Early chemical history of the solar system. *Reviews of Geophysics and Space Physics*, 12: 71 – 101.
- Günther D. and Hattendorf B. (2005). Solid sample analysis using laser ablation inductively coupled plasma mass spectrometry. *Trends in Analytical Chemistry*, 24/3: 255 – 265.
- Guillong M., Hametner K., Reusser E., Wilson S. A., Günther D. (2005). Preliminary Characterization of New Glass Reference Materials (GSA-1G, GSC-1G, GSD-1G and GSE-1G) by Laser Ablation-Inductively Coupled Plasma-Mass Spectrometry Using 193 nm, 213 nm and 266 nm Wavelengths. *Geostandards and Geoanalytical Research* 29/3: 315 – 331.
- Halicz L., and Günther D. (2004). Quantitative analysis of silicates using LA-ICP-MS with liquid calibration. *Journal of Analytical Atomic Spectrometry*, 19: 1539 – 1545.
- Harkins W. D. (1917). The evolution of the elements and the stability of complex atoms. I. A new periodic system which shows a relation between the abundance of the elements and the structure of the nuclei of atoms. *Journal of the American Chemical Society*, 39(5): 856 – 879.
- Hewins R. H., Bourot-Denise M., Zanda B., Leroux H., Barrat J.-A., Humayun M., Göpel C., Greenwood R. C., Franci I. A., Pont S., Lorand J.-P., Cournède C., Gattacceca J., Rochette P., Kuga M., Marrocchi Y., Marty B. (2014). The Paris meteorite, the least altered CM chondrite so far. *Geochimica et Cosmochimica Acta*, 124: 190 – 222.
- Hezel D. C., Mucerschi D., Friend P., and Palme H. (2014). Chondrule zonation in carbonaceous chondrites. *77th Annual Meteoritical Society Meeting*: A5248.
- Hezel D. C. and Palme H. (2008). Constrains for chondrule formation from Ca – Al distribution in carbonaceous chondrites. *Earth & Planetary Science Letters*, 265: 716 – 725.
- Hezel D. C. and Palme H. (2010). The chemical relationship between chondrules and matrix complementarity. *Earth & Planetary Science Letters*, 294: 65 – 93.
- Hoffmann E., Lüdke C., and Scholze H. (1997). “Is Laser-Ablation-ICP-MS an Alternative to Solution Analysis of Solid Samples?” *Fresenius' Journal of Analytical Chemistry*, 359: 394 – 98.
-

-
- Horn I., Guillon M., and Günther D. (2001). Wavelength dependant ablation rates for metals and silicate glasses using homogenized laser beam profiles – implications for LA-ICP-MS. *Applied Surface Science*, 182: 91 – 102.
- Horstmann M., Humayun M., and Bischoff A. (2014). Clues to the origin of metal in Almahata Sitta EL and EH chondrites and implications for primitive E chondrite thermal histories. *Geochimica et Cosmochimica Acta*, 140: 720 – 744
- Howard K. T., Benedix G. K, Bland P. A., and Cressey G. (2011). Modal mineralogy of CM chondrites by X-ray diffraction (PSD-XRD): Part 2. Degree, nature and settings of aqueous Alteration. *Geochimica et Cosmochimica Acta*, 75: 2735 – 2751.
- Hoyle F., (1946). The synthesis of the elements from hydrogen. *Monthly Notices of the Royal Astronomical Society*, 106: 343.
- Hoyle F., (1954). On Nuclear Reactions Occuring in Very Hot STARS. I. the Synthesis of Elements from Carbon to Nickel. *The Astrophysical Journal Supplement Series*, 1: 121.
- Huang S., Benoit P. H., and Sears D. W. G. (1993). Metal and sulfide in Semarkona chondrules and rims: evidence for reduction, evaporation, and recondensation during chondrule formation. *Meteoritics*, 28/3: 367.
- Humayun M. and Clayton R. N. (1995). Potassium isotope geo-chemistry: Genetic implications of volatile element depletion. *Geochimica et Cosmochimica Acta*, 59, 2131 - 2148.
- Humayun M., Simon S. B. and Grossman L. (2007). Tungsten and hafnium distribution in calcium aluminum inclusions (CAIs) from Allende and Efremovka. *Geochimica et Cosmochimica Acta*, 71: 4609 – 4627.
- Huss G. R. (2004). Implications of isotopic anomalies and presolar grains for the formation of the solar system. *Antarct. Meteorite Res.*, 17: 133 – 153.
- Huss G. R., Alexander C. M. O'D., Palme H., Bland P. A., Wasson J. T. (2005). Genetic Relationship between chondrules, fine-grained rims, and interchondrule matrix. *Chondrites and the Protoplanetary Disk ASP Conference Series*, 341: 701 – 731.
- Huss G. R., Meshik A. P., Smith J. B., and Hohenberg C. M. (2003). Presolar diamond, silicon carbide, and graphite in carbonaceous chondrites: Implications for thermal processing in the solar nebula. *Geochimica et Cosmochimica Acta* 67: 4823 – 4848.
- Hyman M. and Rowe M. W. (1983). Magnetite in CI chondrites. *Journal of Geophysical Research*, 88: A736 – A740.
- Ikramuddin M., Matza S., and Lipschutz M.E. (1977). Thermal metamorphism of primitive meteorites. V. Ten trace elements in Tieschitz H3 chondrite heated at 400–1000 °C. *Geochimica et Cosmochimica Acta*, 41: 1247 – 1256.
-

-
- Ireland T. R. and Fegley B., Jr. (2000). The solar system's earliest chemistry: systematics of refractory inclusions. *Int. Geol. Rev.*, 42: 865 – 894.
- Itoh S., Rubin A. E., Kojima H., Wasson J. T. and Yurimoto H. (2002). Amoeboid olivine aggregates and AOA-bearing chondrule from Y81020 CO3.0 chondrite: Distributions of oxygen and magnesium isotopes. *Lunar & Planetary Science Conference*, A1490.
- Jarosewich E. (1966). Chemical analyses of ten stony meteorites. *Geochimica et Cosmochimica Acta*, 30: 1261 - 1265.
- Jochum K.P., Dingwell D.B., Rocholl A., Stoll B., Hofmann A.W., Becker S., Besmehn A., Bessette D., Dietze H.-J., Dulski P., Erzinger J., Hellebrand E., Hoppe P., Horn I., Janssens K., Jenner G.A., Klein M., McDonough W.F., Maetz M., Mezger K., Münker C., Nikogosian I.K., Pickhardt C., Raczek I., Rhede D., Seufert H.M., Simakin S.G., Sobolev A.V., Spettel B., Straub S., Vincze L., Wallianos A., Weckwerth G., Weyer S., Wolf D., and Zimmer M. (2000). The preparation and preliminary characterisation of eight geological MPI-DING reference glasses for in-situ microanalysis. *Geostandards Newsletter: The Journal of Geostandards and Geoanalysis*, 24: 87 - 133.
- Jochum K.P., Pfänder J., Woodhead J.D., Willbold M., Stoll B., Herwig K., Amini M., Abouchami W. and Hofmann A.W. (2005). MPI-DING glasses: New geological reference materials for in situ Pb isotope analysis. *Geochemistry Geophysics Geosystems* 6: doi: 10.1029/2005GC000995. issn: 1525-2027.
- Jochum K. P., Stoll S., Herwig K., and Willbold M. (2007). Validation of LA-ICP-MS trace element analysis of geological glasses using a new solid-state 193 nm Nd:YAG laser and matrix-matched calibration. *Journal of Analytical Atomic Spectrometry*, 22: 112 – 121.
- Jochum K. P., Stoll B., Herwig K., Willbold M., Hofmann A. W., Amini M., Aarburg S., Abouchami W., Hellebrand E., Mocek B., Raczek I., Stracke A., Alard O., Bouman C., Becker S., Dücking M., Brätz H., Klemm R., de Bruin D., Canil D., Cornell D., de Hoog C.-J., Dalpé C., Danyushevsky L., Eisenhauer A., Gao Y., Snow J. E., Groschopf N., Günther D., Latkoczy C., Guillong M., Hauri E. H., Höfer H. E., Lahaye Y., Horz K., Jacob D. E., Kasemann S. A., Kent A. J. R., Ludwig T., Zack T., Mason P. R. D., Meixner A., Rosner M., Misawa K., Nash B. P., Pfänder J., Premo W. R., Sun W. D., Tiepolo M., Vannucci R., Vennemann T., Wayne D., Woodhead J. D.(2006). MPI-DING reference glasses for in situ microanalysis: New reference values for element concentrations and isotope ratios. *Geochemistry Geophysics Geosystems*, 7: doi: 10.1029/2005GC001060. issn: 1525-2027.
- Jochum K. P., Weis U., Stoll B., Kuzmin D., Yang O., Raczek I., Jacob D. E., Stracke A., Birbaum K., Frick D. A., Günther D., and Enzweiler J. (2011) Determination of Reference Values for NIST SRM 610—617 Glasses Following ISO Guidelines. *Geostandards and Geoanalytical Research*, 35/4: 397 – 429.
- Kaczaral P. W., Dodd R. T., Lipschutz M. E. (1989). Chemical studies of L chondrites: IV. Antarctic/non-Antarctic comparisons. *Geochimica et Cosmochimica Acta*, 53: 491 - 501.
-

- Kadlag Y. and Becker H. (2013a). HSE and S-Se-Te fractionation in components of enstatite chondrites. *Mineralogical Magazine*, 77/5: 1416.
- Kadlag Y. and Becker H. (2013b). Constraints from HSE and S-Se-Te abundances on the origin of components of EH3 chondrites. *Joint Meeting "Paneth Kolloquium" and SPP 1385: The First 10 Million Years of the Solar System*: A0028.
- Kadlag Y. and Becker H. (2014). Highly siderophile and chalcogen element constraints on the origin of components of unequilibrated L chondrites. *Lunar & Planet. Sci. Conf.* 45: A1771.
- Kadlag Y., Becker H., Schubring F., and Giebner T. (2014). Abundances of highly siderophile and chalcogen elements in the components of unequilibrated L chondrites. *92nd Annual Meeting Deutsche Mineralogische Gesellschaft 2014*: MET-T10.
- Kallemeyn G. W. and Wasson J. T. (1981). The compositional classification of chondrites – I. The carbonaceous chondrite group. *Geochimica et Cosmochimica Acta*, 45: 1217 – 1230.
- Kallemeyn G. W. and Wasson J. T. (1986). Compositions of enstatite (EH3, EH4,5 and EL6) chondrites: Implications regarding their formation. *Geochimica et Cosmochimica Acta*, 50: 2153 – 2164.
- Kallemeyn G. W., Rubin A. E., Wang D., and Wasson J. T. (1989). Ordinary chondrites: Bulk compositions, classification, lithophile-element fractionations, and composition-petrographic type relationships. *Geochimica et Cosmochimica Acta*, 53: 2747 - 2767.
- Kallemeyn G. W., Rubin A. E., Wasson J. T. (1996). The compositional classification of chondrites: VII. The R chondrite group. *Geochimica et Cosmochimica Acta*, 60: 2243 – 2256.
- Kita N. T. and Ushikubo T. (2012). Evolution of protoplanetary disk inferred from 26Al chronology of individual chondrules. *Meteoritics & Planetary Science*, 47: 1108 – 1119.
- Kleine T., Münker C., Mezger K., and Palme H. (2002). Rapid Accretion and Early Core Formation on Asteroids and the Terrestrial Planets from Hf-W Chronometry. *Nature*, 418: 952 – 55.
- Klerner S. (2001). Materie im frühen Sonnensystem: die Entstehung von Chondren, Matrix, und refraktären Forsteriten. Ph. D. thesis. Universität zu Köln.
- Koch J. and Günther D. (2011). Review of the state-of-the-art of laser ablation inductively coupled plasma mass spectrometry. *Applied Spectroscopy*, 65/5: 155 – 162.
- Koch J., Wälle M., Pisonero J., Günther D. (2006). Performance characteristics of ultra-violet femtosecond laser ablation inductively coupled plasma mass spectrometry at ~265 and ~200 nm *Journal of Analytical and Atomic Spectrometry*, 21: 932 - 940.
-

-
- Komatsu M., Krot A. N., Kasama T., Pataev M. I., Ulyanov A. A., Keil K., and Miyamoto M. (2001) Mineralogy and petrography of amoeboid olivine aggregates from the reduced CV3 chondrites Efremovka, Leoville and Vigarano: Products of nebular condensation, accretion and annealing. *Meteoritics & Planetary Science* 36: 629 – 641.
- König S., Luguët A., Lorand J.-P., Wombacher F., Lissner M. (2012). Selenium and tellurium systematics of the Earth's mantle from high precision analyses of ultra-depleted orogenic peridotites. *Geochimica et Cosmochimica Acta*, 86: 354 – 366.
- Kornacki A. S. and Fegley B. Jr. (1986). The abundance and relative volatility of refractory trace elements in Allende Ca, Al-rich inclusions: Implications for chemical and physical processes in the solar nebula. *Earth & Planetary Science Letters*, 79: 217 – 234.
- Kuebler K. E., McSween H. Y., Carlson W. D., and Hirsch D. (1999). Sizes and masses of chondrules and metal-troilite grains in ordinary chondrites: possible implications for nebular sorting. *Icarus*, 141: 96 – 106.
- Kurat G., Zinner E., and Brandstätter F. (2002). A plagioclase olivine-spinel-magnetite inclusion from Maralinga (CK): Evidence for sequential condensation and solid-gas exchange. *Geochimica et Cosmochimica Acta*, 66: 2959 – 2979.
- Kroslakova I. and Günther D. (2007). Elemental fractionation in laser ablation-inductively coupled plasma-mass spectrometry: evidence for mass load induced matrix effects in the ICP during ablation of a silicate glass. *Journal of Analytical Atomic Spectrometry*. 22: 51 – 62.
- Krot A. N., Amelin Y., Bland P., Ciesla F. J., Connelly J., Davis A. M., Huss G. R., Hutcheon I. D., Makide K., Nagashima K., Nyquist L. E., Russell S. S., Scott E. R. D., Thrane K., Yurimoto H., and Yin Q.-Z. (2009). Origin and chronology of chondritic components: A review. *Geochimica et Cosmochimica Acta*, 73: 4963 – 4997.
- Krot A. N., Meibom A., Russell S. S., Alexander C. M. O., Jeffries T. E., and Keil K. (2001). A new astrophysical setting for chondrule formation. *Science* 291, 1776 – 1779.
- Krot A. N., Petaev M. I., Russell S. S., Itoh S., Fagan T. J., Yurimoto H., Chizmadia L., Weisberg M. K., Komatsu M., Olyanov A. A., and Keil K. (2004). Amoeboid olivine aggregates and related objects in carbonaceous chondrites: Records of nebular and asteroid processes. *Chemie der Erde*, 64: 185 – 239.
- Krot A. N., Scott E. R. D., and Zolensky M. E. (1995). Mineralogical and chemical modification of components in CV3 chondrite: Nebular or asteroidal processing? *Meteoritics* 30: 748 – 775.
- Larimer J. W. and Anders E. (1967). Chemical fractionation in meteorites-II. Abundance patterns and their interpretation. *Geochimica et Cosmochimica Acta*, 31: 1239 – 1270.
- Larimer, J. W. and Anders, E. (1970). Chemical fractionation in meteorites-III. Major element fractionations in chondrites. *Geochimica et Cosmochimica Acta*, 34: 367 – 387.
-

-
- Larimer J. W. (1967). Chemical fractionations in meteorites-I. Condensation of the elements. *Geochimica et Cosmochimica Acta*, 31: 1215.
- Larimer J. W. and Anders E. (1967). Chemical fractionations in meteorites-II. Abundance patterns and their interpretation. *Geochimica et Cosmochimica Acta*, 31, 1239–1270.
- Leach A. M. and Hieftje G. M. (2002). Identification of alloys using single shot laser ablation inductively coupled plasma time-of-flight mass spectrometry. *Journal of Analytical Atomic Spectrometry*, 17: 852 – 857.
- Lin Y., Kimura M., and Wang D. (2003). Fassaites in compact type A Ca-al-rich inclusions in the Ningqiang carbonaceous chondrite: Evidence for partial melting in the nebula. *Meteoritics & Planetary Science*, 38: 407 – 417.
- Lin Y. and Kimura M. (2000). Two unusual Type B refractory inclusions in the Ningqiang carbonaceous chondrite: Evidence for relicts, zenoliths and multi-heating. *Geochimica et Cosmochimica Acta*, 64: 4031 – 4047.
- Liu Y., Hu Z., Gao S., Günther D., Xu J., Gao C., Chen H. (2008) In situ analysis of major and trace elements of anhydrous minerals by LA-ICP-MS without applying an internal standard. *Chemical Geology*, 257: 34 – 43.
- Liu C., Mao X. L., Mao S., Zeng X., Greif R., and Russo R. E. (2004). Nanosecond and Femtosecond Laser Ablation of Brass: Particulate and ICPMS Measurements. *Analytical Chemistry*, 76: 379.
- Lodders K. (2003). Solar system abundances and condensation temperatures of the elements. *The Astrophysical Journal*, 591: 1220 – 1247.
- Lodders K. and Fegley B. Jr. (1998) *The Planetary Scientist's Companion*, Oxford University Press.
- Lodders K. and Fegley B. Jr. (2011). Chemistry of the solar system. *Cambridge RSC Publishing, Royal Society of Chemistry*: 476.
- Lodders K., Palme H., Gail H. P. (2009). Abundances of the elements in the solar system. In Landolt-Bornstein, New Series, Vol. VI/4B, Chap. 4.4, J.E. Trumper (ed.), Berlin, Heidelberg, New York: Springer-Verlag: 560 - 630.
- Longerich H. P., Jackson S. E., and Günther D. (1996). Laser Ablation Inductively Coupled Plasma Mass Spectrometric Transient Signal Data Acquisition and Analyte Concentration Calculation. *Journal of Analytical Atomic Spectrometry*, 11: 899 – 904.
- Loss R. D., Rosman K. J. R., De Laeter J. R. (1984). Mass spectrometric isotope dilution analyses of palladium, silver, cadmium and tellurium in carbonaceous chondrites. *Geochimica et Cosmochimica Acta*, 48: 1677 – 1681.
-

-
- Luck J.M., Othman D.B., Barrat J.A., and Albarede F. (2003). Coupled ^{63}Cu and ^{16}O excesses in chondrites. *Geochimica et Cosmochimica Acta*, 67: 143–151.
- Luck J.M., Othman D.B., and Albarede F. (2005). Zn and Cu isotopic variations in chondrites and iron meteorites: Early solar nebula reservoirs and parent-body processes. *Geochimica et Cosmochimica Acta*, 69: 5351–5363.
- Lugmair G. W. and Shukolyukov A. (1998). Early solar system timescales according to ^{53}Mn - ^{53}Cr systematics. *Geochimica et Cosmochimica Acta*, 62, 2863 – 2886.
- Makishima A., and Nakamura E. (2001). Determination of Total Sulfur at Microgram per Gram Levels in Geological Materials by Oxidation of Sulfur into Sulfate with in Situ Generation of Bromine Using Isotope Dilution High-Resolution ICPMS. *Analytical Chemistry*, 73/11: 2547 – 2553.
- Makishima A. and Nakamura E. (2009). Determination of Ge, As, Se and Te in silicate samples using isotope dilution-internal standardization octopole reaction cell ICP-QMS by normal sample nebulization. *Geostandards and Geoanalytical Research*, 33-3: 369 – 384.
- Marin L., Lhomme J., and Carignan J. (2001). Determination of selenium concentration in sixty five reference materials for geochemical analysis by GFAAS after separation with thiol cotton. *The Journal of Geostandards and Geoanalysis* 25: 317 – 324.
- Matsunami S., Ninagawa K., Nishimura S., Kubono N., Yamamoto I., Kohata M., Wada T., Yamashita Y., Lu J., Sears D. W. G., and Nishimura H. (1993). Thermoluminescence and compositional zoning in the mesostasis of a Semarkona group A1 chondrule and new insights into the chondrule-forming process. *Geochimica et Cosmochimica Acta*, 57: 2101 – 2110.
- McSween H. Y. and Huss G. R. (2010). Cosmochemistry. *United Kingdom University Press, Cambridge*.
- Meibom A., Petaev M. I., Krot A. N., Keil K., and Wood J. A. (2001). Growth mechanism and additional constraints on FeNi metal condensation in the solar nebula. *Journal of Geophysical Research*, 106: 32797 – 32801.
- Merrill P.W. (1952). Spectroscopic Observations of Stars of Class. *The Astrophys. J.*, 116: 21.
- Mitchell K., Mason P. R. D., Cappellen P., Johnson T. M., Gill B. C., Owens J. D., Diaz J., Ingall E. D., Reichart G.-J., Lyons T. W. (2012). Selenium as paleo-oceanographic proxy: A first assessment. *Geochimica et Cosmochimica Acta*, 89: 302 – 317.
- Mittlefehldt D. W. (2002). Geochemistry of the ungrouped carbonaceous chondrite Tagish Lake, the anomalous CM chondrite Bells, and comparison with CI and CM chondrites. *Meteoritics & Planetary Science*, 37: 703 – 712.
-

-
- Morlok A., Bischoff A., Stephan T., Floss C., Zinner E., and Jessberger E. K. (2006). Brecciation and chemical heterogeneities of CI chondrites. *Geochimica et Cosmochimica Acta*, 70: 5371 – 5394.
- Münker C., Pfänder J. A., Weyer S., Büchl A., Kleine T., and Mezger K. (2003). Evolution of Planetary Cores and the Earth-Moon System from Nb/Ta Systematics. *Science*, 301:: 84 – 87.
- Nagahara H. (1982). Ni-Fe metals in the type 3 ordinary chondrites. *Mem NIPR Spec*: 25: 86 – 96.
- Nagahara H., Kita N. T., Ozawa K., and Morishita Y. (1999). Condensation during chondrule formation: elemental and Mg isotopic evidence. In *Lunar and Planetary Science*, 30: #1342.
- Nakamura F. and Umemura M. (2001). The stellar IMF in very metal-deficient gas. *Astrophysical Journal*, 548: 19 – 32.
- Niederer F. R., Papanastassiou D. A., and Wasserburg G. J. (1985). Absolute isotopic abundances of Ti in meteorites. *Geochimica et Cosmochimica Acta*, 49: 835 – 851.
- Niemeyer S. and Lugmair G. W. (1984). Titanium isotopic anomalies in meteorites. *Geochimica et Cosmochimica Acta*, 48: 1401 – 1416.
- Oddo G. (1914). Die Molekularstruktur der radioaktiven Atome. *Zeitschrift für anorganische Chemie*, 87: 253 - 268.
- Okai T., Terashima S., and Imai N. (2001). Determination of total sulfur in thirty one geochemical reference materials using an inductively coupled plasmaatomic emission spectrometer fitted with a semiconductor photodiode detector. *Geostandards Newsletter: The Journal of Geostandards and Geoanalysis*, 25: 133 – 136.
- Ostriker J. P. and Gnedin N. Y. (1996). Reheating of the universe and population III. *Astrophysical Journal Letters*, 472: L63
- Orthous-Dauney F.-R., Quirico E., Lemelle L., Beck P., deAndrade V., Simionovici A., and Derenne S. (2010). Speciation of sulfur in the insoluble organic matter from carbonaceous chondrites by XANES spectroscopy. *Earth & Planet. Sci. Lett.* 300: 321 – 328.
- Pack A., Yurimoto H., and Palme H. (2004). Petrographic and oxygen-isotopic study of refractory forsterites from R-chondrite Dar al Gani 013 (R3.5–6), unequilibrated ordinary and carbonaceous chondrites. *Geochimica et Cosmochimica Acta*, 68: 1135 – 1157.
- Pack A., Palme H., and Shelley J. M. G. (2005). Origin of chondritic forsterite grains. *Geochimica et Cosmochimica Acta*, 69: 3159 – 3182.
-

- Pack A., Toulouse C. and Przybilla R. (2007). Determination of oxygen triple isotope ratios of silicates without cryogenic separation of NF_3 — technique with application to analyses of technical O_2 gas and meteorite classification. *Rapid Commun. Mass Spectrom.* 21: 3721 – 3728.
- Palme H., and Beer H. (1993). Abundances of the elements in the solar system. In: Landolt-Bornstein, Group VI: Astronomy and Astrophysics, Vol. 3a: Instruments; Methods; Solar System, Springer, Berlin: 196 - 221.
- Palme H., Jones A. (2003). In: *Meteorites, Comets, and Planets* (ed. A.M. Davis) Vol.1 Treatise on Geochemistry (eds. H.D. Holland, K.K. Turekian), Elsevier-Pergamon, Oxford: 41 - 61.
- Palme H., Lodders K., and Jones A. (2014). Solar system abundances of the elements. In: *Meteorites, Comets, and Planets*. Treatise on Geochemistry Vol.2 (eds.) H.D. Holland, K.K. Turekian), Elsevier-Pergamon, Oxford: 15 - 35.
- Palme H., Hezel D. C., Ebel D. S. (2015). The origin of chondrules: Constraints from matrix composition and matrix-chondrule complementarity. *Earth & Planetary Science Letters* 411: 11 – 19.
- Palme H. and Wlotzka F. (1976). A metal particle from a Ca, Al-rich refractory inclusion from the meteorite, Allende, and the condensation of refractory siderophile elements. *Earth and Planetary Science Letters*, 33: 45 – 60.
- Pearson V. K., Sephton M. A., Franchi I. A., Gibson J. M., Gilmour I. (2006). Carbon and nitrogen in carbonaceous chondrites: Elemental abundances and stable isotopic compositions. *Meteoritics & Planetary Science*, 41: 1899 - 1918.
- Petaev M. I., Meibom A., Krot A. N., Wood J. A., and Keil K. (2001). The condensation origin of zoned metal grains in Queen Alexandria Range 94411: Implications for the formation of the Bencubbin-like chondrites. *Meteoritics & Planetary Science*, 36: 93 – 106.
- Petaev M. I., Wood J. A., Meibom A., Krot A. N., and Keil K. (2003). The ZONMET thermodynamic and kinetic model of metal condensation. *Geochimica et Cosmochimica Acta* 67: 1737 – 1751.
- Paul R. L. and Lipschutz M. E. (1990). Consortium study of labile trace elements in some Antarctic carbonaceous chondrites: Antarctic and non-Antarctic meteorite comparisons. Proc. NIPR Symp. Antarct. *Meteorites*, 3: 80 - 95.
- Reed S. J. B. (2005). In: *Electron Microprobe Analysis and Scanning Electron Microscopy in Geology*, Cambridge University Press, second edn. 2005, ch. 7.7: 122 – 126.
- Rose-Weston L., Brenan J. M., Fei Y., Secco R. A., Frost D. J. (2009). Effect of pressure, temperature, and oxygen fugacity the metal-silicate partitioning of Te, Se, and S: Implications for earth differentiation. *Geochimica et Cosmochimica Acta*, 73: 4598 – 4615.
-

-
- Rouxel O., Ludden J., Cerignan J., Marin L., and Fouquet Y. (2002). Natural variations of Se isotopic composition determined by hydride generation multiple collector inductively coupled plasma mass spectrometry. *Geochimica et Cosmochimica Acta*, 66: 3191 – 3199.
- Rubin A. E. and Scott E. R. D. (1997). Abee and related EH chondrite impact-melt breccias. *Geochimica et Cosmochimica Acta*, 61: 425 – 435.
- Russell H. N. (1929). On the composition of the Sun's atmosphere. *Astrophys. J.*, 70: 11 - 82.
- Tabersky D., Luechinger N. A., Rossier M., Reusser E., Hametner K., Aeschlimann B., Frick D. A., Halim S. C., Thompson J., Danyushevsky L., Günther D. (2014). Development and characterization of custom-engineered and compacted nanoparticles as calibration materials for quantification using LA-ICP-MS. *Journal of Analytical Atomic Spectrometry* 29: 955 – 962.
- Tissandier L., Libourel G., and Robert F. (2002). Gas-melt interactions and their bearing on chondrule formation. *Meteoritics & Planetary Science*, 37: 1377 – 1389.
- Toppani, A., G. Libourel, F. Robert, J. Ghanbaja, und L. Zimmermann (2004). Synthesis of refractory minerals by high-temperature condensation of a gas of solar composition. *In Lunar and Planetary Institute Conference Abstracts*, pp. 1726.
- Sanders I. S. and Scott E. R. D. (2012). The origin of chondrules and chondrites: Debris from low-velocity impacts between molten planetesimals? *Meteoritics and Planetary Science* 47: 2170 – 2192.
- Schönbächler M., Carlson R.W., Horan M.F., Mock T.D., and Hauri E.H. (2008). Silver isotope variations in chondrites: Volatile depletion and the initial ^{107}Pd abundance of the Solar System. *Geochimica et Cosmochimica Acta* 72: 5330–5341.
- Scott E. R. D. (1988). A new kind of primitive chondrite. Allan Hills 85085. *Earth Planet. Sci. Lett.*, 91: 1-18.
- Scott E. R. D. (1994). Evaporation and recondensation of volatiles during chondrule formation. *25th Lunar and Planetary Science Conference*: 1227 – 1228.
- Scott E. R. D. and Krot A. N. (2001). Oxygen isotopic compositions and origins of calcium-aluminum-rich inclusions and chondrules. *Meteoritics & Planetary Science*, 36: 1307 – 1319.
- Scott E. R. D. and Krot A. N. (2014). Chondrites and their components. In: *Meteorites and Cosmochemical Processes*. Treatise on Geochemistry (Second edition), Vol.1. (ed. A. M. Davis), Elsevier-Pergamon, Oxford: 65 - 136.
- Scott E. R. D. (2007). Chondrites and the Protoplanetary Disk. *Annu. Rev. Earth Planet. Sci.*, 35: 577 – 620.
-

- Schaefer L., and Fegley Jr. B. (2010). Volatile element chemistry during metamorphism of ordinary chondritic material and some implications for the composition of asteroids. *Ikarus*, 205: 483 – 496.
- Sears D. W. G., Grossman J. N., Melcher C. L., Ross L. M., and Mills A. A. (1980) Measuring the metamorphic history of unequilibrated ordinary chondrites. *Nature*, 287: 791 – 795.
- Sears D. W. G. and Dodd R. T. (1988). Overview and classification of meteorites. In: Kerridge, J. F. and Matthews, M. S. (eds.) *Meteorites and the Early Solar System*, pp. 3 – 31. Tucson, AZ: University of Arizona Press.
- Sears D. W. G. and Lipschutz M. E. (1994). Evaporation and recondensation during chondrule formation. *35th Lunar and Planetary Science Conference*. pp. 1229–1230.
- Seeger P. A., Fowler W. A. and Clayton D. D. (1965). "Nucleosynthesis of heavy elements by neutron capture". *Astrophysical Journal Supplement*, 11: 121 – 66.
- Shu F. H., Shang H., and Lee T. (1996). Toward an astrophysical theory of chondrites. *Science*, 271: 1545 – 1552.
- Shu F. H., Shang H., Gounelle M., Glassgold A. E., and Lee T. (2001) The origin of chondrules and refractory inclusions in chondritic meteorites. *The Astrophysical Journal*, 548: 1029 – 1050).
- Simon S. B., Davis A. M., Grossman L., and McKeegan K. D. (2002). A hibonite-corundum inclusion from Murchison: a first generation condensate from the solar nebula. *Meteorit. Planet. Sci.*, 37: 533 – 548.
- Smith C. L., De Laeter J. R., and Rosman K. J. R (1977). Mass spectrometric isotope dilution analyses of tellurium in meteorites and standard rocks. *Geochimica et Cosmochimica Acta*, 41: 676 – 681.
- Stöffler D., Keil K., and Scott E. R. D. (1991). Shock metamorphism of ordinary chondrites. *Geochimica et Cosmochimica Acta*, 55: 3845 – 3867.
- Stracke A., Herbert P., Gellissen M., Münker C., Kleine T., Birbaum K., Günther D., Bourdon B., and Zipfel J. (2012). Refractory Element Fractionation in the Allende Meteorite: Implications for Solar Nebula Condensation and the Chondritic Composition of Planetary Bodies. *Geochimica et Cosmochimica Acta*, 85: 114 – 141.
- Suess H. E. and Urey H. C. (1956). Abunances of the elements. *Reviews of Modern Physics*, 28: 53 – 74.
- Van Schmus W. R. and Wood J. A. (1967). A chemical-petrologic classification for the chondritic meteorites. *Geochimica et Cosmochimica Acta*, 31: 747 – 754.
-

-
- Wai C. M. and Wasson J. T. (1977). Nebular condensation of moderately volatile elements and their abundance in ordinary chondrites. *Earth and Planetary Science Letters*, 36: 1 – 13.
- Wai, C. M. and Wasson, J. T. (1979). Nebular condensation of Ga, Ge and Sb and the chemical classification of iron meteorites. *Nature*, 282: 790 – 793.
- Wang M.-S. and Lipschutz M. E. (2005). Thermal metamorphism of primitive meteorites - XII. The enstatite chondrites revisited. *Environmental Chemistry*, 2: 215 - 226.
- Wang Z. and Becker, H. (2013b). Ratios of S, Se and Te in the silicate earth require a volatile-rich late veneer. *Nature*, 499: 328 – 331.
- Wang Z. and Becker H. (2014a). Abundances of sulfur, selenium, tellurium, rhenium and platinum-group elements in eighteen reference materials by isotope dilution sector-field ICP-MS and negative TIMS. *Geostandards and Geoanalytical Research*, 38/2: 189 – 209.
- Wang Z., Becker H., and Gawronski T. (2013a). Partial re-equilibration of highly siderophile elements and the chalcogens in the mantle: A case study on the Baldissero and Balmuccia peridotite massifs (Ivrea Zone, Italian Alps). *Geochimica et Cosmochimica Acta*, 108: 21 – 44.
- Wang Z., Becker H., Wombacher F. (2014b). Mass fractions of S, Cu, Se, Mo, Ag, Cd, In, Te, Ba, Sm, W, Tl and Bi in geological reference materials and selected carbonaceous chondrites determined by isotope dilution ICP-MS. *Geostandards and Geoanalytical Research* doi: 10.1111/j.1751-908X.2014.00312.x.
- Wasson J. T. and Chou C.-L. (1974). Fractionation of moderately volatile elements in ordinary chondrites. *Meteoritics*, 9: 69 – 84.
- Weckwerth G. (2014). Instrumental Neutron Activation Analyses of the Most Earth-like Meteorites. *Journal of Radioanalytical and Nuclear Chemistry*, 299: 221 – 228.
- Weisberg M. K., Connolly H. C., and Ebel D. S. (2005). Petrology and origin of amoeboid olivine aggregates in CR chondrites. *Meteoritics & Planetary Science*, 39: 1741 – 1753.
- Weisberg M. K., McCoy T. J., and Krot A. N. (2006). Systematics and Evaluation of Meteorite Classification. In: *Meteorites and the Early Solar System II*. D. S. Lauretta and H. Y. McSween, University of Arizona Press, Tucson.
- Wlotzka F. (1993). A weathering scale for the ordinary chondrites. *Meteoritics* 28: 460.
- Wolf D. and Palme H. (2001). The Solar System Abundances of Phosphorus and Titanium and the Nebular Volatility of Phosphorus. *Meteoritics & Planetary Science*, 36: 559 – 571.
- Wolf S. F. and Lipschutz M. E. (1995). Chemical Studies of H Chondrites .4. New Data and Comparison of Antarctic Suites. *J. Geophys. Res.-Planets*, 100: 3297 – 3316.
-

- Wolf R., Richter G. R., Woodrow A. B., and Anders E. (1980). Chemical fractionations in meteorites--XI. C2 chondrites. *Geochimica et Cosmochimica Acta*, 44: 711 - 717.
- Wolf S. F., Unger D. L. & Friedrich J. M. (2005). Determination of cosmochemically volatile trace elements in chondritic meteorites by inductively coupled plasma mass spectrometry. *Analytical Chimica Acta*, 528: 121 – 128.
- Wombacher F., Rehkämper M., Mezger K., and Münker C. (2003). Stable isotope compositions in geological material and meteorites determined by multicollector ICPMS. *Geochimica et Cosmochimica Acta*, 67: 4639 - 4654.
- Wombacher F., Rehkämper M., Mezger K., Bischoff A., and Münker C. (2008). Cadmium stable isotope cosmochemistry. *Geochimica et Cosmochimica Acta*, 72: 646 - 667.
- Wombacher F., Ziegler A. and Becker H. (2009) Selenium and tellurium abundances in mafic and ultramafic rock reference samples by ID-ICP-MS. *Geochimica et Cosmochimica Acta* 73(13): A1450.
- Wood J. A. (1963). The origin of chondrules and chondrites. *Icarus* 2: 152 – 180.
- Wood J. A. (1985). Meteoritic constraints on processes in the solar nebula. In: Black, D. C., Matthews, M. S. (Eds.). *Protostars and Planets*, vol. II. Univ. of Arizona Press, Tucson. 687 – 702.
- Wood J. A. (2000). The beginning: swift and violent. *Space Sci. Rev.*, 92: 97 – 112.
- Wiik H. B. (1969). On the regular discontinuities in the composition of meteorites. *Commentationes Physico-Mathematicae*, 34: 135 - 145.
- Xiao X. and Lipschutz M. E. (1992). Labile trace elements in carbonaceous chondrites: A survey. *J. Geophys. Res.*, 97 E6: 10199 - 10211.
- Yanai K., Kojima H., Haramura H. (1995). Catalog of the Antarctic Meteorites collected from December 1969 to December 1994, with special reference to those represented in the collections of the National Institute of Polar Research. *National Institute of Polar Research, Tokyo*, 44 – 76: 212 - 213.
- Yoshida N., Bromm V., and Hernquist L. (2004). The era of massive population III stars: Cosmological implications and self-termination. *Astrophysical Journal*, 605: 579 – 590.
- Yin Q.-Z. (2005). From dust to planets: The tale told by moderately volatile elements. In: *Chondrites and the Protoplanetary Disk* (A. N. Krot et al., eds.), pp. 632–644. ASP Conference Series 341, Astronomical Society of the Pacific, San Francisco.
- Yin Q.-Z., Jacobsen S. B, and Yamashita K. (2002). Diverse supernova sources of pre-solar material inferred from molybdenum isotopes in meteorites. *Nature*, 415: 881 – 883.
-

- Yu M., Sun D., Tian W., Wang G., Shen W., and Xu N. (2002). Systematic studies on adsorption of trace elements Pt, Pd, Au, Se, Te, As, Hg, Sb, on thiol cotton fiber. *Analytica Chimica Acta* 456: 147 – 155.
- Zanda B., Yu Y., Bourot-Benise M., and Hewins R. (2000). The history of metal and sulfides in chondrites. *Workshop on Parent-Body and Nebular Modification of Chondritic Materials*. A4042.
- Zanda B., Bourot-Denise M., Perron C., and Hewins R. H. (1994) Origin and metamorphic redistribution of silicon, chromium, and phosphorus in the metal of chondrites. *Science* 265: 1846 – 1849.
- Zolensky M. E., Mittlefehldt D. W., Lipschutz M. E., Wang M.-S., Clayton R. N., Mayeda T. K., Grady M. M., Pillinger C., Barber D. (1997). CM chondrites exhibit the complete petrologic range from type 2 to 1. *Geochimica et Cosmochimica Acta*, 61: 5099 - 5115.
- Zook H. A. (1981). On a new model for the generation of chondrules. *Lunar & Planetary Science*, 12: 1242 – 1244.

DANKSAGUNG

Ich möchte mich zuallererst bei meinem Betreuer Frank Wombacher bedanken. Danke für die Möglichkeit die Du mir mit diesem Projekt gegeben hast, für Deine unermüdliche Unterstützung, Dein Vertrauen, die ausgiebigen und ergiebigen Diskussionen. Danke für die analytischen Skills und Deine geduldige Einweisung in die Welt der Analytik. Du bist ein großartiger Analytiker und Denker – Ich habe viel von Dir gelernt.

Carsten Münker danke ich insbesondere für die offene Begegnung und den Rahmen in dem ich arbeiten durfte, die Diskussionen und die für mich immer wieder hilfreichen Ratschläge und Aufmunterungen.

Dominik danke ich für die Inspiration in letzter Minute für die angenehmen Diskussionen und die Unterstützung an der Mikrosonde.

Ashlea and Maxwell – I thank you so much for your incredible, unequivocal support during the last stages of my PhD. Ashlea thanks for the honey! Maxwell thanks for the Californian Sun!

Ich danke Jochen Schlüter und Addi Bischoff, die mir den Weg hier her geebnet haben und mich ermuntert haben den Weg nach Köln einzuschlagen.

Alessandro – mio Twin Taurus – mio piccolo chinghialino – without you my time here in the Schloß would have been much more meaningless. Thanks for the light – thanks for your sincere friendship! I thank “iddu” or whoever is hanging around upstairs for our encounter. I thank you heartfelt for the scientific discussions about awesome food – and the awesome food during scientific work. Without your apples and pears I would have been lost. May our paths cross again!

Alexander – Danke für die entspannten Gespräche, die flachen Witze, Dein Wohlwollen, Deine Freundschaft und den „Ersatzitaliener“.

Stefan Peters & Quinten van der Meeeeeer – Thanks for unforgettable Nightflights!

I thank Raul for technical support, discussion and incredible evenings together with Maria, Johanna, Christoph, FTOM, Hendrik, Jacek, and all the other people from the Schloss community.

Moritz, Zaizong and Jogita – Thanks for support and constructive Se – Te discussions!

DANKE MO DU MACHST MICH FROH!

Lars, ohne Dich wäre das Alles von vorn herein nicht möglich gewesen – Danke für den unerschütterlichen Rückhalt. Ich weiß dass ich das alles nie zurückzahlen kann – es ist beruhigend zu wissen dass Du das nicht erwartest.

Ich danke meinen Eltern. Danke für das starke Fundament! Danke für Eure Hilfe (Einzelheiten würden Seiten füllen), Danke für Euer Vertrauen!

Ein besonders farbenprächtiger Dank gebührt Philippe Wolk – Danke dass Du mit aufgesprungen bist auf dieses „intergalaktische Reittierchen“ – Danke dass Du mich immer wieder wohl behalten nach Hause gebracht hast.

ERKLÄRUNG

Ich versichere, dass ich die von mir vorgelegte Dissertation selbständig angefertigt, die benutzten Quellen und Hilfsmittel vollständig angegeben und die Stellen der Arbeit – einschließlich Tabellen, Karten und Abbildungen – , die anderen Werken im Wortlaut oder dem Sinn nach entnommen sind, in jedem Einzelfall als Entlehnung kenntlich gemacht habe; dass diese Dissertation noch keiner anderen Fakultät oder Universität zur Prüfung vorgelegen hat; dass sie – abgesehen von unten angegebenen Teilpublikationen – noch nicht veröffentlicht worden ist, sowie, dass ich eine solche Veröffentlichung vor Abschluss des Promotionsverfahrens nicht vornehmen werde. Die Bestimmungen der Promotionsordnung sind mir bekannt. Die von mir vorgelegte Dissertation ist von Prof. Dr. Carsten Münker betreut worden.

Teilpublikationen liegen nicht vor.

Datum:

Unterschrift:

LEBENS LAUF (März 2015)

Name: Claudia Funk
Geburtsdatum: 11.05.1980
Geburtsort: Hagenow, Deutschland
Staatsangehörigkeit: Deutsch
Familienstand: Ledig

Schullaufbahn

1986 – 1996

Realschulabschluss

August-Bebel Realschule, 19258 Boizenburg

2001 – 2003

Abitur

Abendschule vor dem Holstentor, 20355 Hamburg

Studium

2004 – 2011

Mineralogie Studium (Diplom), Universität Hamburg

Thema der Diplomarbeit: „Xenoliths in Chondrites“

Diplomhauptprüfungen:

- Petrologie – Geochemie – Lagerstättenkunde
- Allgemeine und angewandte Mineralogie
- Geologie
- Geophysik

Promotionsstudium

Mai 2011

Beginn der Dissertation am Institut für Mineralogie und Geologie, Universität zu Köln

- Unter der Betreuung von Prof. Dr. Carsten Münker